Precambrian Research 332 (2019) 105397

Contents lists available at ScienceDirect

Precambrian Research

journal homepage: www.elsevier.com/locate/precamres

Neoproterozoic granitoid magmatism and granulite metamorphism in the Chu-Kendyktas terrane (Southern Kazakhstan, Central Asian Orogenic Belt): Zircon dating, Nd isotopy and tectono-magmatic evolution

A.A. Tretyakov[a,*], A.V. Pilitsyna[a], K.E. Degtyarev[a], E.B. Salnikova[b], V.P. Kovach[b], H.-Y. Lee[c], V.G. Batanova[e,f], K.-L. Wang[c,d], N.A. Kanygina[a], E.V. Kovalchuk[g]

[a] Geological Institute, Russian Academy of Sciences, Pyzhevsky lane, 7a, Moscow, Russia
[b] Institute of Precambrian Geology and Geochronology, Russian Academy of Sciences, Makarova emb. 2, Saint Petersburg, Russia
[c] Institute of Earth Sciences, Academia Sinica, P.O. Box 1-55, Nangang, Taipei 11529, Taiwan
[d] Department of Geosciences, National Taiwan University, No. 1, Sec. 4, Roosevelt Rd., Taipei 10617, Taiwan
[e] Univ. Grenoble Alpes, Univ. Savoie Mont Blanc, CNRS, IRD, IFSTTAR, ISTerre, 38000 Grenoble, France
[f] Vernadsky Institute of Geochemistry and Analytical Chemistry, Russian Academy of Sciences, Kosygin Str. 19, Moscow, Russia
[g] Institute of Geology of Ore Deposits, Petrography, Mineralogy and Geochemistry of Russian Academy of Sciences, Staromonetny lane, 35, Moscow, Russia

ARTICLE INFO

Keywords:
Central Asian Orogenic Belt
Neoproterozoic
Zircon dating
Sm-Nd isotope systematics
High-temperature granulite
Granitoid magmatism

ABSTRACT

Within the Chu-Kendyktas Precambrian terrane located in Southern Kazakhstan (in the western part of the Central Asian Orogenic Belt), medium- and high-grade metamorphic formations have been identified and attributed to the Aydaly and Shukyr Complexes. The Aydaly Complex is predominantly composed of orthogneisses with a Neoproterozoic protolith age of 790 Ma and subordinate high-temperature granulites comprising a succession of amphibolites, amphibole-rich granulites, mesocratic granulites, and melanocratic (clinopyroxene-rich) and leucocratic (melt-rich) granulites, which were evidently formed at moderate pressures of 6–9 kbar and high temperatures, increasing from 700 to 900 °C or more. The clinopyroxene-rich granulites of the Aydaly Complex contain detrital zircon grains of mainly Palaeoproterozoic (1790–2058 Ma) and, to a more limited extent, Neoarchean (~2500 Ma) ages, with preserved magmatic zoning and indicating a sedimentary origin of the protolith via mafic greywackes that were subsequently metamorphosed to amphibolites. The age estimates of the leucocratic melt-rich granulites, which form veins or layers within the clinopyroxene-rich melanosome, correspond to the range 770–790 Ma and define the Neoproterozoic stage of magmatism and granulite metamorphism. Hence, the deposition of the sedimentary protolith for the Aydaly Complex granulites and its subsequent emplacement at mid-crustal levels occurred from the middle Palaeoproterozoic (~1800 Ma) to the late Tonian (~770–790 Ma). In turn, the Shukyr Complex consists of garnet-biotite schists, which are characterised by a significantly lower grade of metamorphism compared to the Aydaly Complex, at around T ~600 °C. The garnet-biotite schists are thought to represent moderate-temperature hornfels, located at the contact between the protolith (shales) and the Early Palaeozoic Ulken massif granitoids. The deposition of the Shukyr Complex protolith occurred during the Ediacaran–Cambrian, as a result of the erosion of mainly Mesoproterozoic (1000 Ma), and to a lesser extent Palaeoproterozoic (2460 Ma), rocks. The Sm-Nd whole-rock isotopic compositions suggest that the formation of the protoliths of the Aydaly and Shukyr Complexes was related to the reworking of Palaeoproterozoic continental crust.

1. Introduction

Precambrian terranes located in the western and southern parts of the Palaeozoides of the Kazakh Uplands and extending to the Kyrgyz and Chinese Tien Shan play an essential role in the structure of the western part of the Central Asian Orogenic Belt (CAOB) (Fig. 1). These Precambrian terranes are separated by Early Palaeozoic accretionary wedge complexes with ophiolites and island arc formations (Degtyarev et al., 2017), and generally consist of Meso- and Neoproterozoic, weakly metamorphosed sedimentary and volcanogenic lithologies

* Corresponding author at: Pyzhevsky lane, 7-1, room 302-b, Moscow zip-code 119017, Russia.
E-mail addresses: and8486@yandex.ru (A.A. Tretyakov), degtkir@mail.ru (K.E. Degtyarev), katesalnikova@yandex.ru (E.B. Salnikova), haoyanglee@earth.sinica.edu.tw (H.-Y. Lee), valentina.batanova@univ-grenoble-alpes.fr (V.G. Batanova), klwang@gate.sinica.edu.tw (K.-L. Wang).

https://doi.org/10.1016/j.precamres.2019.105397
Received 9 January 2019; Received in revised form 19 July 2019; Accepted 23 July 2019
Available online 25 July 2019

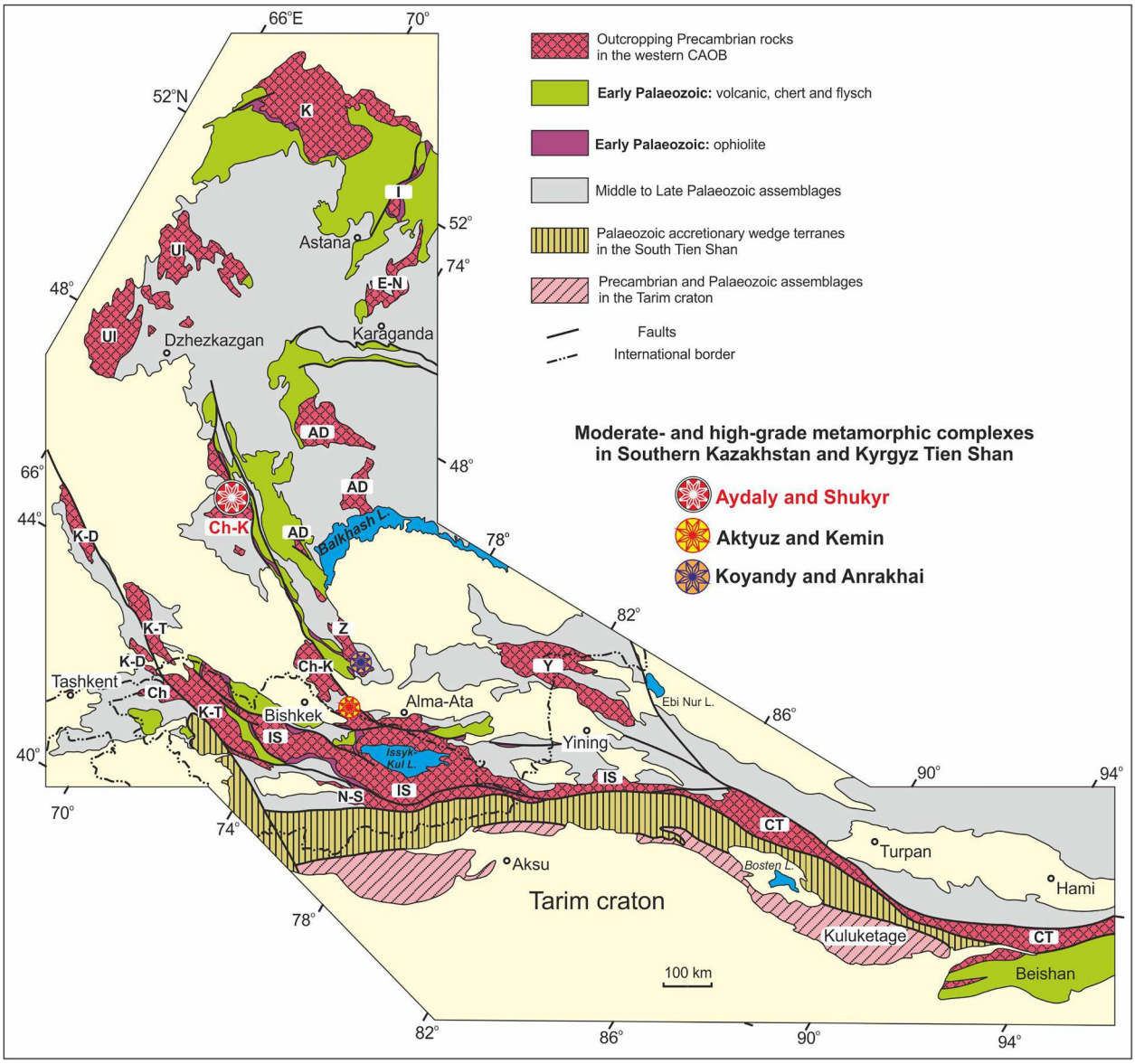

Fig. 1. Precambrian terranes of the western CAOB: AD – Aktau-Dzhungar, Y – Yili, CT – Chinese Central Tien Shan, E-N – Erementau-Niyaz, IS – Issyk-Kul, K – Kokchetav, I – Ishkeolmes, Z – Zheltau, Ch – Chatkal, Ch-K – Chu-Kendyktas, K-D – Karatau-Dzhebagly, K-T – Karatau-Talas, N-S – Naryn-Sarydzhaz, Ul – Ulutau (after Degtyarev et al., 2017).

along with granitoids (e.g., Kröner et al., 2012; Kröner et al., 2013; Wang et al. 2014a; He et al., 2015; Tretyakov et al., 2015; Degtyarev et al., 2017; Kovach et al., 2017; Kanygina et al., 2018; Zhu et al. 2019; Xiong et al., 2019).

A number of recent comprehensive studies have allowed two main groups of Precambrian terranes to be distinguished in the western CAOB, the Issedonian (north-eastern) and Ulutau-Moyunkum (south-western) groups, based on the zircon ages of magmatic and sedimentary rocks, their structural inter-relationships and differences in their Meso- and Neoproterozoic tectono-magmatic evolution. The Issedonian group includes the Kokchetav, Aktau-Dzhungar, Yili, Issyk-Kul (Kyrgyz North Tien Shan) and Chinese Central Tien Shan terranes (Degtyarev et al., 2017). This group is characterised by a wide distribution of Mesoproterozoic (1450–1050 Ma) granitoids, rhyolite–basalt or rhyolitic volcanic series, which have been described in the Chinese Central Tien Shan, Kokchetav and Issyk-Kul terranes (Shi et al., 2010; Tretyakov et al., 2011; Turkina et al., 2011; Kröner et al., 2013; Liu et al., 2014; He et al., 2015; He et al., 2018). The evolution of the Issedonian group of terranes is notable for the presence of thick (more than 1000 m) quartzite-schist sequences, which are best-exposed within the Kokchetav and Aktau-Dzhungar terranes. The inception of the deposition of the quartzite-schist sequences is thought to correspond to the boundary of the Meso- and Neoproterozoic (~1000 Ma), and the deposition continued for 100 Ma in sub-platform settings (Kovach et al., 2017; Kanygina et al., 2018; Huang et al., 2019). The accumulation of these sequences apparently ended with the formation of Early Neoproterozoic granitoids and rhyolite–granite associations around 870–930 Ma, which are widespread within the Aktau-Dzhungar, Yili and Chinese Central Tien Shan terranes (Wang et al., 2014a; Tretyakov et al, 2015; Huang et al., 2015; Gao et al., 2015; Zhu et al. 2019; Xiong et al., 2019). From the Early Neoproterozoic to the Early Palaeozoic, the Issedonian group terranes were covered by terrigenous carbonates, and in the eastern part of the Yili and Chinese Central Tien Shan terranes Late Neoproterozoic intraplate gabbroids, alkaline granitoids and contrasting volcanic–plutonic associations formed around 730–780 Ma are locally exposed (Wang et al., 2014b; Gao et al., 2015

The Ulutau-Moyunkum group includes the Ulutau, Karatau-Talas, Naryn-Sarydzhaz (Kyrgyz Middle Tien Shan), the Zheltau terranes and,

apparently, the Chu-Kendyktas terrane. Within this group, Palaeoproterozoic complexes have been identified (Kröner et al., 2007; Tretyakov et al., 2016; Pilitsyna et al., 2019) and Mesoproterozoic and Early Neoproterozoic formations are represented by variegated sedimentary rocks. Late Neoproterozoic felsic or rhyolitic to basaltic volcanogenic and sedimentary rocks along with anorogenic granitoids formed around 750–850 Ma play a crucial role in the structure of the terranes of this group (Kröner et al., 2007; Glorie et al., 2011; Tretyakov et al., 2015; Pilitsyna et al., 2019). The Precambrian evolution of the terranes of the Ulutau-Moyunkum group ended with the formation of the tillite-bearing volcanogenic-sedimentary complexes of the Late Cryogenian–Ediacaran, preceded by the intrusion of a syenite massif (Tretyakov et al., 2012; Degtyarev et al., 2017).

The Chu-Kendyktas terrane is located in Southern Kazakhstan and extends to the NW over 650 km, with an average width of ~50 km. This terrane includes several blocks (Zhuantobe, Chu, Kendyktas and Aktyuz), which are separated by Middle- to Upper-Palaeozoic and Cenozoic volcanogenic and sedimentary formations from the NW to the SE (Fig. 1). The Precambrian complexes of the Chu-Kendyktas terrane are poorly investigated. Detailed information is available for the Precambrian formations of the Aktyuz Block, where the orthogneisses and gneissic granites of the Aktyuz and Kemin Complexes, which were formerly thought to be Palaeoproterozoic in age (Bakirov et al., 2003), were reassessed using geochemical and isotopic signatures and determined to have Late Neoproterozoic protolith ages (Kröner et al., 2012). In addition, the metagabbros and greenschists of the Kopurelisay Complex that were formerly thought to be Palaeoproterozoic in age have been re-assigned to the Early Palaeozoic (Kröner et al., 2012). Data regarding the ages of the Zhuantobe, Chu and Kendyktas Blocks of the Chu-Kendyktas Precambrian terrane are based mainly on wider regional correlations (Abdulin, 1980; Kozakov, 1993). An investigation of the complexes associated with these blocks is key for understanding the Precambrian evolution of the entire Chu-Kendyktas terrane and determining its tectonic affinity in the western CAOB. The moderate- and high-grade metamorphic formations, which have been traditionally referred to as Archean-Palaeoproterozoic (Abdulin, 1980; Kozakov, 1993), are of great importance as these may reflect the earliest stages of the evolution of the Chu-Kendyktas terrane. In the north-western part of the Chu Block, orthogneisses and high-temperature granulites have been identified, comprising the Aydaly Complex along with the garnet-bearing schists of the Shukyr Complex. However, information regarding the geological positions, formation stages, protolith sources, geochemical signatures and mineral chemistry, along with P-T paths for the observed complexes, is virtually absent. Furthermore, regional correlations have never been conducted between the observed complexes and those from the well-studied Aktyuz and Kemin Complexes in the Aktyuz Block (Kröner et al., 2012), corresponding to the structures of the south-eastern part of the Chu-Kendyktas terrane, or with the Anrakhai and Koyandy Complexes in the Zheltau terrane in Southern Kazakhstan (Pilitsyna et al., 2019) (Fig. 1).

In this paper, we provide a comprehensive study of the structural positions, geochemical affiliations, zircon dating results and Nd isotopic compositions of the meta-magmatic and metasedimentary rocks of the Chu Block, comprising the north-western part of the Chu-Kendyktas terrane in Southern Kazakhstan, together with their tectono-magmatic evolution. We show that the studied complexes record different tectono-magmatic evolutions and possess distinct protolith ages. Based on our results, we suggest a Precambrian tectonic affinity for these complexes within the Chu Block and propose a model of the Precambrian–Early Palaeozoic tectonic evolution of the Chu-Kendyktas terrane.

2. Geological structure of the NW part of the Chu-Kendyktas terrane

In the NW part of the Chu-Kendyktas terrane, the Precambrian and Early Palaeozoic complexes comprise the Chu and Zhuantobe Blocks (Fig. 2A). The major part of the Chu Block consists of strongly deformed

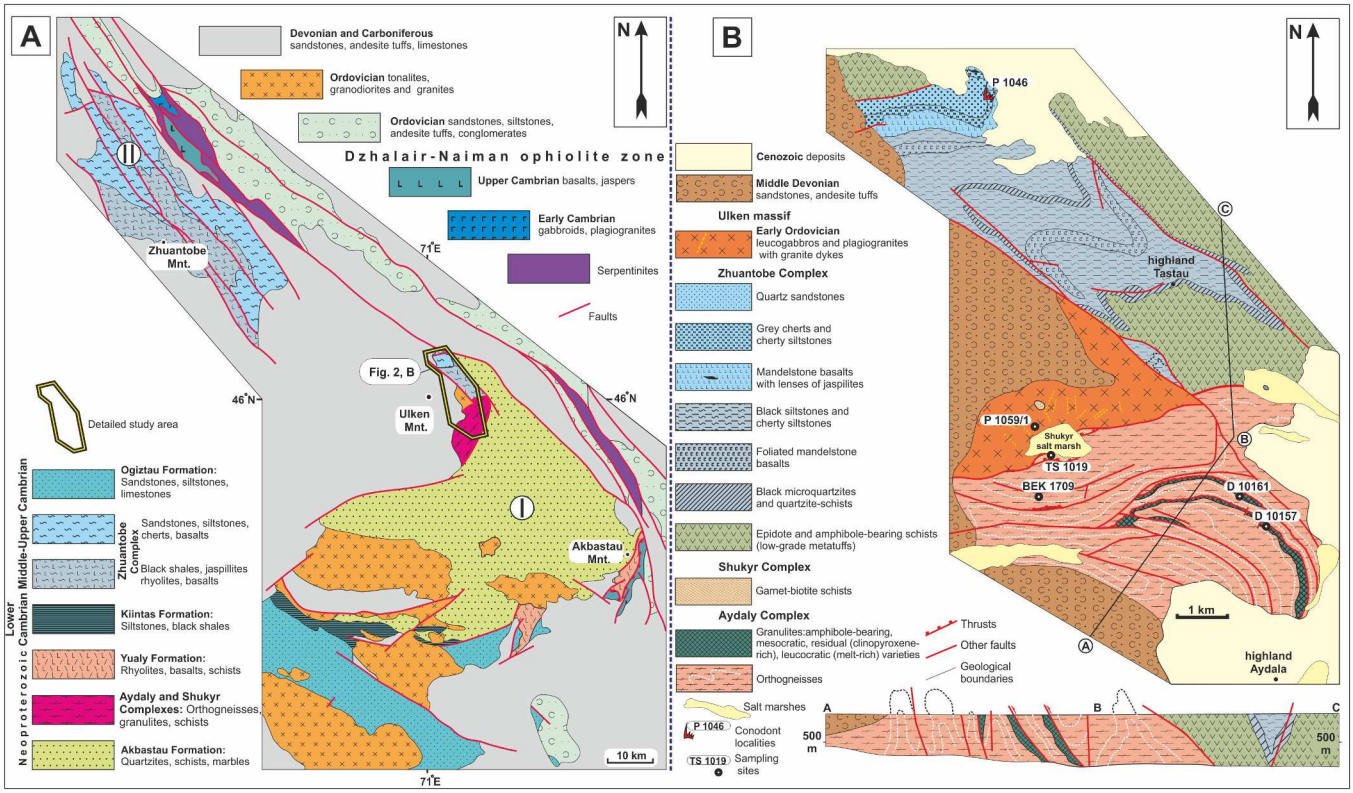

Fig. 2. A. Geological scheme of the Chu (I) and Zhuantobe (II) blocks (NW part of the Chu-Kendyktas terrane). B. Geological map and cross-section of the NW part of the Chu block (near the Aydala and Tastau highlands).

quartzite-schist sequences of the Akbastau Formation. Based on the chemical compositions and structures of the quartzite-schist sequences of the Chu Block, these rocks are thought to be consistent with those described from Northern Kazakhstan or the Aktau-Dzhungar terrane (Central and Southern Kazakhstan), and correspond to the lowest Neoproterozoic (Abdulin, 1980; Degtyarev et al., 2017). In the SE part of the Chu Block, the quartzite-schist sequences are overlain by metamorphosed intermediate or felsic volcanic rocks; tuffs and volcanogenic sequences; and sedimentary lithologies of the Yualy Formation, with a faulted contact between these two groups. The structures and compositions of the Yualy Formation rocks are similar to those described from the Kopi Formation of the Kendyktas Block, with an estimated Neoproterozoic age of 780 Ma (Kröner et al., 2007). Early Palaeozoic complexes in the SW part of the Chu Block are composed of quartz-sericite, graphite-mica, cherty carbon-bearing schists with graphite-bearing quartzites (of the lower Cambrian Kiintas Formation) and quartz–chlorite–sericite schists and quartz or quartz–feldspar sandstones (of the middle–upper Cambrian Ogiztau Formation) with a total thickness of up to 1500 m (Abdulin, 1980). The NW part of the Chu Block is made up of formations of the Zhuantobe Complex, also comprising the cognominal block (Fig. 2A). The Zhuantobe Complex, which is thought to be Ediacaran–lower Cambrian in age, consists of mainly black shales, quartzites or rarely jaspilites, as well as variably metamorphosed (low- to moderate-grade) felsic (rhyolites) or basic volcanic rocks or tuffs (Rozanov et al., 1974; Rozanov, 1976). The ages of the Early Palaeozoic complexes of the Chu and Zhuantobe Blocks are generally based on regional correlations with the faunistically-characterised complexes of the adjacent terranes in Kazakhstan (Abdulin, 1980; Rozanov et al., 1974). The medium- and high-grade metamorphic Aydaly and Shukyr Complexes are exposed within a small area of 10 × 5 km in the NW part of the Chu Block. The metamorphic complexes have faulted contacts with the Precambrian quartzite-schists of the Akbastau Formation in the SE, and are in thrust-faulted contact with the silicic and terrigenous formations of the Zhuantobe Complex in the NW. Both the Precambrian and Early Palaeozoic complexes of the Chu Block are cut by large granitoid massifs of presumed Ordovician age (Abdulin, 1980).

2.1. Geological structure of the NW part of the Chu Block

Medium- and high-grade metamorphic formations, represented by the Aydaly and Shukyr Complexes together with the Lower Palaeozoic silicic, terrigenous and volcanogenic lithologies of the Zhuantobe Complex and Early Palaeozoic granitoids of the Ulken massif, are best exposed near the highlands of Aydala and Tastau, and the Shukyr salt marshes in the NW part of the Chu Block (Fig. 2B). The sampling localities are given in Table 1.

2.1.1. The Aydaly Metamorphic Complex

The Aydaly Complex includes mainly two rock types, based on their mineralogical and chemical compositions. Orthogneisses are the predominant lithology, making up ~80% of the Aydaly Complex, and comprising pinkish, slightly banded and foliated rocks that commonly constitute the cores of the isoclinal folds (e.g. sample BEK 1709; Fig. 2B). Granulites, including amphibole-bearing, melanocratic residual (clinopyroxene-rich) and leucocratic (melt-rich) varieties, constitute the limbs of the isoclinal folds and are multiply repeated in the thrust systems. These rocks tend to preserve clear evidence of pervasive partial melting, reflected in a transition from amphibolite–amphibole-rich granulites to mesocratic granulites, and then to segregated melt-rich veins (injections of plagiogranite leucosomes of variable thickness (e.g. sample D 10161; Fig. 2B) with residual (clinopyroxenite melanosomes, e.g. sample D 10157; Fig. 2B) granulites (Fig. 5). In some cases, the leucocratic granulites form bodies up to several metres in size. The observed orthogneisses and granulites have been synchronously deformed and may represent as a single tectonic unit. The Aydaly

Table 1
Summary of sample localities, rock types, geological associations, and zircon ages for the rock types from the NW part of the Chu-Kendyktas terrane (the Chu block).

Sample	N. latitude	E. longitude	Locality	Rock type	Complex	Age (Ma)
BEK 1709	46° 00′ 16.4″	71° 04′ 44.0″	900 m to the south from the Shukyr salt marsh	Quartz-feldspar orthogneiss	Aydaly Complex	789 ± 5
D 10161	46° 00′ 19.7″	71° 07′ 54.3″	3.5 km to the north from the Aydala highland	Leucocratic melt-rich granulite (tonalite)	Aydaly Complex	769 ± 2
D 10157	45° 59′ 47.0″	71° 08′ 29.8″	2.5 km to the NNE from the Aydala highland	Melanocratic residual (clinopyroxene-rich) granulite	Aydaly Complex	793 ± 4 1790 – 2680
TS 1019	46° 00′ 41.8″	71° 04′ 49.2″	Southern bank of the Shukyr salt marsh	Garnet-biotite schist	Shukyr Complex	548 – 3175
P 1059/1	46° 01′ 01.2″	71° 04′ 37.6″	NW bank of the Shukyr salt marsh	Leucogabbro	Ulken massif	489 ± 5

Complex has been overthrust from the NW by poorly developed garnet-biotite schists of the Shukyr Complex (Fig. 2B).

2.1.2. The Shukyr Metamorphic Complex

The garnet-biotite schists of the Shukyr Complex are the least developed rock type in the studied area and are locally exposed near the cognominal Shukyr salt marshes (e.g. sample TS 1019; Fig. 2B). These rocks are strongly deformed into tight E–W trending isoclinal folds, cut by reverse faults and thrusts. The garnet-biotite schists are characterised by a higher structural position compared to the Aydaly Complex, making up an individual tectonic slice, and are frequently cut by Early Palaeozoic granitic dykes.

2.1.3. The Zhuantobe Complex

The Zhuantobe Complex is located in the northern part of the studied area, close to the Tastau highlands, and also makes up the cognominal Zhuantobe Block (Fig. 2A). The Zhuantobe Complex is deformed into a NW-trending fold system (Fig. 2B). The lowest parts of the Complex are represented by low-grade banded epidote- and amphibole-bearing metatuffs and metabasalts, followed upwards by black shales, micro-quartzites or quartzites, jaspilites with foliated basalts and rhyolites. The upper parts of the Complex consist of mandelstone basalts, overlain by grey, weakly-layered cherts and quartz sandstones. Sparse lenses of jaspilites are spatially associated with the contacts with the mandelstone basalts and cherts. The total thickness of the Zhuantobe Complex is around 1000 m. In the upper parts of the sequence, a number of upper Cambrian paraconodonts (*Prooneotodus* spp.) have been identified (e.g. sample P 1046; Fig. 2B), therefore the studied Complex is thought to be middle- to late-Cambrian in age. The Zhuantobe Complex occupies a structurally higher position relative to the Aydaly and Shukyr Complexes, and is characterised by a progressive up-section decrease of metamorphic grade from moderate to low (epidotised metavolcanic rocks), then to the lowest grades (foliated mandelstone basalts and cherts) whilst moving away from the faulted contact with the medium- and high-grade metamorphic formations.

2.1.4. The Ulken granitoid massif

The Ulken massif is located to the north and west of the Shukyr salt marshes and consists of moderately deformed plagiogranites and minor leucogabbro (e.g. sample P 1059/1; Fig. 2B), cut by numerous leucocratic dykes of granite and pegmatite. It is worth noting that similar dykes also cut the garnet-biotite schists of the Shukyr Complex. The Ulken massif rocks have a faulted (tectonic) contact with the Shukyr Complex, however the presence of xenoliths of the garnet-biotite schists and similar granitic dykes in both complexes indicate a primarily intrusive contact between the tectonic units.

The Aydaly, Shukyr and Zhuantobe Complexes along with the Ulken massif are unconformably overlain by Middle Devonian volcanogenic and sedimentary formations (Fig. 2B).

3. Results

To decipher the tectono-magmatic evolution of the crustal complexes of the Chu Block in the NW part of the Chu-Kendyktas terrane, and to compare the obtained results with those from the adjacent complexes in the SE part of the Chu-Kendyktas terrane (Aktyuz and Kemin Complexes, Kröner et al., 2012) or the Zheltau terrane (Anrakhai and Koyandy Complexes, Pilitsyna et al., 2019), petrographic,

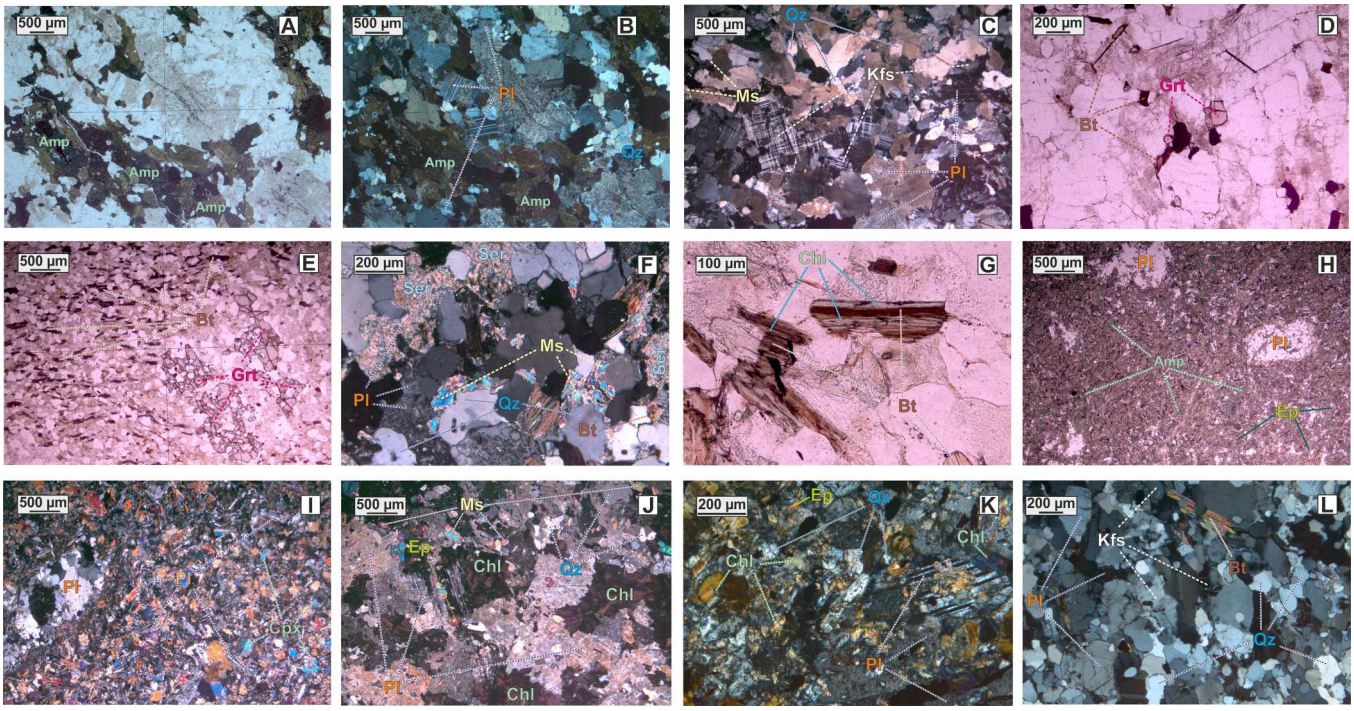

Fig. 3. Photomicrographs of the main minerals and microtextures of the orthogneisses of the Aydaly Complex (amphibole-bearing orthogneiss: A, B; quartz-feldspar orthogneiss – C, D), garnet-biotite schists of the Shukyr Complex (E – G), metatuffs and basalts of the Zhuantobe Complex (H, I), granitoids of the Ulken massif (J – L): A) Subhedral and anhedral crystals of amphibole in the matrix (plane light); B) General microtexture of the amphibole-bearing orthogneiss (crossed nicols); C) Weakly foliated microtexture, composed of plagioclase, quartz, K-feldspar, minor muscovite (crossed nicols); D) Flakes of biotite and garnet grains in the matrix (plane light); E) General foliated microtexture of the garnet-biotite schist (plane light); F) Flakes of muscovite and sericite with biotite in the matrix (crossed nicols); G) Replacement of biotite by chlorite (plane light); H) Amphibolitised and epidotised matrix (plane light); I) Partly altered phenocryst of plagioclase in the matrix of clinopyroxene, plagioclase, magnetite and glass (crossed nicols); J) Plagiogranite general microtexture, composed of plagioclase, chlorite, quartz, muscovite and epidote (crossed nicols); K) Leucogabbro general microtexture, composed of mainly plagioclase and chlorite with overprinted epidote and quartz (crossed nicols); L) Leucogranite with abundant quartz and feldspars (crossed nicols). Qz – quartz; Pl – plagioclase; Kfs – K-feldspar; Chl – chlorite; Amp – amphibole; Bt – biotite; Ep – epidote; Grt – garnet; Ms – muscovite; Cpx – clinopyroxene; Ser – sericite.

mineralogical, whole-rock chemistry, geochronological and Sm-Nd isotopic studies were conducted. The analytical techniques, standards, approaches, and software used for whole-rock and mineral chemistry studies, and the determination of metamorphic evolution paths, zircon ages, and Sm-Nd whole-rock isotopic systematics measurements, are provided in Appendices A, B and C. Mineral abbreviations are after Whitney and Evans (2010).

3.1. Petrography and mineral chemistry of the main rock types

For the most variegated metamorphic rocks of the Aydaly and Shukyr Complexes, mineral chemistry and element mapping studies together with field observations and petrography were used to constrain the P-T evolutions, where possible. For the rest of the studied rocks, field geology and structural information were used, together with petrographic observations.

3.1.1. Aydaly Complex

3.1.1.1. The orthogneisses. Comprise mesocratic amphibole-bearing varieties and leucocratic quartz-feldspar varieties with minor micas. The amphibole-bearing orthogneisses are weakly foliated, medium-grained rocks composed of subhedral plagioclase (Pl) in the size range 0.4–1.5 mm, with a composition corresponding to andesine, and subhedral green amphibole in the size range 0.3–0.7 mm (Fig. 3A, B). Anhedral grains of quartz (Qz) and K-feldspar (Kfs) are subordinate in this rock type.

The leucocratic quartz-feldspar orthogneisses are similarly weakly foliated, medium- to coarse-grained rocks, consisting of mostly subhedral crystals of sodic Pl (X_{ab} = 0.88) and Kfs (X_{or} = 0.90–0.94) (Fig. S1a, Tables S2, S3) in the size range 0.4–1.2 mm, with well-preserved twinning bands and grating structures (Fig. 3C). The modal contents of Kfs and Pl are nearly equal. Qz forms poorly expressed ribbons of rounded or anhedral grains of a wide range of sizes, which normally do not exceed 0.8–1 mm and are characterised by clouded extinctions. The feldspars together with quartz display a weak orientation, following the metamorphic lineation. Micas are poorly developed in this rock type (< 5 vol%) and include biotite (Bt) with muscovite (Ms) in equal proportions. The micas form small, weakly-oriented flakes up to 0.2–0.3 mm in size with preserved cleavage. The Bt records a moderate $Mg/(Mg + Fe_{tot})$ ratio of 0.4 and notably high concentrations of fluorine (1.5–1.7 wt%; Table S9) and is frequently replaced by chlorite (Chl). Sporadic roundish grains of garnet (0.1–0.3 mm in size) are distributed in the matrix (Fig. 3D). Notable accessory minerals include zircon, rutile, and apatite, present in both varieties of the orthogneisses.

3.1.1.2. 3.1.1.2. The granulites. Comprise several varieties with transitional contacts. Within the *amphibolites–amphibole-rich granulites*, relict metamorphic layering is partly preserved, and the rocks are characterised by fine- to medium-grained textures (Fig. 4A). The amphibole (Amp) is pleochroic in dark green to slightly bluish-green colours (with Na comprising 0.48–0.51 atoms per formula unit (a.p.f.u.), and Al^{VI} comprising 0.51–0.65 a.p.f.u.; Table S8), and forms both subhedral crystals with prominent cleavage and anhedral grains with resorbed rims of 0.1–0.6 mm in size. Amp generally follows the metamorphic lineation and corresponds to pargasite in composition (Fig. S1c). Slightly greenish clinopyroxene (Cpx) is also present in this rock type and is spatially associated with pockets or patches of Qz-feldspar assemblages. Cpx forms both subhedral crystals and anhedral, corroded grains in the size range 0.1–0.5 mm, with a $Mg/(Mg + Fe^{2+})$ ratio of 0.70 and Na_2O contents of 0.60–0.68 wt% (Fig. S1b, Table S4). The Qz-feldspar patches are mostly composed of Qz and Pl (X_{ab} = 0.50–0.68) with lesser Kfs (Or_{93-94}), and are up to 1 mm thick (Fig. S1a, Tables S2, S3). The Qz-feldspar segregations are interpreted to have been formed at the early stages of anatexis and indicate a low melt fraction. This is in agreement with the observed elemental migrations (Fig. 4A), expressed in the conspicuous increase of albite in plagioclase from core to rim, along with the decrease of anorthite in the same direction, which is characteristic for the crystallisation of melt lenses. Yellowish epidote (Ep) is extensively developed in the rock matrix.

Mesocratic granulites are characterised by the nearly complete disappearance and destruction of the earlier metamorphic layered structures, which is evidently related to the progress of anatexis, and this is also confirmed by the predominance of Qz-feldspar assemblages (leucosomes) relative to the dark-coloured minerals (Fig. 4B). Instead, coarser-grained igneous structures and textures, made up of Qz, Cpx and feldspars, predominate and notable modal contents of anhedral, corroded Amp of hastingsite composition (with Na: 0.50–0.57 a.p.f.u. and Al^{VI}: 0.35–0.44 a.p.f.u.; Fig. S1c, Table S8) are present. Cpx forms slightly greenish, rounded and resorbed crystals 0.2–0.5 mm in size, with a $Mg/(Mg + Fe_{tot})$ ratio of 0.67–0.69, higher Na_2O contents of 0.70–1.0 wt% (Fig. S1b, Table S4), and rarely possesses good cleavage. Amph and Cpx are frequently surrounded by yellowish worm-like aggregates of Ep and Qz. The leucosomes mainly consist of sodic Pl (X_{ab} = 0.7–0.94) and Qz, and Kfs of Or_{94} is not unusual at the boundaries with Pl, marked by an appearance of mirmekites (Tables S2, S3). It is noteworthy that the plagioclase within the Qz-feldspar leucosomes similarly displays a rimward enrichment in sodium and a decrease in calcium content (Fig. 4B), reflecting a melt crystallisation process. An abundance of accessory minerals (zircon, rutile, allanite, and titanite) is characteristic for these granulites.

With progressing anatexis, the melt-residuum separation evidently leads to the segregation of *melanocratic residual granulites* (clinopyroxenite melanosomes) and *leucocratic melt-rich granulites* (plagiogranite leucosomes) (Fig. 5). The plagiogranite leucosomes are medium- to coarse-grained rocks with an igneous structure, made up of anhedral crystals of sericitised Pl (0.5–1 mm in size) and Qz (small roundish grains up to 0.5 mm in size), with rare Kfs (Fig. 4C). The chemical compositions of Pl in the melt-rich leucocratic granulites are characterised by variable contents of Na_2O and CaO (Fig. S1a, Table S2), generally corresponding to andesine-labradorite compositions, with rare bytownite and occasional nearly purely albitic (X_{ab} = 0.99) compositions (Fig. 4C, Table S2). Kfs is represented by orthoclase (X_{or} in the range 0.90–0.95; Fig. S1a, Table S3). The minerals have evidently been deformed to some extent, which is expressed in their prominent undulating extinctions along with the appearance of kinks. It is worth noting that the leucocratic granulites contain minor (< 10 vol%) green Cpx similar to that of the residuum, corresponding to diopside-hedenbergite with a $Mg/(Mg + Fe_{tot})$ ratio varying from 0.67 to 0.60 on average (Fig. S1b, Table S4), together with zircon, allanite (Table S6) and rutile with titanite. In many cases allanite and relics of the least magnesian Cpx ($Mg/(Mg + Fe_{tot})$ = 0.3–0.4) are replaced by aggregates of epidote–clinozoisite (Ep-Czo) with Qz (Fig. 4C, Tables S5, S6). Pale orange garnet (Grt) of andradite-grossular composition (Fig. S2, Table S7) occurring in association with zoned Ep-Czo ($Fe^{3+}/(Fe^{3+} + Al)$ varies considerably in the range of 0.07–0.29; Table S5, Fig. S2, from element mapping) is often present in the matrix, and these associations may have been formed during a later metasomatic overprinting event. In the most melt-rich varieties of the leucocratic granulites, only sporadic anhedral grains of Cpx occur, evidently replaced by later Amp of hastingsite-magnesiohornblende composition (Fig. S1c, Table S8). White mica in this rock type is solely present when replacing plagioclase, and corresponds to sericite (Fig. 4C, Table S9). Conversely, the clinopyroxenite melanosomes (or melanocratic residual granulites) represent a virtually monomineralic rock type, composed of pale-green subhedral Cpx with sizes of 0.3–0.5 mm on average, rarely enclosing layers of leucocratic Qz–feldspar material up to 0.4 mm thick (Fig. 4D). In contrast to these melt-rich granulites, the clinopyroxene in the residuum-rich granulites is characterised by significantly higher $Mg/(Mg + Fe_{tot})$ ratios in the range from 0.75 (in the core) to 0.68 (in the rims) (Fig. S1b, Table S4), reflecting prominent zoning with a gradual decrease of MgO and SiO_2 from cores to rims with an increase in FeO_{tot}

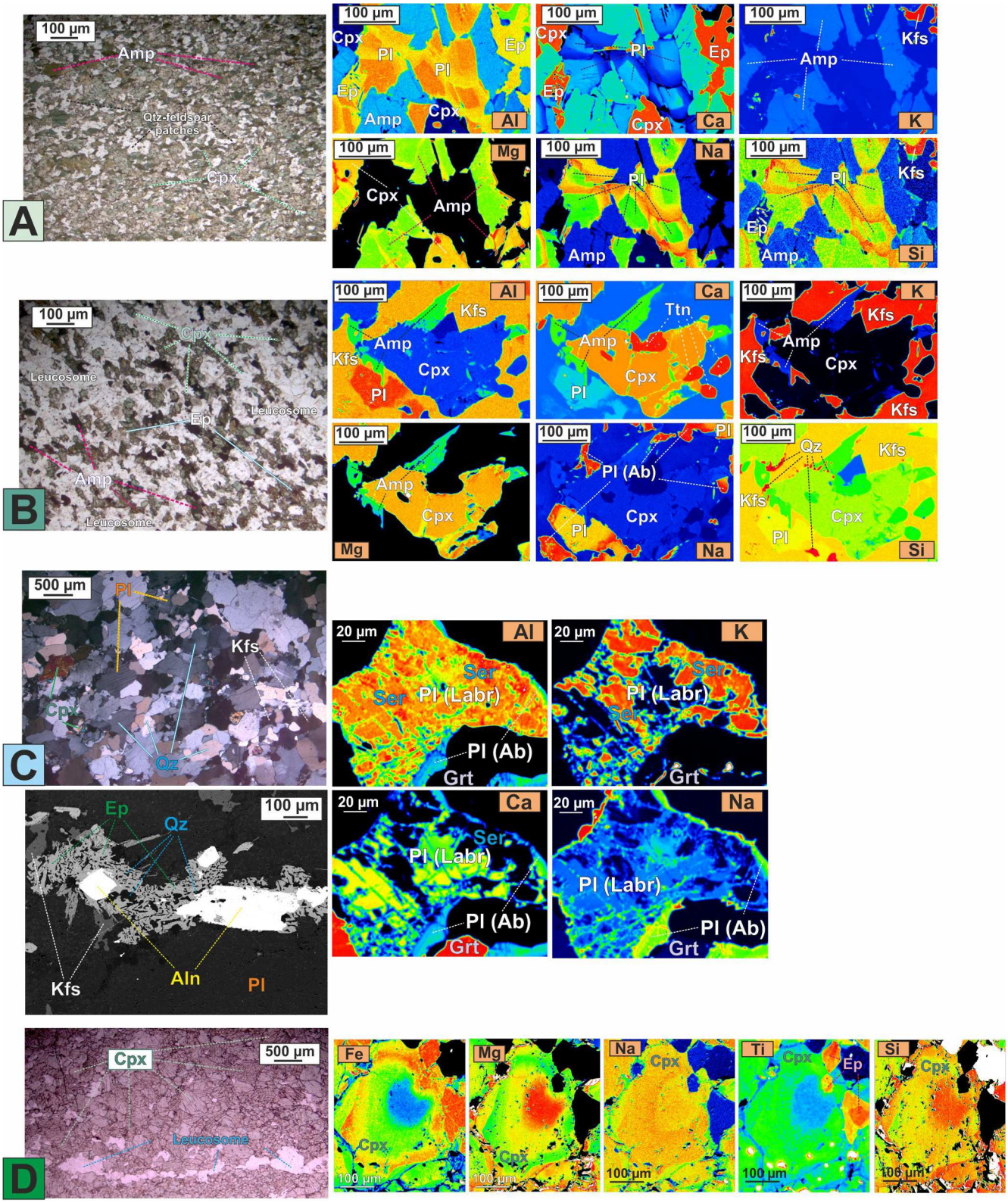

Fig. 4. Photomicrographs and X-ray element mapping images of the Aydaly Complex granulites varieties. A) Amphibolite – amphibole-rich granulite microtexture with preserved metamorphic layering (plane light); B) Mesocratic granulite with nearly destroyed metamorphic layering and low modal contents of amphibole (plane light); C) Leucocratic melt-rich granulite with minor clinopyroxene and allanite replaced by epidote (crossed nicols and BSE images). D) Melanocratic residual clinopyroxene-rich granulite with layer of quartz-feldspar leucosome (plane light). Element mapping shows a prominent clinopyroxene zoning with decrease of Mg and Si from core to rims and increase of Fe, Na, Ti in the same direction; Qz – quartz; Pl – plagioclase; Kfs – K-feldspar; Aln – allanite; Ep – epidote; Grt – garnet; Cpx – clinopyroxene; Ser – sericite; Amp – amphibole.

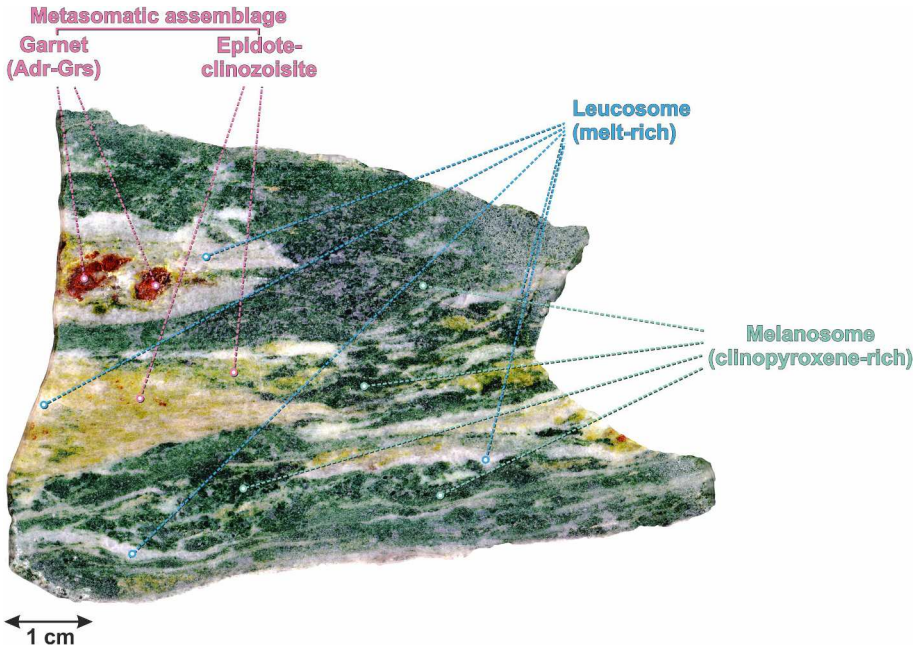

Fig. 5. Polished sample of the granulite of the Aydaly Complex (scanned image).

in the same direction (Fig. 4D, from element mapping). In addition, the plagioclase from the leucocratic layers is characterised by high anorthite contents of An_{62}–An_{77}, corresponding to labradorite-bytownite compositions (Table S2). Cpx is replaced from the rims by epidote–-clinozoisite to various extents (Table S5). These rocks contain numerous grains of zircon, including detrital varieties (see Section 3.4.1 below).

3.1.2. Shukyr Complex

The garnet-biotite schists that compose the Shukyr Complex are moderately foliated rocks with medium- to coarse-grained textures, comprising large (up to 2–2.5 mm) porphyroblasts of slightly pinkish garnet of almandine composition (Table S7) with an anhedral appearance. Bt, Ms and Qz with sericitised Pl make up the groundmass and follow the metamorphic lineation (Fig. 3E–G). The garnet does not display any chemical zoning features and shows nearly equal contents of MnO, FeO, CaO, and MgO in the core, mantle, and marginal parts of the porphyroblasts (Table S7). The Grt contains numerous inclusions of Pl and Qz (of generally 0.1–0.5 mm in size), which are also present in the rock matrix. The plagioclase compositions cover a wide range of An content (An_4–An_{32}), corresponding to albite-andesine compositions (Fig. S1a, Table S2). Biotite forms subhedral flakes of 0.4–0.6 mm in size, prevails over muscovite and may show an anhedral or xenomorphic habit (Fig. 3F). Similarly, the micas do not contain chemical zoning and the biotite displays stable high contents of TiO_2 in the range of 3.5–3.8 wt%, with a moderate $Mg/(Mg + Fe_{tot})$ ratio varying from 0.41 to 0.49 (Table S9). In many cases Bt is replaced by Chl, up to the extent of complete biotite disappearance (Fig. 3G, Table S10). White mica mostly replaces Pl or forms separated flakes (rarely) and is characterised by a high SiO_2 content (Si = 3.17–3.20 a.p.f.u.) with low TiO_2 concentrations (~0.1 wt%), corresponding to muscovite-sericite compositions (Table S9). Yellowish tourmaline (Tur) of dravite-magnesiofoitite composition (Fig. S1d, Table S11) with Qz inclusions, as well as rutile together with ilmenite, are sporadically distributed in the rock matrix. These rocks also contain numerous grains of detrital zircon in the size range 50–100 μm.

3.1.3. Zhuantobe Complex

The epidote- and amphibole-bearing schists, with rarer epidosites (low-grade metatuffs), of the Zhuantobe Complex are foliated rocks with a matrix made up predominantly of Ep with lesser Amp with pleochroic in yellowish to green colours, as well as magnetite and porphyroblasts (relics of phenocrysts) of partly epidotised Pl up to 2 mm in size (Fig. 3H). The Cpx is completely replaced by Amp. In the *weakly-foliated mandelstone basalts* of the upper parts of the sequence, phenocrysts of Pl are normally preserved, however these are replaced by calcite in many cases. The matrix of the basalts consists of nearly unaltered Cpx, Pl and magnetite (Fig. 3I).

3.1.4. Ulken massif

The weakly deformed plagiogranites and leucogabbros of the Ulken massif are characterised by medium- to coarse-grained textures and generally magmatic structures. The *plagiogranites* contain strongly sericitised sodic Pl, forming anhedral tablets up to 1–1.2 mm in size, and abundant anhedral roundish grains of Qz. Concentric aggregates of Chl are characteristic for this rock type. Ms and Ep, the sizes of which do not exceed 0.3–0.5 mm, are normally developed as separate flakes and grains in the rock groundmass (Fig. 3J). The *leucogabbros*, which display a subordinate distribution compared to the plagiogranites, are composed of strongly chloritised dark-coloured minerals with sericitised Pl (up to 1 mm in size) (Fig. 3K). Epidote and quartz are also developed in these rocks as later phases. Both the leucogabbros and the plagiogranites contain accessory zircons and apatites. The rocks are cut by leucogranitic dykes, mainly of a fine- to medium-grained texture, and are composed of abundant rounded or anhedral grains of Qz, ranging from 0.1 to 0.8 mm in size, and Pl with Kfs in equal proportions (Fig. 3L). The leucogranites contain minor Bt and Ms (< 5 vol%), forming small flakes up to 0.3 mm in size, and anhedral grains of yellowish Ep.

3.2. Whole-rock major and trace element compositions of the principal rock types

3.2.1. Aydaly Complex

On the Ab-An-Or ternary diagram, the amphibole-bearing orthogneisses of the Aydaly Complex correspond to tonalites, whilst the quartz-feldspar orthogneisses fall into the granitic field (Fig. 6a). The moderately ferroan tonalite corresponds to a calcic-alkalic series and displays a low ASI of 0.76, consistent with a metaluminous series (Table 2; Fig. 6d–f). On the chondrite-normalised diagram, the

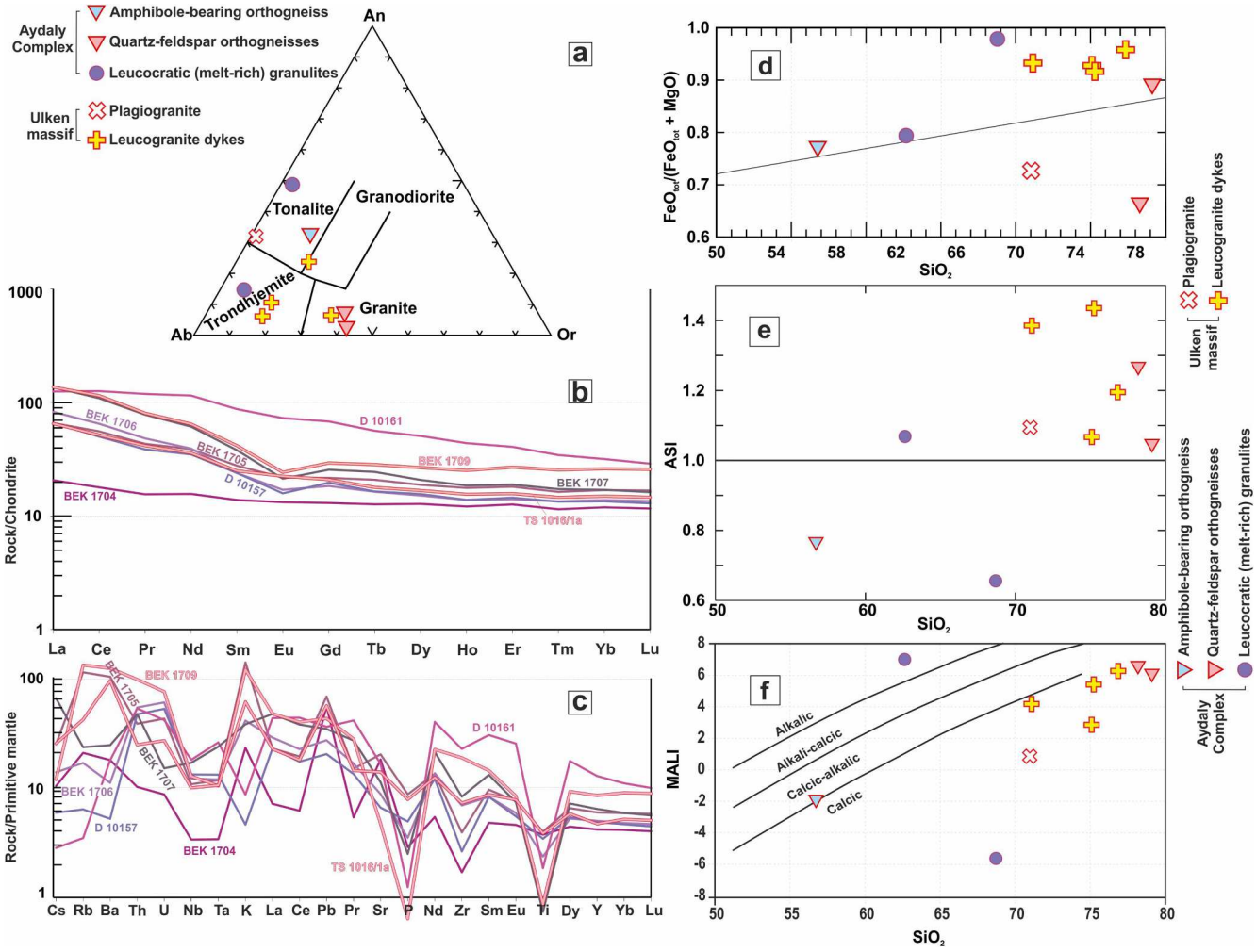

Fig. 6. a) Ab-An-Or classification of the Aydaly Complex and Ulken massif granitoids (Barker, 1979); b – c) chondrite- and primitive mantle- normalised patterns for the Aydaly Complex rock types; d – f) variation diagrams for the Aydaly Complex and Ulken massif granitoids: d) $FeO_{tot}/(FeO_{tot} + MgO)$ vs. SiO_2 plot (Frost et al., 2001); e) ASI (aluminum saturation index) vs. SiO_2 plot (Frost and Frost, 2011); f) MALI (modified alkali lime index) vs. SiO_2 plot (Frost et al., 2001).

amphibole-bearing orthogneiss demonstrates a high content of rare earth elements (REE), with a moderate enrichment in light REEs (LREEs) relative to heavy REEs (HREEs) and lacks an Eu anomaly (Eu/Eu* 0.98) (Fig. 6b). These features are characteristic for early intrusive phases, in other words, primary melts that were not significantly affected by differentiation processes. The quartz-feldspar orthogneisses show lower Al_2O_3 contents, with a wide range of FeO_{tot} concentrations ($FeO_{tot}/(FeO_{tot} + MgO)$ 0.6–0.9), and correspond to a calcic series (SiO_2 = 78–79 wt%; ASI = 1.05–1.27; MALI = 6.06–6.61; Table 2, Fig. 6d–f). An enrichment of the quartz-feldspar orthogneisses in LREEs $((La/Yb)_n$ 4.9), along with the presence of a prominent negative Eu anomaly (Eu/Eu* 0.69) and a leucocratic modal composition could indicate its formation from the differentiated granitoid melts of the later phases. Furthermore, in comparison to the amphibole-bearing orthogneisses, the observed LREEs enrichment, negative Eu anomaly, and high Rb/Sr ratio (0.84) in the quartz-feldspar orthogneisses may have resulted from fractionation of the feldspars, whereas the higher HREE content could reflect the final stages of crystallisation with the formation of accessory minerals (e.g. allanite, zircon). The orthogneisses of the Aydaly Complex display generally similar trace element distribution patterns (e.g. a depletion in Nb and Ta, and an enrichment in large-ion lithophile elements (LILEs), Zr, and Y; Fig. 6c), indicating that the protoliths may be derived from the evolution of a single melt, with the amphibole-bearing and quartz-feldspar orthogneiss protoliths corresponding to earlier and later intrusive phases, respectively. According to the 'Rb vs. Y + Nb' and 'Rb vs. Yb + Ta' diagrams (Pearce et al., 1984), the orthogneisses correspond to volcanic arc granites (Fig. S3c–d), and the rocks fall into the field of I-, S- and M-type granites (Fig. S3e–g) on the discriminative diagrams of Whalen et al. (1987).

The whole-rock major and trace element compositions of selected granulites of the Aydaly Complex are provided in Table 2. These rocks display wide ranges of major components, reflecting progressive partial melting and the consequent segregation of mineral assemblages with different chemical compositions and grain sizes. Given that the melanocratic residual granulites contain a number of detrital zircons (Section 3.4.1), their protolith is thought to have been a series of sedimentary rocks. Following from this interpretation, the sample that was least affected by anatexis, i.e. the amphibolite–amphibole-rich granulite BEK 1704, which preserves metamorphic layering and inferred pre-anatexis minerals, can be plotted in the Th-La-Sc diagram of Cullers (1994) for sedimentary rocks. This rock type falls into the metabasic source field, and more particularly amphibolite (Fig. 7a), indicating a formation at the expense of sedimentary rocks of predominantly mafic compositions. This interpretation is also confirmed by the ratios of La/Sc (0.13), Th/Sc (0.02), La/Co (0.13) and Th/Co (0.02), which cover a range of compositions corresponding to those resulting from the erosion of mafic rocks (Cullers, 2000). On the diagram of Herron (1988), the amphibolite–amphibolite-rich granulite falls into the field of iron-rich shales (Fig. S3a). This rock type is therefore characterised by a low chemical index of alteration (CIA) of

Table 2
Selected chemical analyses of the rock types of the Aydaly, Shukyr Complexes and Ulken massif. Major elements are in wt.%, trace elements are in ppm. $FeO_{(tot)} = 0.9Fe_2O_3 + FeO$; n.d. is 'not determined'; LOI is 'loss on ignition'; MALI is 'modified alkali-lime index' = $Na_2O + K_2O$-CaO (Frost et al., 2001); ASI is 'aluminum saturation index' = Al/(Ca − 1.67P + Na + K) (Frost and Frost, 2011); CIA is 'chemical index of alteration' = $Al_2O_3/(Al_2O_3 + CaO + Na_2O + K_2O)$*100 (Nesbitt and Young, 1982, 1984; Taylor and McLennan, 1985).

	Aydaly Complex									Shukyr Complex	
	Granulites						Orthogneisses				
	Amphibole-rich	Mesocratic		Melanocratic (clinopyr-oxene-rich)	Leucocratic (melt-rich)		Mesocratic amphibole-bearing	Leucocratic quartz-feldspar		Garnet-biotite schists	
	BEK 1704	BEK 1705	BEK 1706	D 10157	D 10161	BEK 1707	TS 1016/1a	BEK 1709	TS 1016	P 1062/1	P 1062/4
SiO_2	46.88	55.95	61.36	54.13	68.72	62.63	56.73	79.09	78.18	57.15	57.30
TiO_2	0.81	0.86	0.51	0.74	0.40	0.16	0.83	0.19	0.08	1.07	1.15
$Al2O_3$	15.03	15.96	10.65	6.71	12.98	22.59	17.75	11.36	12.53	21.36	20.43
FeO	4.89	2.42	1.96		0.40	0.13	4.00	0.13	0.20	4.64	5.30
Fe_2O_3	5.12	4.57	3.12		5.78	0.89	3.36	0.96	0.87	0.14	0.39
MnO	0.15	0.08	0.15	0.17	0.09	0.03	0.14	0.02	0.01	0.09	0.12
MgO	6.07	2.70	4.30	9.02	0.12	0.23	2.08	0.12	0.50	3.77	4.30
CaO	16.20	9.04	15.32	19.26	8.44	3.04	7.98	0.84	0.32	0.40	0.66
K_2O	0.69	2.89	0.36	0.14	0.26	1.14	1.82	3.31	3.67	5.31	4.07
Na_2O	2.51	4.17	1.23	1.14	2.55	8.78	4.28	3.59	3.26	1.06	1.23
P_2O_5	0.06	0.19	0.08	0.11	0.03	0.05	0.17	0.01	0.02	0.13	0.14
LOI	1.03	0.65	0.42	1.21	0.18	0.20	0.47	0.20	0.38	4.36	4.33
Total	99.43	99.49	99.45	99.08	99.94	99.87	99.61	99.81	100.01	99.48	99.42
FeO_{tot}	9.49	6.53	4.77	6.45	5.60	0.93	7.03	0.99	0.98	4.77	5.65
CIA	43.66									75.93	77.42
$\log(FeO_{tot}/K_2O)$	1.14									−0.05	0.14
$\log(SiO_2/Al_2O_3)$	0.49									0.43	0.45
K_2O/Na_2O					0.10	0.13	0.43	1.08	1.13		
MALI					−5.63	6.88	−1.88	6.06	6.61		
ASI					0.66	1.07	0.76	1.05	1.27		
$FeO_{tot}/(FeO_{tot} + MgO)$	0.61	0.71	0.53	0.42	0.98	0.80	0.77	0.89	0.66	0.56	0.57
$MgO/(FeO_{tot} + MgO)$	0.39	0.29	0.47	0.58	0.02	0.20	0.23	0.11	0.34	0.44	0.43
Li	9.2	9.1	8.8	13.7	0.7	1.4	7.0	3.3	–	15.2	18.1
Be	0.8	0.9	1.9	2.2	0.8	1.1	0.9	1.5	–	5.4	6.7
Sc	38.1	22.2	22.5	25.3	18.7	2.8	20.8	5.6	–	14.2	11.1
V	248.8	198.3	100.7	106.0	20.5	19.2	160.4	6.8	–	202.9	178.0
Cr	162.8	19.5	72.2	104.9	4.8	13.1	18.3	10.4	–	124.3	132.4
Co	36.6	24.9	16.5	22.4	1.2	1.1	18.8	1.1	–	22.0	27.0
Ni	84.7	44.1	55.3	72.3	13.9	9.8	42.9	5.7	–	53.7	65.9
Cu	56.1	105.1	4.2	11.0	3.1	2.4	5.1	3.1	–	9.0	26.9
Zn	71.9	60.8	101.9	108.8	21.1	8.2	77.6	11.6	–	115.3	108.3
Ga	13.8	14.7	12.1	8.3	13.4	15.0	16.2	11.8	–	30.5	30.3
As	n.d.	0.3	1.6	1.5	n.d.	0.1	0.4	0.4	–	1.1	3.3
Rb	13.2	71.4	10.6	4.0	2.2	14.8	26.5	83.1	–	28.6	27.2
Sr	380.4	424.1	184.2	138.7	346.6	235.8	292.5	98.7	–	81.0	75.4
Y	18.9	27.0	22.7	22.1	58.0	29.1	21.3	38.7	–	12.3	12.9
Zr	19.0	43.7	77.2	29.3	252.5	92.8	81.0	209.6	–	151.6	131.5
Nb	2.4	7.7	8.6	9.4	12.8	12.0	7.1	9.1	–	18.4	18.9
Mo	0.3	1.1	1.0	1.4	0.4	0.4	0.3	0.4	–	0.8	1.0
Cs	0.3	0.8	0.4	0.2	0.1	2.1	0.8	0.4	–	2.3	1.8
Ba	124.5	713.9	77.4	36.3	124.1	170.2	657.6	854.5	–	755.8	662.4
La	4.9	15.6	19.6	15.7	29.6	32.3	15.4	32.4	–	25.8	18.3
Ce	10.9	34.1	39.8	30.6	77.0	66.7	31.7	70.3	–	60.3	45.0
Pr	1.5	4.1	4.6	3.7	11.3	7.4	3.9	7.6	–	6.7	4.8

(*continued on next page*)

Table 2 (*continued*)

	Aydaly Complex									Shukyr Complex	
	Granulites						Orthogneisses				
	Amphibole-rich	Mesocratic		Melanocratic (clinopyr-oxene-rich)	Leucocratic (melt-rich)		Mesocratic amphibole-bearing	Leucocratic quartz-feldspar		Garnet-biotite schists	
	BEK 1704	BEK 1705	BEK 1706	D 10157	D 10161	BEK 1707	TS 1016/1a	BEK 1709	TS 1016	P 1062/1	P 1062/4
Nd	7.3	18.1	18.3	16.3	53.7	28.6	16.8	30.1	–	25.7	18.7
Sm	2.1	4.3	3.7	3.7	13.4	5.8	3.8	6.4	–	4.6	3.7
Eu	0.8	1.3	1.0	0.9	4.2	1.2	1.3	1.4	–	1.0	1.0
Gd	2.7	4.5	3.8	4.0	14.0	5.3	4.3	6.0	–	3.3	3.0
Tb	0.5	0.8	0.6	0.6	2.1	0.9	0.7	1.1	–	0.5	0.5
Dy	3.2	4.8	3.8	4.0	12.9	5.3	4.3	6.8	–	2.6	2.7
Ho	0.7	1.0	0.8	0.8	2.5	1.1	0.9	1.4	–	0.5	0.5
Er	2.1	3.0	2.3	2.4	6.7	3.1	2.6	4.5	–	1.5	1.7
Tm	0.3	0.4	0.3	0.3	0.9	0.4	0.4	0.7	–	0.2	0.2
Yb	2.0	2.9	2.3	2.3	5.4	2.9	2.5	4.4	–	1.7	1.7
Lu	0.3	0.4	0.3	0.3	0.7	0.4	0.4	0.7	–	0.3	0.3
Hf	0.8	1.7	2.2	1.1	5.6	2.7	2.5	5.7	–	4.2	3.8
Ta	0.1	0.5	0.5	0.5	1.1	1.0	0.4	0.4	–	1.4	1.4
W	0.5	0.4	1.1	0.8	0.3	0.1	0.3	0.1	–	1.7	2.6
Tl	0.1	0.4	0.0	0.0	0.0	0.1	0.1	0.4	–	0.5	0.5
Pb	10.2	12.5	5.0	3.7	6.6	6.3	10.3	7.9	–	8.4	9.1
Bi	0.2	0.1	0.3	0.2	0.0	0.0	0.2	n.d.	–	0.3	0.3
Th	0.9	3.2	4.6	4.0	4.5	4.0	2.1	8.2	–	16.9	9.3
U	0.2	0.9	1.3	1.1	0.9	0.3	0.6	1.6	–	1.1	1.1
ΣREE	39.3	95.2	101.3	85.6	234.4	161.4	89.0	173.7		134.7	102.1

	Shukyr Complex Garnet-biotite schists					Ulken massif Leucogabbro	Plagiogranite	Leucogranite dykes			
	P 1062/2	TS 1019/b	TS 1019/3	TS 1019/a	TS 1019/1	P 1059/1	BEK 1708	P 1059/2	TS 1018	TS 1019/2	D 10171
SiO_2	55.62	62.03	58.01	64.33	67.31	51.06	70.97	71.09	76.86	75.23	75.09
TiO_2	1.07	0.95	1.09	0.85	0.79	1.00	0.03	0.04	0.14	0.08	0.07
$Al2O_3$	22.10	18.92	20.97	17.37	15.67	17.74	18.41	13.41	13.18	15.04	14.55
FeO	5.18	4.05	4.50	3.98	3.13	4.92	0.13	0.20	0.11	0.14	0.40
Fe_2O_3	0.13	0.83	0.13	0.97	1.94	4.27	0.19	0.80	1.62	1.49	0.71
MnO	0.09	0.10	0.08	0.08	0.08	0.18	0.01	0.01	0.01	0.02	0.03
MgO	4.19	2.78	3.19	2.54	2.60	3.16	0.11	0.07	0.03	0.14	0.08
CaO	0.83	0.75	0.45	0.90	0.68	5.86	4.48	1.03	0.76	0.70	2.93
K_2O	3.64	4.52	5.76	4.44	3.56	0.73	0.17	1.33	3.37	1.47	2.06
Na_2O	1.33	1.37	1.02	1.25	1.28	5.99	5.17	3.88	3.67	4.65	3.73
P_2O_5	0.13	0.15	0.15	0.15	0.15	0.16	0.01	0.01	0.02	0.03	0.05
LOI	5.11	3.12	4.14	2.69	2.75	4.37	0.20	8.12	0.22	0.98	0.42
Total	99.42	99.56	99.49	99.55	99.94	99.45	99.89	99.98	99.98	99.98	100.11
FeO_{tot}	5.30	4.80	4.62	4.85	4.88	8.76	0.30	0.92	1.57	1.48	1.04
CIA	79.21	74.02	74.36	72.50	73.95						
$\log(FeO_{tot}/K_2O)$	0.16	0.03	−0.10	0.04	0.14						
$\log(SiO_2/Al_2O_3)$	0.40	0.52	0.44	0.57	0.63						
K_2O/Na_2O						0.12	0.03	0.34	0.92	0.32	0.55
MALI						0.86	0.86	4.18	6.28	5.42	2.86
ASI						0.84	1.09	1.39	1.19	1.44	1.07
$FeO_{tot}/(FeO_{tot} + MgO)$	0.56	0.63	0.59	0.66	0.65	0.74	0.72	0.93	0.98	0.91	0.93

(*continued on next page*)

Table 2 (*continued*)

	Shukyr Complex Garnet-biotite schists					Ulken massif Leucogabbro	Plagiogranite	Leucogranite dykes			
	P 1062/2	TS 1019/b	TS 1019/3	TS 1019/a	TS 1019/1	P 1059/1	BEK 1708	P 1059/2	TS 1018	TS 1019/2	D 10171
$MgO/(FeO_{tot} + MgO)$	0.44	0.37	0.41	0.34	0.35	0.26	0.28	0.07	0.02	0.09	0.07
Li	23.9	22.7	23.9	12.5	25.9	16.3	1.1	1.9	1.3	9.6	–
Be	6.3	4.3	5.1	3.5	3.3	0.9	4.5	1.3	1.5	1.7	–
Sc	22.0	17.6	14.4	15.4	13.7	20.8	1.0	0.6	1.8	1.3	–
V	224.7	91.3	132.6	101.0	88.6	128.8	6.6	6.2	13.7	10.3	–
Cr	138.9	106.6	90.2	79.6	59.9	12.2	14.5	7.5	n.d.	4.1	–
Co	22.0	21.2	23.1	17.1	13.7	20.9	0.9	0.5	0.5	1.9	–
Ni	53.3	52.5	44.7	36.7	33.8	18.1	8.8	4.7	5.4	4.2	–
Cu	15.3	49.9	43.9	24.8	43.2	8.6	1.8	0.6	4.6	2.3	–
Zn	135.7	79.8	109.4	85.5	80.4	79.2	n.d.	5.0	18.2	14.0	–
Ga	33.6	25.4	29.0	23.4	19.9	12.1	16.1	7.4	11.3	14.8	–
As	4.4	2.4	5.3	3.5	2.2	1.9	n.d.	1.1	2.2	0.3	–
Rb	33.5	83.8	35.9	175.0	93.3	16.1	2.0	28.0	71.6	36.3	–
Sr	76.7	116.3	56.0	90.4	83.4	187.5	655.0	189.7	40.7	174.7	–
Y	10.0	33.0	23.0	29.7	22.2	9.8	7.7	3.5	8.3	7.0	–
Zr	118.9	165.6	154.2	151.0	153.5	33.2	32.8	15.3	205.9	49.4	–
Nb	20.2	16.7	18.2	15.3	12.2	8.2	2.0	0.9	10.6	4.7	–
Mo	0.9	0.8	0.8	0.6	0.6	0.2	0.2	0.1	0.3	0.2	–
Cs	2.2	3.9	3.4	5.8	2.0	0.3	0.1	1.0	0.6	1.0	–
Ba	858.4	788.2	644.4	681.0	560.3	165.7	177.0	570.7	747.4	454.3	–
La	17.4	39.0	39.6	45.1	30.6	6.9	3.5	4.4	13.9	5.0	–
Ce	43.8	74.4	80.9	87.3	57.3	15.7	10.0	7.3	35.2	8.3	–
Pr	4.8	8.5	9.2	9.7	6.9	1.9	0.9	0.6	3.5	1.1	–
Nd	18.5	32.0	35.3	37.0	26.4	8.3	3.9	2.0	13.4	4.4	–
Sm	3.2	6.5	7.1	7.2	5.2	2.0	0.9	0.4	2.6	1.0	–
Eu	1.1	1.4	1.1	1.3	1.1	0.7	0.2	0.3	0.4	0.3	–
Gd	2.2	5.8	5.9	6.3	4.4	2.2	0.9	0.5	2.1	1.0	–
Tb	0.3	1.0	0.9	1.0	0.7	0.3	0.2	0.1	0.3	0.2	–
Dy	2.0	5.8	4.8	5.5	4.1	2.1	1.1	0.6	1.6	1.1	–
Ho	0.4	1.2	0.9	1.0	0.8	0.4	0.2	0.1	0.3	0.2	–
Er	1.4	3.5	2.5	3.1	2.5	1.3	0.8	0.5	1.0	0.8	–
Tm	0.2	0.5	0.3	0.4	0.4	0.2	0.1	0.1	0.2	0.1	–
Yb	1.6	3.3	2.2	2.8	2.4	1.3	0.9	0.7	1.2	0.8	–
Lu	0.3	0.5	0.3	0.4	0.4	0.2	0.1	0.1	0.2	0.1	–
Hf	3.4	4.6	4.3	4.3	4.2	1.0	1.4	0.7	5.0	2.0	–
Ta	1.4	1.2	1.2	1.2	0.9	0.5	0.2	0.1	0.6	0.4	–
W	0.9	0.8	0.8	1.5	0.7	1.2	0.1	0.4	0.1	0.5	–
Tl	0.4	0.5	0.8	0.8	0.4	0.1	0.0	0.1	0.3	0.2	–
Pb	14.1	21.5	9.2	15.7	17.0	2.8	9.2	4.5	11.5	6.4	–
Bi	0.2	0.3	0.2	0.4	0.2	0.0	0.0	0.0	0.0	0.0	–
Th	16.7	23.1	22.4	20.0	19.2	0.8	3.6	4.1	3.3	2.4	–
U	1.0	2.6	1.7	3.1	2.3	0.5	0.5	0.4	0.6	0.7	–
ΣREE	97.3	183.3	190.8	208.1	143.0	43.5	23.7	17.6	76.1	24.5	–

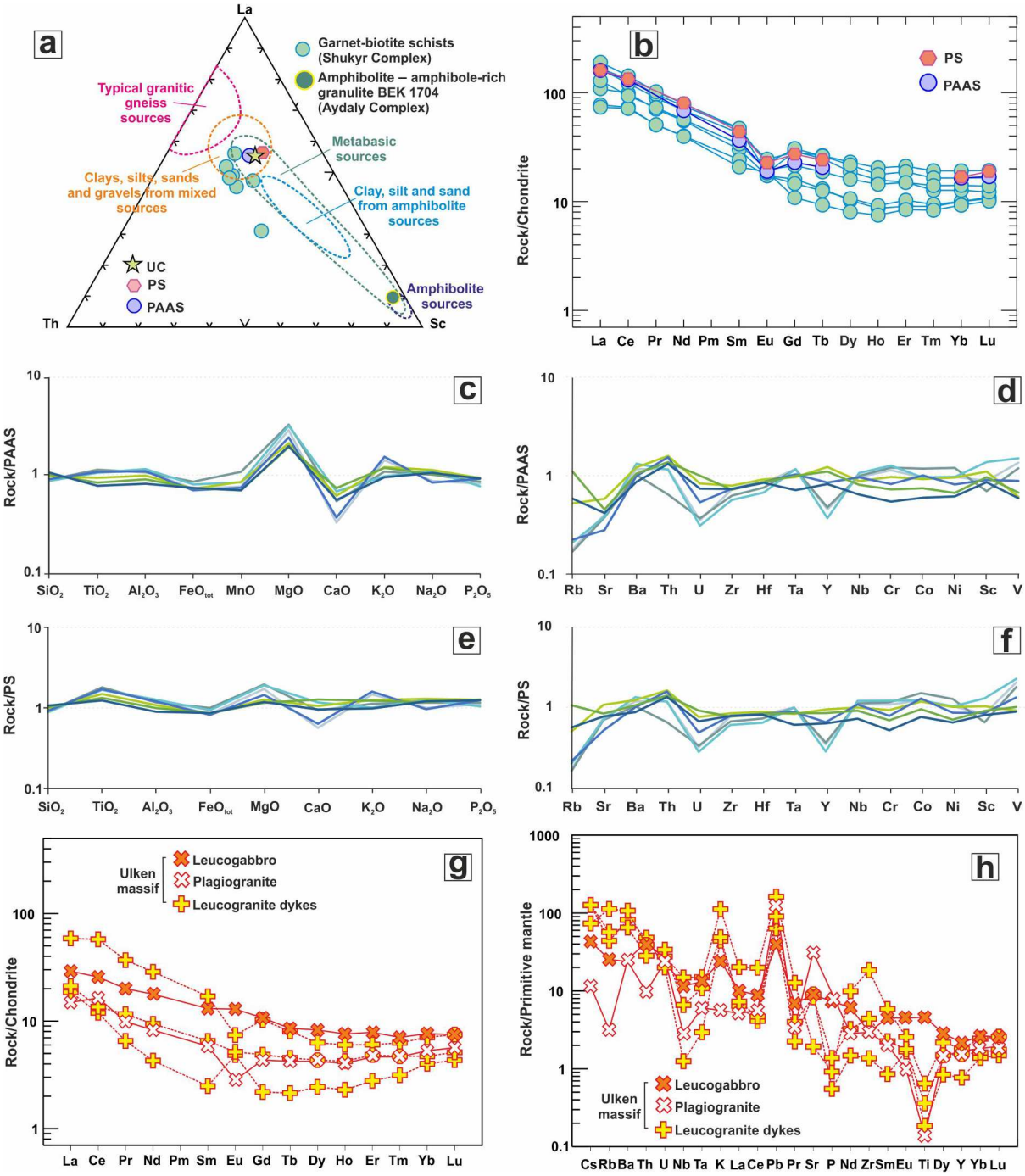

Fig. 7. a) La–Th–Sc ternary diagram for the metasedimentary rocks of the Aydaly and Shukyr Complexes (Cullers, 1994); b) chondrite-normalised patterns for the garnet-biotite schists of the Shukyr Complex; c – d) PAAS-normalised patterns for the garnet-biotite schists of the Shukyr Complex (major and trace elements); e – f) PS-normalised patterns for the garnet-biotite schists of the Shukyr Complex (major and trace elements); g – h) chondrite- and primitive mantle- normalised patterns for the Ulken massif rock types. Chondrite and primitive mantle values are from Sun and McDonough (1989). PS – Proterozoic Shale (Condie, 1993), PAAS – Post-Archaean Australian Shale, UC – Upper Crust (Taylor and McLennan, 1985).

43.7, which is common for poorly eroded igneous rocks. Moreover, the observed SiO_2, MgO, FeO_{tot} and Al_2O_3 contents are typical for basalts. On the chondrite-normalised plot, the amphibolite–amphibole-rich granulite shows a slightly differentiated spectrum of REE distribution ($(La/Yb)_n$ = 1.6) and an absence of Eu anomaly (Eu/Eu* = 0.99) (Fig. 6b), which is consistent with E-MORB basalts.

The mesocratic, residuum- and melt-rich granulites represent a neosome with conspicuous magmatic structures, therefore these should not be considered as metasedimentary complexes, but rather correspond to newly formed igneous rocks. With regards to the major components, the observed granulites display a general increase in SiO_2 and Al_2O_3 and a decrease in MgO and TiO_2 from the mesocratic to the melt-rich varieties (Table 2). The trace element concentrations show similar tendencies of increasing total REE and Zr and decreasing Co, Sc and V from the mesocratic to the melt-rich varieties (Table 2). Moreover, all the granulites possess higher total contents of REE, LILE and Zr with Y compared to the amphibolite–amphibole-rich granulite (Fig. 6b–c). On the chondrite-normalised diagram, the studied granulites are characterised by mostly similar REE distribution patterns with the exception of the melt-rich granulite D 10161 (Fig. 6b). The

granulites are enriched in LREEs relative to HREEs and show obvious negative Eu anomalies (Eu/Eu* in the range 0.68–0.89). The melt-rich granulite D 10161 contains the largest amounts of andradite-grossular garnet and epidote (Fig. S2), which are thought to have been formed during the overprinting processes. Hence, the observed enrichment of the rock type in REE might be related to an interaction with metasomatic fluids. In addition, the studied granulites display negative Ti, Nb, and P anomalies with an enrichment in Y, Th, U on the PM-normalised plot, whilst Zr anomalies tend to show a progressive character in terms of the rock type (Fig. 6c). The melt-rich granulites fall into the tonalite and trondhjemite fields on the Ab-An-Or diagram (Fig. 6a) and correspond to a slightly peraluminous (ASI = 1.07) and alkalic series with a moderate $FeO_{tot}/(FeO_{tot} + MgO)$ ratio of 0.80, and a metaluminous (ASI = 0.66) and calcic series with a high $FeO_{tot}/(FeO_{tot} + MgO)$ ratio of 0.98 (Table 2, Fig. 6d–f). The observed differences in the compositions of the melt-rich granulites, particularly with respect to the unusually high Al_2O_3 (22.6 wt%) and Na_2O (8.8 wt%) contents in sample BEK 1707 (Table 2), may reflect processes related to the diffusional interaction of the pre-existing amphibolite with the granitoid melt, producing local zones of hybrid granitoids enriched in alumina and alkalis (e.g. Skjerlie & Patino Douce, 1995; Khodorevskaya, 2002). On the 'Rb vs. Y + Nb' and 'Rb vs. Yb + Ta' diagrams (Pearce et al., 1984), the melt-rich variety D 10161 plots in the field of volcanic arc granites (Fig. S3c–d), and the rock type corresponds to I-, S- and M-type granites (Fig. S3e–g) on the diagrams of Whalen et al. (1987). It should be noted that the geochemical signatures of the granulites (in particular the melt-rich varieties) are generally similar to those observed in the orthogneisses, which together with the granulites comprise the Aydaly Complex.

3.2.2. Shukyr Complex

The mineral compositions of the garnet-biotite schists indicate that they are derived from sedimentary rocks, which correspond to shales (Fig. S3a) according to the diagram of Herron (1988). The schists have CIA values in the range of 70–80, reflecting moderate extents of weathering of the protolith (Nesbitt and Young, 1982). Based on the Th/Sc vs. Zr/Sc diagram (McLennan et al., 1993; Fig. S3b), the protoliths of the observed formations were not significantly enriched in heavy minerals during clastic transportation. Hence, the chemical compositions of the protoliths of the garnet-biotite schists were controlled by the compositions of the original source rocks. On the PS- and PAAS-normalised plots, the schists display slightly increased TiO_2, MgO and K_2O contents, and lower CaO and Na_2O contents (Fig. 7c–e). The trace element distributions of the garnet-biotite schists are generally consistent with those of the PS and PAAS, with the exception of a prominent depletion in Rb, Sr, U, and somewhat in Y, and an enrichment in Th, Co, V, Ni and Sc (Fig. 7d–f).

On the chondrite-normalised diagram, the schists display differentiated spectra of REE distributions with a prominent LREE enrichment relative to HREE ($(La/Yb)_n$ = 7.5–12.5), virtually flat patterns of HREE ($(Gd/Yb)_n$ = 1.2–2.3) and a wide range of Eu anomalies (Eu/Eu* = 0.50–1.24; Fig. 7b, Table 2). Thus, the observed patterns are generally similar to those of the PS and PAAS, however the total REE content of the schists is lower compared to the PS and PAAS. The range of Eu/Eu* anomalies from negative to positive values may be related to the presence of both felsic and basic rocks in the source. The latter are thought to be essential in the source due to the high contents of TiO_2, MgO, Co, Ni, Sc and V compared to the PS and PAAS, which is characteristic for basic rocks. In addition, the increased contents of K_2O and Th in the schists in comparison to the PS and PAAS are indicative of the presence of felsic rocks in the source. This is also confirmed by the low Cr/Th ratios in the garnet-biotite schists (varying in the range 3.1–14.2), consistent with the erosive products of felsic rocks (Cullers, 2000). Other indicative ratios such as La/Sc (0.8–2.9), Th/Sc (0.8–1.6), La/Co (0.8–2.6) and Th/Co (0.3–1.4) also indicate a mixed source (Fig. 7a) (Cullers, 1994; Cullers, 2000).

3.2.3. Zhuantobe Complex

The basic volcanics of the Zhuantobe Complex include basalts with high TiO_2 contents (1.9–3.15 wt%) and a $FeO_{tot}/(FeO_{tot} + MgO)$ ratio in the range of 0.6–0.85, corresponding to a tholeiitic series (Table S1, Fig. S4). In addition, the felsic volcanic rocks are rhyolites with a K_2O/Na_2O ratio of 1.32–1.62, corresponding to a calcic series (the MALI varies from 1.57 to 3.84) with a moderate to high $FeO_{tot}/(FeO_{tot} + MgO)$ ratio of 0.61–0.88 (Table S1, Fig. S4).

3.2.4. Ulken massif

According to the Ab-An-Or diagram, the observed plagiogranite is consistent with tonalite (Fig. 6a) and shows high Al_2O_3 contents (ASI = 1.09) with a $FeO_{(tot)}/(FeO_{(tot)} + MgO)$ ratio of 0.72, and corresponds to a calcic series (Fig. 6d–f, Table 2). The leucogabbro is more enriched in total REE content compared to the plagiogranite and demonstrates a smooth positive Eu anomaly on the chondrite-normalised plot (Eu/Eu* = 1.07), whereas the plagiogranite is considerably more depleted in REE with a clear negative Eu anomaly (Eu/Eu* = 0.56, Fig. 7g–h). This may reflect an evolution of crystallisation, assuming that the plagiogranite formed from highly differentiated melts.

The leucogranitic dykes predominantly fall into the fields of trondhjemites and granites on the Ab-An-Or diagram (Fig. 6a). The granitoids are characterised by high Al_2O_3 contents (the ASI varies in the range of 1.07–1.44) and show a wide range of K_2O/Na_2O ratios from 0.32 to 0.92. These rocks correspond to a calcic series with a high $FeO_{(tot)}/(FeO_{(tot)} + MgO)$ ratio of 0.91–0.98 (Fig. 6d–f, Table 2). Furthermore, the granitoids display variable REE total contents with Eu anomalies ranging from negative (Eu/Eu* = 0.56–0.88) to positive (Eu/Eu* = 2.08) (Fig. 7g). On the PM-normalised diagram, the granitoids show mostly similar elemental distribution patterns, characterised by a general depletion in Nb, P, and Ti and an enrichment in LILEs (e.g. K, Cs, Rb, Ba, Sr) and High field strength elements (HFSE) (Zr, Hf) (Fig. 7h). The plagiogranite and leucogranites of the Ulken massif correspond to volcanic arc granites based on the 'Rb vs. Y + Nb' and 'Rb vs. Yb + Ta' diagrams (Pearce et al., 1984) (Fig. S3c–d), and to I-, S- and M-type granites (Fig. S3e–g) according to the diagrams of Whalen et al. (1987).

3.3. Metamorphism of the principal rock types

A major portion of the rocks in the NW part of the Chu Block have undergone various extents of metamorphic changes. We now describe the main features and stages of the metamorphic evolution of the rocks in the Aydaly and Shukyr Complexes, and partially for the Zhuantobe Complex.

3.3.1. Aydaly Complex

The rock type that has been the least affected by partial melting processes is the amphibolite–amphibole-rich granulite (Fig. 4A). This rock type shows clear micro-textural evidence of interactions with melt, but also generally preserves the metamorphic appearance of a common medium-grained amphibolite, indicating a low extent of anatexis (Sawyer, 2008). Taking into consideration the coexistence of Cpx with Amph in an assemblage without garnet, and presuming a low melt fraction in the rock type, a generalised P-T pseudosection can be constructed for sample BEK 1704 using the whole-rock composition (Fig. S5). The 'melt-in area' constrains the temperature to 700–800 °C at pressures of 6–9 kbar (Table S8) (Hammarstrom and Zen, 1986; Hollister et al., 1987; Johnson and Rutherford, 1989; Schmidt, 1992). The early stages of partial melting and interaction of the reactant amphiboles in the inferred mafic amphibolite with the haplogranitic melt may have occurred at these P-T conditions, along with an increase in Mg and Si in the amphiboles with increasing temperature. The consequent destruction of the pre-existing metamorphic lineation is related to the formation of the mesocratic granulites with minor preserved amphibole (Fig. 4B). The temperature limit for the mesocratic granulite

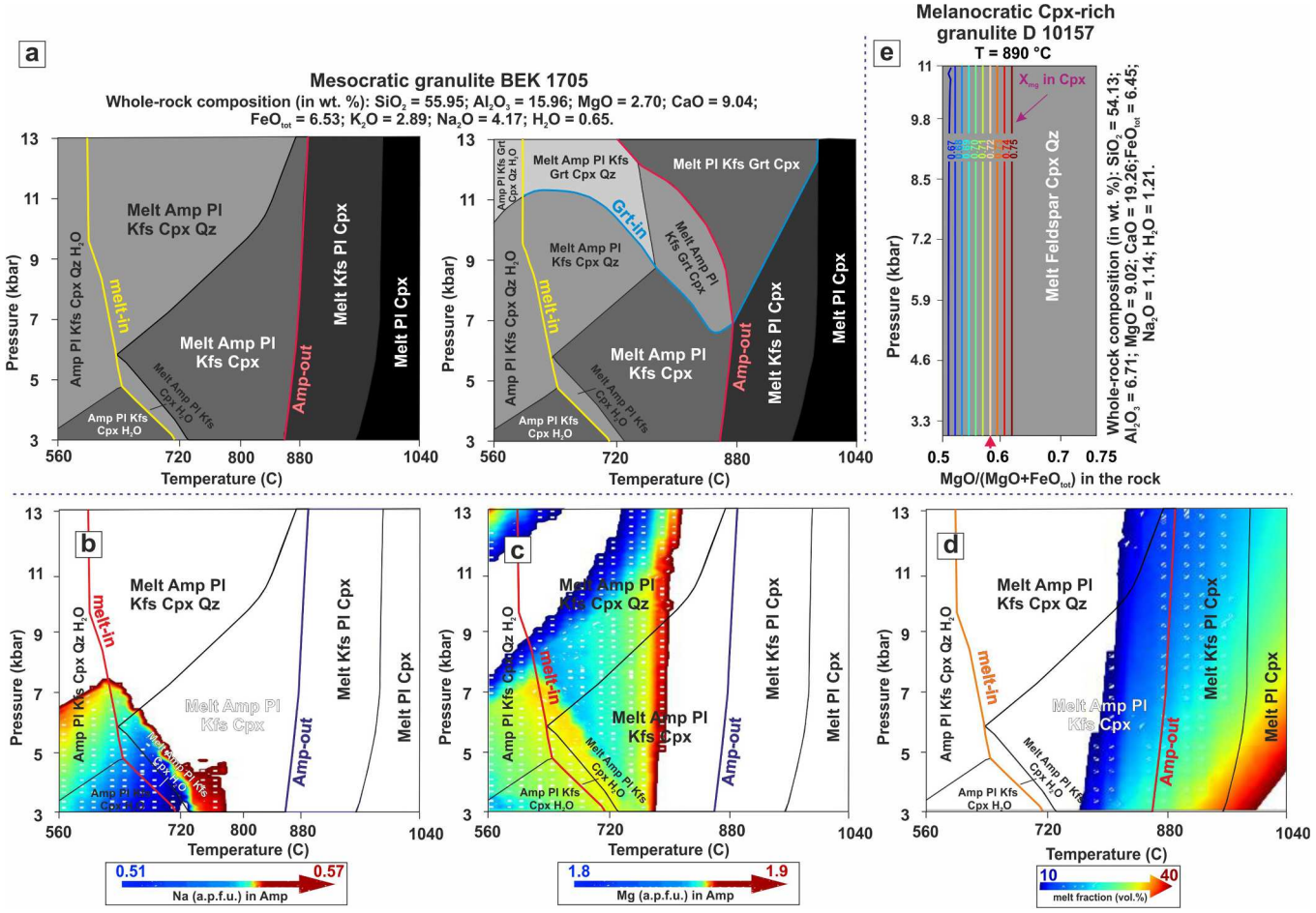

Fig. 8. a – d) P-T pseudosections for CFMNKASH system based upon the whole-rock composition for mesocratic granulite BEK 1705: a) pseudosections with the observed mineral assemblages without garnet (left) and with garnet introduced (right); b) compositional isopleths of Na (a.p.f.u.) in Amp; c) compositional isopleths of Mg (a.p.f.u.) in Amp; d) modal proportions of melt (in vol.%); e) P vs. $Mg/(Mg + Fe_{tot})$ pseudosection (T = 890 °C) for CFMNASH system based upon the whole-rock composition for melanocratic residual clinopyroxene-rich granulite D 10157 (colored lines are compositional isopleths of $Mg/(Mg + Fe_{tot})$ in Cpx (Table S4); red arrow corresponds to $MgO/(FeO_{tot} + MgO)$ of the sample D 10157 of 0.58 (Table 2)). Incorporated solution models and details of recalculations are provided in Appendix B. (For interpretation of the references to colour in this figure legend, the reader is referred to the web version of this article.)

BEK 1705 is marked by the complete disappearance of amphibole, which shows an increase in Mg and Si with increasing temperature (Fig. 8a–d), and the production of magnesian clinopyroxene at T ≈ 870 °C. According to experimental studies, a high-temperature reaction may have resulted from incongruent dehydration melting of the earlier amphibolite with clinopyroxene + melt production (Wyllie and Wolf, 1993), indicating *in situ* melting (i.e. migmatisation). Alternatively, this reaction may have resulted from the interaction of the initial amphibolite with overheated granitic melts, derived from the partial melting of the *external* source unrelated to the amphibolite, followed by the formation of a granulite facies assemblage of clinopyroxene + melt at T = 900 °C (Khodorevskaya, 2002). An absence of almandine-pyrope garnet among the resulting minerals implies a formation of the clinopyroxene-bearing granulites at moderate to low pressures of 7–9 kbar for T = 870–900 °C (Fig. 8a, Table S8), which is consistent with mid-crustal levels of 15–20 km. This is also supported by the observed segregation of the melanocratic residual clinopyroxene-rich (sample D 10157) and leucocratic melt-rich (samples D 10161, BEK 1707) granulites (Fig. 5), which is expected to occur at T greater than 900 °C according to experimental studies (Khodorevskaya, 2002). For the indicated whole-rock composition of the melanocratic granulite (sample D 10157) with an $MgO/(MgO + FeO_{tot})$ ratio of 0.58 (Table 2), the formation of the most magnesian clinopyroxene with a X_{mg} of 0.72–75 (Table S4) is consistent with a temperature of ~890 °C (Fig. 8e). In turn, a subsequent rimward decrease of X_{mg} in Cpx (Fig. 4D, from element mapping) along with pervasive epidote-clinozoisite growth is apparently related to overprinting retrograde and/or metasomatic processes. Similarly, late amphiboles and andradite-grossular garnet exist together in the associated leucocratic melt-rich granulites (Fig. 4C, S2), with widely-developed epidote-clinozoisite. All the granulites contain plagioclase with variable compositions from bytownite to almost pure albite (Fig. S1a, Table S2), reflecting an evolution of the rock types in response to progressive partial melting and crystallisation (Sawyer, 2008). To summarise, the granulites of the Aydaly Complex were evidently formed at moderate pressures of 6–9 kbar and high temperatures, gradually increasing from 700 to 900 °C or even slightly more, and followed the metamorphic succession of amphibolite–amphibole-rich granulite–mesocratic granulite–melanocratic (clinopyroxene-rich) and leucocratic (melt-rich) granulites. These rocks were subsequently affected by later overprinting processes.

The mineral assemblages of the amphibole-bearing and quartz-feldspar orthogneisses, which are structurally related with the granulites in the Aydaly Complex, are not representative for the purposes of constraining their formation conditions. Taking into account the mostly leucocratic mineral compositions of the orthogneisses, their structural and spatial proximity with the granulites, the similar U-Pb and $t_{Nd(DM)}$ model ages of the melt-rich granulites and the observed quartz-feldspar

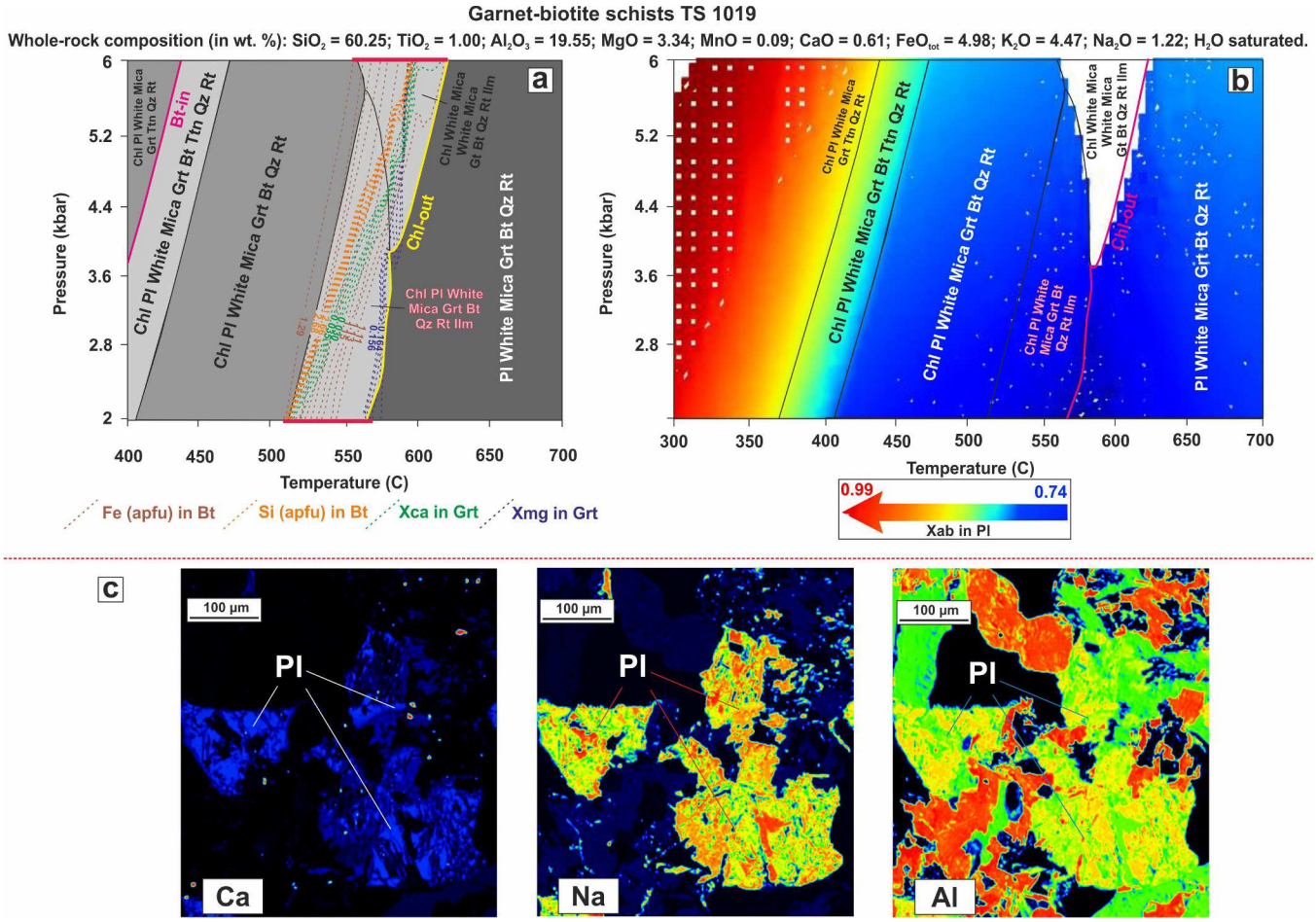

Fig. 9. a – b) P-T pseudosections for CFTiMMnNKASH system based upon the averaged whole-rock composition for the garnet-biotite schist TS 1019: a) P-T pseudosection with the compositional isopleths of X_{ca} with X_{mg} in garnet (Table S7) and Si (a.p.f.u.) with Fe (a.p.f.u.) in biotite (Table S9); b) X_{ab} in plagioclase (Table S2) compositional isopleths; c) X-ray element mapping (Ca, Na, Al) displaying replacement of andesine by sodic plagioclase with sericite.

orthogneisses (considered below), these rocks could be interpreted as melt-rich leucosomes, formed after partial melting of the unknown crustal source. However, any direct petrological evidence of their anterior existence has been obscured.

3.3.2. Shukyr Complex

The garnet-biotite schists of the Shukyr Complex are spatially associated with the contact with the granitoids of the Ulken massif (Fig. 2B). The mineralogy and chemical compositions of the schists indicate a metasedimentary origin after shales (Fig. S3a). The rocks are characterised by generally similar whole-rock compositions, therefore an averaged composition was introduced for the purposes of pseudosection modelling to constrain their metamorphic evolution. Fig. 9a shows the compositional isopleths of garnet (X_{ca} and X_{mg}) and biotite (Fe and Si, in a.p.f.u), which do not display any zoning features and fall into a multivariate field covering the temperature range from 510 to 600 °C for a wide pressure interval, where biotite and chlorite are stable and plagioclase displays the lowest X_{ab} contents (Fig. 9b). Applying the conventional Grt-Bt geothermometers of Perchuk and Lavrent'eva (1983) or Goldman and Albee (1977) gave slightly higher temperatures of 650–680 °C and 600–650 °C, respectively. In summary, an average temperature peak for the garnet-biotite schists could be estimated around ~580–630 °C. The later retrograde metamorphic alterations are linked with an increase of X_{ab} in Pl and the replacement of biotite with plagioclase by sericite and chlorite, reflecting cooling processes (Fig. 9b–c). Taking into consideration the near complete absence of chemical zoning in garnet and biotite in the schists, which is characteristic for metamorphic metapelites, as well as the spatial proximity of the rocks with the granitoids of the Ulken massif, the garnet-biotite schists may represent moderate-temperature contact hornfels, which were deformed by later tectonic events, resulting in the appearance of the metamorphic schistose micro-textures.

3.3.3. Zhuantobe Complex

The mineral paragenesis and micro-textural features of the observed amphibole (optically actinolite) and the epidote-bearing schists or epidosites of the Zhuantobe Complex, which have been referred to as metatuffs, indicate a formation under low-grade conditions of the greenschist or lower epidote–amphibolite facies, where temperature played a key role in the appearance of the metamorphic alterations.

3.4. U-Pb geochronology and Sm-Nd whole-rock isotopic systematics

3.4.1. Aydaly Complex

The zircons from the quartz-feldspar orthogneiss (sample BEK 1709) are euhedral, prismatic, transparent or semi-transparent and pale-yellow. The grain sizes range from 40 to 300 µm, with a common length/width ratio of 1.5–3.0. Most of the grains consist of bright, weakly-zoned cores, in some cases fractured, and are characterised by the presence of prominent homogeneous dark rims in cathodoluminescence (CL) (Fig. 10). The rims, as well as cloudy structures observed in some cores, may be related to metamorphic or metasomatic reworking. We studied 28 zircon grains in total, and the cores and rims were both analysed where possible. The average of twelve core analyses

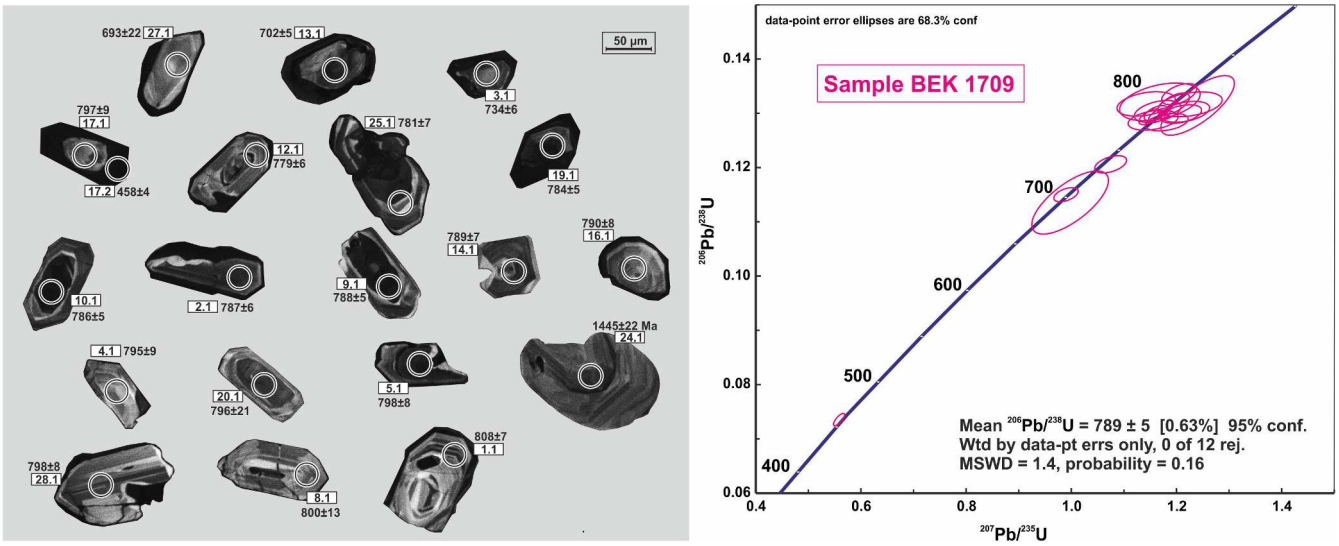

Fig. 10. Cathodoluminescence (CL) photographs of zircon grains (left) from the quartz-feldspar orthogneiss BEK 1709 (the circles are SHRIMP analytical spots; the numbers in the squares are in accordance with Table 3) and U-Pb concordia diagram (right) with the U-Pb isotope data of the analysed zircons (SHRIMP II).

gave a result of 789 ± 5 Ma (MSWD = 1.4) (Fig. 10). One inherited core analysis yielded a $^{207}Pb/^{206}Pb$ age of 1445 Ma (Table 3). The CL-dark rims of the studied zircons are characterised by relatively high U contents (800–1400 ppm), and one of the most representative domains yielded a $^{206}Pb/^{238}U$ age of 458 ± 4 Ma (Fig. 10, Table 3). It is worth noting that there are several core analyses ranging from 693 to 734 Ma ($^{206}Pb/^{238}U$). These age estimates were obtained from the structureless cloudy dark or medium-intensity CL areas, and were evidently affected by late recrystallisation or diffusive Pb loss, and are therefore considered as misleading.

Accessory zircon from the leucocratic melt-rich granulite (sample D 10161) is typically represented by subhedral, euhedral prismatic, and short prismatic (up to equant) crystals shaped by the {1 0 0} and {1 1 0} prisms and {1 0 1}, {2 0 1} and {1 1 1} bipyramids (Fig. 11a). The crystal sizes vary from 30 to 80 μm, with an elongation coefficient ranging from 1.0 to 3.0. The zircons display light yellow colours with a high birefringence and are characterised by the presence of magmatic zoning, partially distorted in the marginal parts. Fig. 11a shows that all the data points plot on the concordia (the discordance degree is < 3%), while their $^{207}Pb/^{206}Pb$ age is 769 ± 2 Ma (MSWD = 2.6), corresponding to the middle of the Neoproterozoic (Table 4). The morphology of the studied zircons indicates a magmatic origin. Hence, the obtained age estimate may be considered to represent the timing of the crystallisation of the parental melts for the leucocratic melt-rich granulites.

The zircon population from the melanocratic residual granulite (sample D 10157) is heterogeneous and at least two groups of zircons were identified. Group I makes up ~40% of the bulk zircon population and consists of transparent or translucent, euhedral, pale-yellow prismatic and short-prismatic grains. The zircons feature a clear magmatic zoning and are overgrown by bright, thin luminescent rims (Fig. 11b). The grain sizes are in the size range of 30–200 μm, and the common

Table 3
Results of ion-microprobe (SHRIMP II) U-Th-Pb analyses of zircons from the quartz-feldspar orthogneiss (Sample BEK 1709).

Spot	% $^{206}Pb_c$	Ppm U	Ppm Th	Ppm $^{206}Pb^*$	$^{232}Th/^{238}U$	(1) $^{206}Pb/^{238}U$ Age		(1) $^{207}Pb/^{206}Pb$ Age		% Dis-cor-dant	(1) $^{238}U/^{206}Pb^*$	± %	(1) $^{207}Pb^*/^{206}Pb^*$	± %	(1) $^{207}Pb^*/^{235}U$	± %	(1) $^{206}Pb^*/^{238}U$	± %	err corr
17.2	–	1604	125	102	0.08	458	± 4	433	± 15	−6	13.6	1.0	0.056	0.7	0.56	1.2	0.074	1.0	0.8
27.1	0.20	76	46	7.37	0.63	693	± 22	732	± 73	+6	8.8	3.4	0.064	3.4	1.00	4.8	0.114	3.4	0.7
13.1	0.09	325	257	32.1	0.82	702	± 5	689	± 29	−2	8.7	0.7	0.062	1.4	0.99	1.5	0.115	0.7	0.5
3.1	–	172	94	17.9	0.57	734	± 6	762	± 35	+4	8.3	0.9	0.065	1.6	1.07	1.9	0.121	0.9	0.5
12.1	–	212	183	23.4	0.89	779	± 6	830	± 44	+7	7.8	0.8	0.067	2.1	1.18	2.3	0.128	0.8	0.4
25.1	–	137	73	15.1	0.55	781	± 7	778	± 54	−0	7.8	0.9	0.065	2.6	1.16	2.7	0.129	0.9	0.3
19.1	–	589	716	65.5	1.26	784	± 5	756	± 20	−4	7.7	0.7	0.064	1.0	1.15	1.2	0.129	0.7	0.6
10.1	–	718	1008	79.9	1.45	786	± 5	784	± 20	−0	7.7	0.7	0.065	0.9	1.17	1.2	0.130	0.7	0.6
2.1	–	265	218	29.6	0.85	787	± 6	854	± 40	+8	7.7	0.9	0.068	1.9	1.21	2.1	0.130	0.9	0.4
9.1	–	463	423	51.7	0.94	788	± 5	766	± 22	−3	7.7	0.7	0.065	1.1	1.16	1.3	0.130	0.7	0.6
14.1	–	173	153	19.3	0.92	789	± 7	860	± 48	+9	7.7	1.0	0.068	2.3	1.22	2.5	0.130	1.0	0.4
16.1	–	99	50	11.1	0.52	790	± 8	767	± 48	−3	7.7	1.0	0.065	2.3	1.16	2.5	0.130	1.0	0.4
17.1	–	112	67	12.7	0.62	797	± 9	854	± 64	+7	7.6	1.1	0.068	3.1	1.23	3.3	0.132	1.1	0.3
5.1	–	447	414	50.6	0.96	798	± 8	799	± 28	+0	7.6	1.0	0.066	1.3	1.19	1.7	0.132	1.0	0.6
8.1	0.13	98	55	11.1	0.58	800	± 13	746	± 84	−8	7.6	1.7	0.064	4.0	1.17	4.3	0.132	1.7	0.4
1.1	–	117	133	13.5	1.17	808	± 7	789	± 33	−3	7.5	1.0	0.065	1.6	1.21	1.8	0.134	1.0	0.5
24.1	0.09	123	87	26.7	0.73	1451	± 14	1445	± 22	−1	4.0	1.1	0.091	1.2	3.16	1.6	0.253	1.1	0.7

Errors are 1-sigma; Pb_c and Pb* indicate the common and radiogenic portions, respectively.
Error in Standard calibration was 0.15% (not included in above errors but required when comparing data from different mounts).
(1) Common Pb corrected using measured ^{204}Pb.

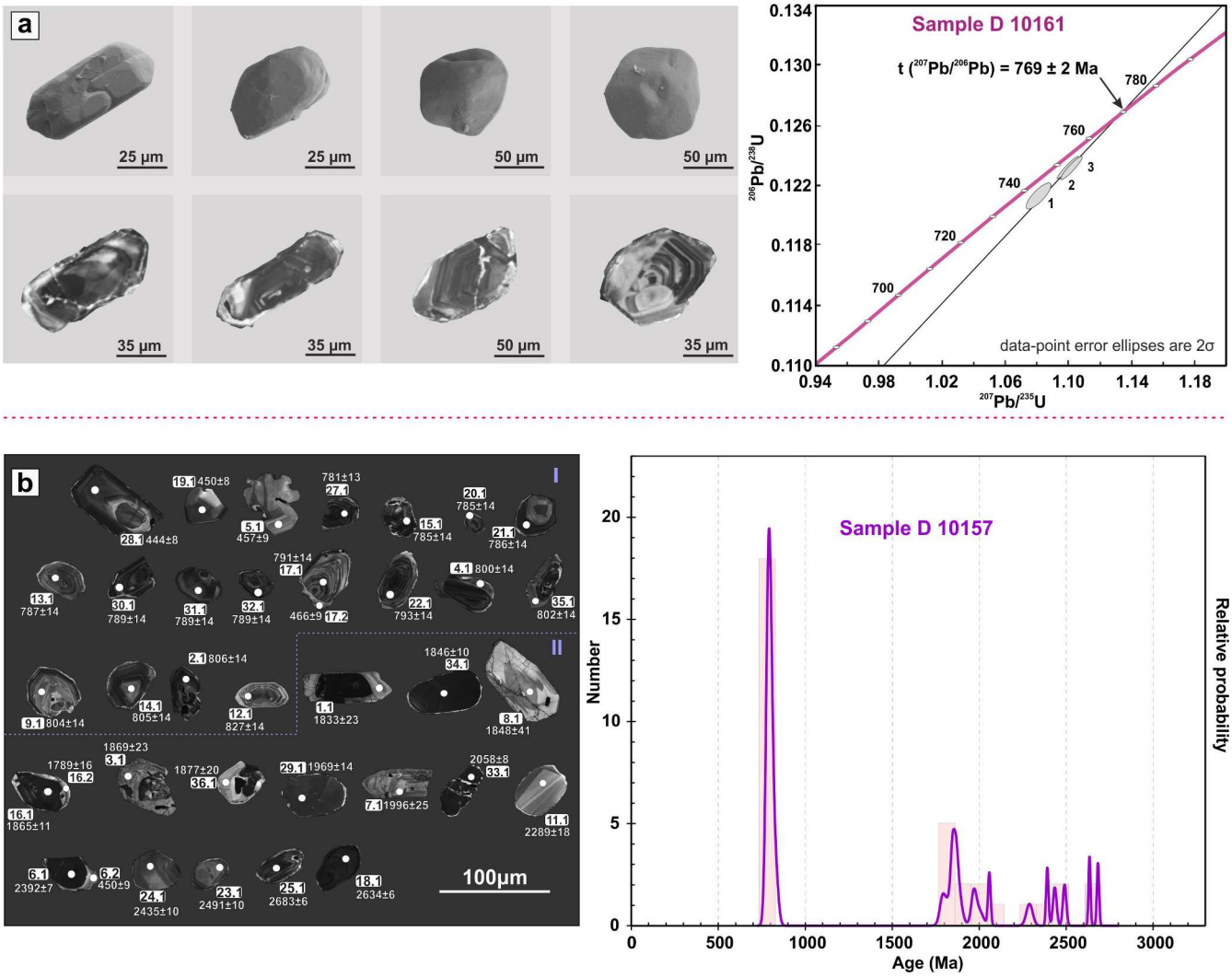

Fig. 11. a) Scanning electron microscopy (SEM) and CL photographs of zircon grains (left) from the leucocratic (melt-rich) granulite D 10161 and U-Pb concordia diagram (right) with the U-Pb isotope data of the analysed zircons (ID TIMS). The numbers of the points correspond to those from Table 4. b) CL photographs of zircon grains (left) from the melanocratic (clinopyroxene-rich) granulite D 10157 (the white circles are SHRIMP analytical spots; the numbers in the squares are in accordance with Table 5) and normalised probability plot (Gehrels, 2012) for detrital zircon ages from the melanocratic (clinopyroxene-rich) granulite (SHRIMP II).

Table 4
U-Pb isotopic data (ID TIMS) for zircons from the leucocratic (melt-rich) granulite (sample D 10161).

№	Zircon size (μm) and type of treatment	Weight, (mg)	Pb, ppm	U, ppm	Isotopic ratios corrected for blank and common Pb					Rho	Age, Ma		
					$^{206}Pb/^{204}Pb$	$^{207}Pb/^{206}Pb^{a}$	$^{208}Pb/^{206}Pb^{a}$	$^{207}Pb/^{235}U$	$^{206}Pb/^{238}U$		$^{207}Pb/^{235}U$	$^{206}Pb/^{238}U$	$^{207}Pb/^{206}Pb$
1	< 50	1.05	7.2	56	7840	0.0646 ± 1	0.1868 ± 1	1.0808 ± 14	0.1213 ± 1	0.87	744 ± 1	738 ± 1	762 ± 1
2	< 50, CA 2 h.	-*	U/Pb = 7.56		27,318	0.0649 ± 1	0.1783 ± 1	1.1014 ± 12	0.1231 ± 1	0.96	754 ± 1	749 ± 1	770 ± 1
3	< 50, CA 2.5 h.	-*	U/Pb = 7.63		5716	0.0647 ± 1	0.1708 ± 1	1.0987 ± 17	0.1232 ± 1	0.97	753 ± 1	749 ± 1	764 ± 1

Notes: all errors are 2 σ and refer to last digits of corresponding ratios; CA- zircons after chemical abrasion;
a – measured ratio; −* – U/Pb ratios for unweighted grains or residues after the acid treatment were determined using the $^{202}Pb/^{235}U$.

magmatic length/width ratio is ~1.0–3.0. Sixteen group I zircon grains were dated by SHRIMP II and the obtained $^{206}Pb/^{238}U$ age estimates are in the range from 781 to 827 Ma (Table 5). Ten analyses with a discordance of < 5% yielded a mean $^{206}Pb/^{238}U$ age of 794 ± 9 Ma (MSWD = 0.94) and concordia age of 793 ± 4 Ma (MSWD = 1.3). The group II zircons are represented by semi-transparent or transparent, fractured subhedral, pale-pink, prismatic, rounded or irregular-shaped grains with sizes in the range 50–300 μm and partially preserved oscillatory zoning and corroded cores (Fig. 11b). Sixteen group II zircons with different features in CL were analysed, and ten analyses showed $^{207}Pb/^{206}Pb$ age estimates in the interval of 1790–2058 Ma, whereas the remaining six analyses yielded $^{207}Pb/^{206}Pb$ ages in the range of 2290–2680 Ma (Table 5). We note that the observed zircons from both groups possess variously luminescent rims. Four points from the rims were analysed and the obtained $^{206}Pb/^{238}U$ age estimates range from 444 to 466 Ma (Table 5).

Thus, several groups of ages were obtained from the SHRIMP II investigations of the melanocratic (clinopyroxene-rich) granulite D

Table 5
Results of ion-microprobe (SHRIMP II) U-Th-Pb analyses of zircons from the melanocratic (clinopyroxene-rich) granulite (Sample D 10157).

Spot	% $^{206}Pb_c$	ppm U	ppm Th	ppm $^{206}Pb^*$	$\frac{^{232}Th}{^{238}U}$	(1) $\frac{^{206}Pb}{^{238}U}$ Age	±	(1) $\frac{^{207}Pb}{^{206}Pb}$ Age	±	% Dis-cor-dant	(1) $\frac{^{238}U}{^{206}Pb^*}$	± %	(1) $\frac{^{207}Pb^*}{^{206}Pb^*}$	± %	(1) $\frac{^{207}Pb^*}{^{235}U}$	± %	(1) $\frac{^{206}Pb^*}{^{238}U}$	± %	err corr
28.1	–	138	15	8.47	0.12	444	± 8	622	± 63	+30	14.0	1.9	0.061	2.9	0.59	3.5	0.071	1.9	0.5
19.1	0.11	161	16	9.98	0.10	450	± 8	419	± 48	−8	13.8	1.9	0.055	2.1	0.55	2.8	0.072	1.9	0.7
6.2	–	63	3	3.94	0.05	450	± 9	566	± 80	+21	13.8	2.1	0.059	3.7	0.59	4.2	0.072	2.1	0.5
5.1	0.16	42	0	2.66	0.00	457	± 9	359	± 105	−28	13.6	2.1	0.054	4.6	0.54	5.1	0.074	2.1	0.4
17.2	0.26	90	12	5.78	0.14	466	± 9	512	± 72	+9	13.4	1.9	0.058	3.3	0.59	3.8	0.075	1.9	0.5
27.1	0.02	446	564	49.4	1.31	781	± 13	819	± 17	+5	7.8	1.8	0.066	0.8	1.18	2.0	0.129	1.8	0.9
15.1	–	181	151	20.2	0.86	785	± 14	847	± 25	+8	7.7	1.8	0.067	1.2	1.20	2.2	0.129	1.8	0.8
20.1	0.13	178	157	19.8	0.91	785	± 14	803	± 29	+2	7.7	1.8	0.066	1.4	1.18	2.3	0.130	1.8	0.8
21.1	0.15	183	127	20.4	0.72	786	± 14	808	± 35	+3	7.7	1.8	0.066	1.7	1.18	2.5	0.130	1.8	0.7
13.1	0.18	228	164	25.5	0.74	787	± 14	759	± 27	−4	7.7	1.8	0.065	1.3	1.16	2.2	0.130	1.8	0.8
31.1	–	112	82	12.6	0.75	789	± 14	895	± 40	+13	7.7	1.9	0.069	1.9	1.24	2.7	0.130	1.9	0.7
32.1	–	281	218	31.5	0.80	789	± 14	864	± 19	+9	7.7	1.8	0.068	0.9	1.22	2.0	0.130	1.8	0.9
30.1	0.18	89	57	10	0.66	789	± 14	807	± 40	+2	7.7	1.9	0.066	1.9	1.19	2.7	0.130	1.9	0.7
17.1	0.07	114	49	12.8	0.45	791	± 14	826	± 34	+5	7.7	1.9	0.067	1.6	1.20	2.5	0.131	1.9	0.8
22.1	–	205	160	23.1	0.81	793	± 14	796	± 24	+0	7.6	1.9	0.066	1.1	1.19	2.2	0.131	1.9	0.9
4.1	0.17	129	94	14.6	0.75	800	± 14	862	± 34	+8	7.6	1.9	0.068	1.7	1.24	2.5	0.132	1.9	0.8
35.1	–	99	58	11.2	0.60	802	± 14	810	± 41	+1	7.6	1.9	0.066	2.0	1.21	2.7	0.132	1.9	0.7
9.1	–	109	98	12.5	0.93	804	± 14	858	± 35	+7	7.5	1.9	0.068	1.7	1.24	2.5	0.133	1.9	0.7
14.1	0.16	98	60	11.2	0.63	805	± 14	780	± 41	−3	7.5	1.9	0.065	2.0	1.20	2.7	0.133	1.9	0.7
2.1	–	157	90	17.9	0.59	806	± 14	851	± 33	+6	7.5	1.9	0.067	1.6	1.24	2.4	0.133	1.9	0.8
12.1	–	433	505	50.9	1.21	827	± 14	850	± 17	+3	7.3	1.8	0.067	0.8	1.27	2.0	0.137	1.8	0.9
3.1	–	57	36	14.3	0.67	1658	± 29	1869	± 23	+13	3.4	2.0	0.114	1.3	4.62	2.4	0.293	2.0	0.8
8.1	–	18	20	4.53	1.18	1696	± 36	1848	± 41	+9	3.3	2.4	0.113	2.3	4.69	3.3	0.301	2.4	0.7
16.2	0.06	93	65	24.2	0.72	1711	± 29	1789	± 16	+5	3.3	1.9	0.109	0.9	4.59	2.1	0.304	1.9	0.9
34.1	–	224	166	59.8	0.76	1742	± 28	1846	± 10	+6	3.2	1.8	0.113	0.5	4.83	1.9	0.310	1.8	1.0
16.1	0.00	164	128	44.3	0.81	1766	± 29	1865	± 11	+6	3.2	1.9	0.114	0.6	4.96	2.0	0.315	1.9	0.9
36.1	0.02	48	36	13.2	0.77	1773	± 32	1877	± 20	+6	3.2	2.0	0.115	1.1	5.01	2.3	0.317	2.0	0.9
29.1	0.01	138	231	37.8	1.73	1782	± 29	1969	± 14	+11	3.1	1.9	0.121	0.8	5.31	2.0	0.318	1.9	0.9
1.1	0.04	40	25	11.3	0.63	1815	± 33	1833	± 23	+1	3.1	2.1	0.112	1.3	5.02	2.5	0.325	2.1	0.9
7.1	–	35	25	9.72	0.75	1815	± 34	1996	± 25	+10	3.1	2.1	0.123	1.4	5.50	2.5	0.325	2.1	0.8
33.1	–	284	271	80.2	0.98	1832	± 29	2058	± 8	+13	3.0	1.8	0.127	0.4	5.76	1.9	0.329	1.8	1.0
11.1	0.10	53	45	18.8	0.88	2234	± 38	2289	± 18	+3	2.4	2.0	0.145	1.1	8.29	2.3	0.414	2.0	0.9
24.1	0.08	121	64	45.8	0.54	2354	± 38	2435	± 10	+4	2.3	1.9	0.158	0.6	9.60	2.0	0.441	1.9	1.0
23.1	0.00	96	46	36.4	0.50	2360	± 38	2491	± 10	+6	2.3	1.9	0.163	0.6	9.96	2.0	0.442	1.9	1.0
6.1	0.00	228	93	88.7	0.42	2403	± 37	2392	± 7	−1	2.2	1.8	0.154	0.4	9.60	1.9	0.452	1.8	1.0
18.1	–	253	96	100	0.39	2447	± 37	2634	± 6	+9	2.2	1.8	0.178	0.3	11.33	1.9	0.462	1.8	1.0
25.1	0.01	184	183	73.4	1.03	2457	± 38	2683	± 6	+10	2.2	1.9	0.183	0.4	11.72	1.9	0.464	1.9	1.0

Errors are 1-sigma; Pb_c and Pb* indicate the common and radiogenic portions, respectively.
Error in Standard calibration was 0.34% (not included in above errors but required when comparing data from different mounts).
(1) Common Pb corrected using measured ^{204}Pb.

10157, which included a wide range of Neoarchean, Palaeoproterozoic, Neoproterozoic and Early Palaeozoic age determinations (Fig. 11b). The zircons with Neoarchean and Palaeoproterozoic ages are apparently detrital and reflect the metasedimentary origin of the granulite protolith. However, the most prominent age peak of ~790 Ma obtained from the group I zircons is in agreement with the previously-discussed $^{207}Pb/^{206}Pb$ ID TIMS zircon age of 770 Ma from the melt-rich granulite D 10161, which forms veins and layers of leucosomes within the melanocratic clinopyroxene-rich variety, including sample D 10157 (Fig. 5). Hence, clear similarities exist in the zircon morphologies and the obtained age estimates in the range of 770–790 Ma from samples D 10161 and D 10157 (Fig. 11a–b), representing a single granulite complex (Section 3.3.1. above). These observations define the timing of the leucosome crystallisation, rather than an additional Neoproterozoic peak of sedimentary protolith formation for the observed melanocratic granulites. Furthermore, the Palaeoproterozoic age peak of 1790 Ma reflects the lower limit of deposition for the sedimentary protolith of the granulites of the Aydaly Complex, whereas the interval of 770–790 Ma marks the timing of high-temperature granulite metamorphism. In turn, the obtained Early Palaeozoic ages for the zircon rims from the granulites (444–466 Ma) may be interpreted as resulting from the overprinting metasomatism. It is worth noting that the previously-discussed, similar estimate of 458 Ma obtained from the quartz-

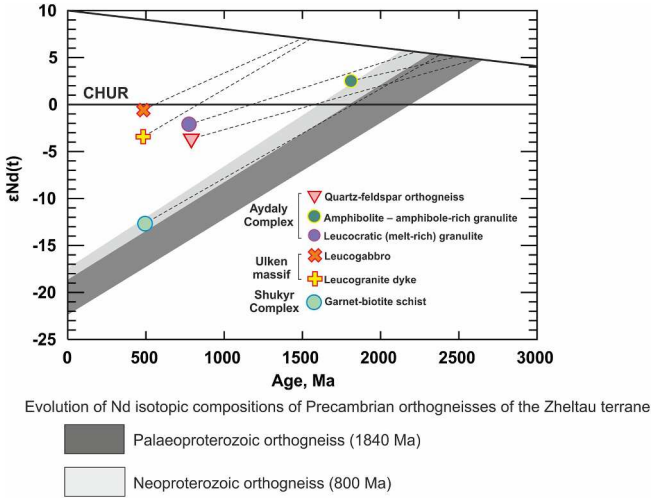

Fig. 12. Nd isotope evolution diagram for the Aydaly, Shukyr Complexes and Ulken massif rock types. Grey lines are evolution of isotopic compositions of the Neo- (~800 Ma) and Palaeoproterozoic (~1840 Ma) orthogneisses of the adjacent Zheltau terrane. CHUR is 'chondritic uniform reservoir' (Jacobsen and Wasserburg, 1984). Depleted mantle evolution curve is after Depaolo (1981).

Table 6
Sm-Nd isotopic data for the principal rock types of the Aydaly, Shukyr Complexes and Ulken massif.

Sample	Rock type		Age, Ma	Sm, ppm	Nd, ppm	$^{147}Sm/^{144}Nd$	$^{143}Nd/^{144}Nd$ (± σm)	$\varepsilon_{Nd}(t)$	$t_{Nd(DM)}$
TS 1016	Orthogneiss	Aydaly Complex	800	1.13	4.25	0.1611	0.512258	−3.7	2575
BEK 1704	Amphibole-rich granulite		1800	1.98	6.84	0.1749	0.512515	2.6	2489
D 10161	Melt-rich granulite		770	12.31	48.34	0.1539	0.512315	−2.1	2124
TS 1019	Garnet-biotite schist	Shukyr Complex	500	4.10	20.4	0.1216	0.511745	−12.6	2319
P 1059/1	Leucogabbro	Ulken massif	489	2.70	11.90	0.1372	0.512418	−0.5	1459
D 10171	Leucogranite		489	1.31	6.49	0.1222	0.512218	−3.4	1552

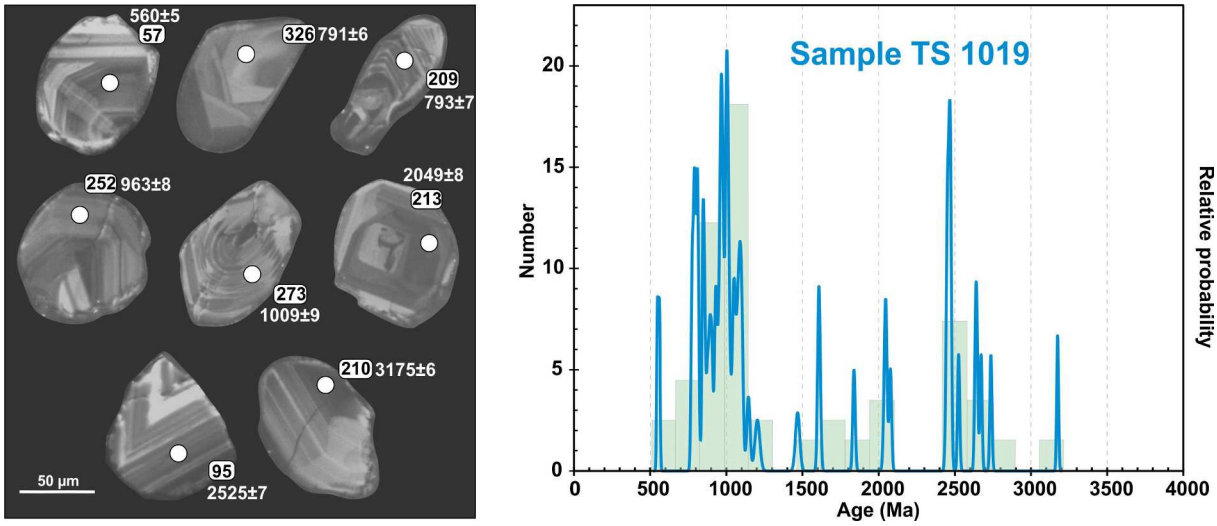

Fig. 13. CL photographs of detrital zircons (left) from the garnet-biotite schists TS 1019 (the white circles are LA-ICP MS analytical spots; the numbers in the squares and age estimates are in accordance with Table S12) and normalised probability plot (Gehrels, 2012) for detrital zircon ages from the schists (right).

feldspar orthogneiss BEK 1709 (Fig. 10), which is structurally related to the granulites of the Aydaly Complex, is evidently related to the same overprinting processes.

The quartz-feldspar orthogneiss displays a negative $\varepsilon_{Nd(t)}$ of −3.8 and a Neoarchean-Palaeoproterozoic model age $t_{Nd(DM)}$ of 2.5 Ga. The leucocratic melt-rich granulite is similarly characterised by a negative $\varepsilon_{Nd(t)}$ of −2.1 and a Palaeoproterozoic model age $t_{Nd(DM)}$ of 2.1 Ga (Fig. 12, Table 6). The amphibolite–amphibole-rich granulite records a positive $\varepsilon_{Nd(t)}$ of 2.6 and a Palaeoproterozoic model age $t_{Nd(DM)}$ of 2.5 Ga (Fig. 12, Table 6). Thus, the Sm-Nd whole-rock isotopic compositions of the granulites indicate an involvement of a Palaeoproterozoic 'juvenile' source during the protolith formation.

3.4.2. Shukyr Complex

57 concordant age estimates, generally ranging within the intervals 779–862 Ma, 935–1107 Ma and 2444–2485 Ma, were acquired for detrital zircons (103 grains in total) from the garnet-biotite schists of the Shukyr Complex (sample TS 1019; Tables 7, S12). On the relative probability plot, there are several conspicuous age peaks, corresponding to 791, 809, 849, 968, 1004, 1051, 1090 and 2467 Ma (Fig. 13, Table 7). It is worth noting that sporadic zircon grains yielded Meso- and Palaeoproterozoic concordant ages of 1145–2077 Ma and two grains were characterised by Neoarchean and Mesoarchean ages of 2737 ± 7 Ma and 3175 ± 5 Ma (Table S12). Furthermore, individual zircon grains from these schists yielded Ediacaran–early Cambrian ages of 548–560 Ma (Fig. 13, Table S12).

Table 7
Selected results of age peaks (Gehrels, 2012) calculations for detrital zircons from the garnet-biotite schists of the Shukyr Complex (Sample TS 1019).

MIN AGE	MAX AGE	# GRAINS	PEAK AGE	# GRAINS
779	820	6	791	3
844	862	3	809	3
935	943	1	849	3
947	1027	12	968	5
1030	1107	7	1004	6
2444	2485	6	1051	3
			1090	5
			2467	5

The garnet-biotite schists show a negative $\varepsilon_{Nd(t)}$ value of −12.6 and a Palaeoproterozoic model age $t_{Nd(DM)}$ of 2.3 Ga (Fig. 12, Table 6).

3.4.3. Ulken massif

The zircon population of the leucogabbro (sample P 1059/1) consists of subhedral or euhedral, transparent or semi-transparent, yellow-to-brownish prismatic and stubby grains. The grain sizes are in the range of 30–300 μm with a typical magmatic length/width ratio of 1.0–3.0. The observed crystals are faceted by {1 0 0}, {1 1 0} prisms and {1 0 1}, {1 1 1} and {2 1 1} bipyramids (Fig. 14). The zircons display oscillatory and sectorial zoning, as well as inherited irregularly-shaped core relics occurring mainly in the short prismatic grains (Fig. 14). Three fractions of the cleanest untreated and air-abraded prismatic zircon grains (20–35 grains in each fraction) were analysed (Table 8). The analytical data are well aligned on the concordia diagram and define a discordia line (MSWD = 2) with intercept ages of 480 ± 14 and −8 ± 13 Ma, respectively (Fig. 14). The three fractions of zircons in total yielded a mean $^{207}Pb/^{206}Pb$ age of 489 ± 5 Ma (MSWD = 1.6), which is interpreted as the timing of the leucogabbro crystallisation.

The studied leucogabbros and plagiogranites of the Ulken massif are characterised by negative $\varepsilon_{Nd(t)}$ values (-0.5) and a Mesoproterozoic model age $t_{Nd(DM)}$ of 1.5 Ga (Fig. 12, Table 6). Moreover, the

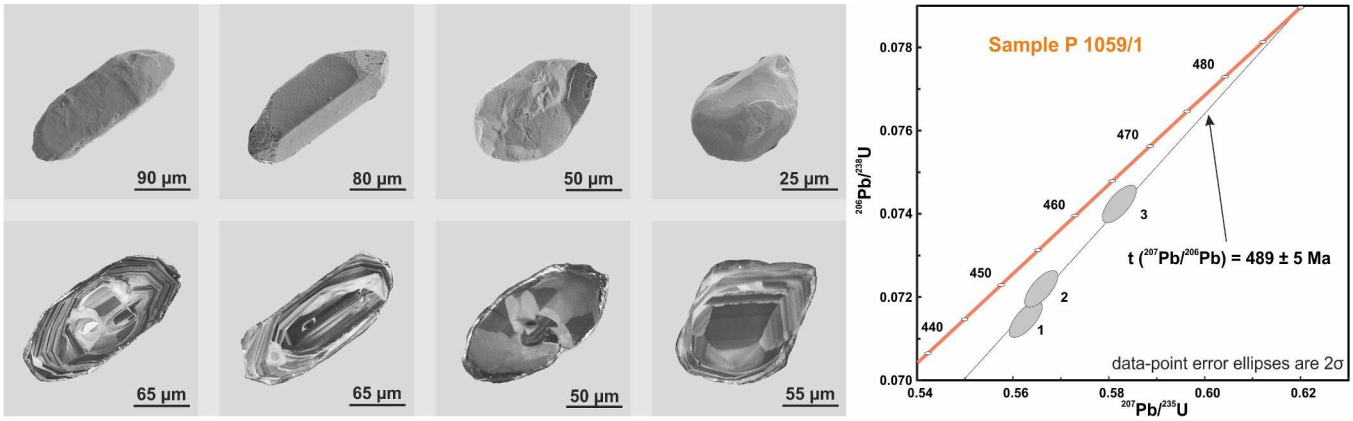

Fig. 14. SEM and CL photographs of zircon grains (left) from the leucogabbro P 1059/1 of the Ulken massif and U-Pb concordia diagram (right) with the U-Pb isotope data of the analysed zircons (ID TIMS). The numbers of the points correspond to those from Table 8.

leucogranite dykes from the same massif show similar negative $\varepsilon_{Nd(t)}$ values of −3.4 and a Mesoproterozoic model age $t_{Nd(DM)}$ of 1.5 Ga (Fig. 12, Table 6).

4. Discussion

Our results shed light on the timing and tectonic settings of the formation of the complexes associated with the Chu Block, and allow us to reconstruct their tectono-magmatic evolution with respect to the adjacent complexes of the Chu-Kendyktas terrane. We first conduct general regional correlations with the Precambrian terranes in Southern Kazakhstan and determine a Precambrian tectonic affinity for the Chu Block. We then propose a model of the tectonic evolution of the Chu-Kendyktas terrane during the Precambrian–Early Palaeozoic.

4.1. Timing, sources, and tectonic settings of the studied complexes in the NW part of the Chu Block

The metamorphic rocks of the Aydaly Complex show evidence of a multi-stage evolution, including both Precambrian and Early Palaeozoic stages. The oldest formations of the Aydaly Complex consist of the amphibolites–amphibole-rich granulites and their derivatives, comprising mesocratic, leucocratic and melanocratic granulites. The geochemical signatures of the amphibolite–amphibole-rich granulite are consistent with those observed in basalts, such as a weakly differentiated spectrum of REE distribution ($(La/Yb)_n$ = 1.6) and an absence of Eu anomaly (Eu/Eu* = 0.99) as well as characteristic La/Sc, Th/Sc, La/Co and Th/Co ratios (Fig. 6, Table 2). Moreover, this rock type corresponds to a mafic source on a La-Th-Sc diagram (Fig. 7a). These rocks also contain a number of detrital zircons (Fig. 11b, group II) with maximum concordant age estimates at 1794 and 1856 Ma, and sparse age estimates in the range of 2290–2680 Ma, confirming a sedimentary origin of the protolith. This implies an involvement of clastic material, derived from the erosion of intermediate and/or basic magmatic rocks that originally contained the zircons. Compared to basalts, these rock types display higher CaO and K_2O contents, and an enrichment in LILEs (Fig. 6c, Table 2). However, the small number of detrital zircons in this rock type, along with a strong similarity with basalts in terms of whole-rock chemical compositions, could indicate that the role of a felsic source was insignificant. The protolith of the granulites is therefore likely to have consisted of mafic greywackes, formed from the erosion of predominantly mafic rocks. The greywackes were transformed to para-amphibolites, and then experienced high-temperature granulite facies metamorphism at mid-crustal levels. This high-temperature metamorphism stage is defined by the Neoproterozoic age (770 Ma) of the leucocratic melt-rich granulites with a generally tonalitic composition (Fig. 11a), which form veins and layers within the melanocratic clinopyroxene-rich granulites, or more rarely constitute separate bodies. This age determination is consistent with that obtained for the group I zircons from the melanocratic granulites of ~790 Ma (Fig. 11b, group I), implying a magmatic origin for the zircon population, derived from the newly formed tonalite leucosome veins (Section 3.4.1). From these observations, we conclude that the accumulation of the protolith for the Aydaly Complex granulites and its subsequent emplacement at mid-crustal levels likely occurred from the middle Palaeoproterozoic (~1800 Ma) to the latter half of Tonian (~770–790 Ma). Moreover, from the results of the geochronological studies, Neoproterozoic (late Tonian) granitoids of ~790 Ma are thought to represent the protolith for the associated orthogneisses (Fig. 10). Taking into consideration the spatial and structural proximity of the Aydaly Complex granulites and the orthogneisses, the obtained age estimates of ~770–790 Ma could reflect a single stage of Neoproterozoic magmatism, which resulted in the formation of the granitoids. The Neoproterozoic rock types are characterised by high $K_2O + Na_2O$ and Al_2O_3 contents, corresponding

Table 8
U-Pb isotopic data (ID TIMS) for zircons from the leucogabbro of the Ulken massif (Sample P 1059/1).

№	Zircon size (μm) and type of treatment	Weight, (mg)	Pb, ppm	U, ppm	Isotopic ratios corrected for blank and common Pb					Rho	Age, Ma		
					$^{206}Pb/^{204}Pb$	$^{207}Pb/^{206}Pb^a$	$^{208}Pb/^{206}Pb^a$	$^{207}Pb/^{235}U$	$^{206}Pb/^{238}U$		$^{207}Pb/^{235}U$	$^{206}Pb/^{238}U$	$^{207}Pb/^{206}Pb$
1	85–100, 30 grains	0.29	5.9	80	3697	0.0568 ± 1	0.1505 ± 1	0.5545 ± 25	0.0708 ± 2	0.97	448 ± 2	441 ± 2	484 ± 3
2	85–100, 35 grains	0.29	5.1	65	711	0.0571 ± 1	0.1602 ± 1	0.5628 ± 16	0.0715 ± 1	0.78	453 ± 1	445 ± 1	495 ± 4
3	100–150, 30 grains, A10%	0.24	3	48	2347	0.0569 ± 1	0.1899 ± 1	0.5829 ± 10	0.0742 ± 1	0.76	466 ± 1	462 ± 1	489 ± 2

Notes: all errors are 2 σ and refer to last digits of corresponding ratios; A10% – air-abraded zircons, shown percentage – amount of zircon removed during of the air-abrasion; a – measured ratio; −* – U/Pb ratios for unweighted grains or residues after the acid treatment were determined using the $^{202}Pb/^{235}U$.

to a peraluminous or metaluminous series, and fall into the fields of I- and S-type granites, with some samples being close to the boundary with the A-type granites (Fig. S3c–g). However, no evidence for the existence of a mantle source has been found, thus the melt-rich granulites and orthogneisses cannot be referred to as A-type granites. Negative $\varepsilon_{Nd(t)}$ values in the leucocratic melt-rich granulites and orthogneisses are thought to relate to the general features of the melt sources rather than the setting of the granitoid magmatism. The obtained Nd model age values of 2.5 and 2.1 Ga for the leucocratic granulites and orthogneisses indicate their derivation from Palaeoproterozoic crust. Moreover, the presence of an older zircon core of ~1450 Ma in the orthogneisses (Fig. 10) could reflect an involvement of Mesoproterozoic magmatic complexes along with the older formations in the structure of the deeper crustal horizons of the Chu Block. It is worth noting that the observed negative $\varepsilon_{Nd(t)}$ value (−2.1) of the leucocratic melt-rich granulite of the Aydaly Complex indicates a crustal source for the protolith, whereas the mafic amphibolite–amphibole-rich granulite, which is thought to represent an inferred precursor for the granulites, displays a positive $\varepsilon_{Nd(t)}$ of 2.6 (Table 6), implying a key role of a juvenile source in the formation of the protolith. This is also confirmed by strong ensimatic signatures in the amphibolite–amphibole-rich granulite, expressed in the REE-depleted whole-rock compositions along with the high MgO with FeO_{tot} contents and the Th-La-Sc-Co ratios that are compatible with a mafic source. Hence, the different layers and veins of the leucocratic tonalites in the clinopyroxene-rich melanosome (Fig. 5), and the observed high-temperature granulite facies metamorphic transformations from the amphibolite–amphibole-rich granulite to the mesocratic and then leucocratic with melanocratic granulites, are evidently related to the interaction between the pre-existing para-amphibolite with the haplogranitic melt derived from the external crustal source, rather than from in-situ melting of the amphibolites (i.e. migmatisation). This interaction led to the formation of the granulite facies mineral assemblages of clinopyroxene and feldspar along with the gradual decomposition of the reactant amphibole. Moreover, during clinopyroxene crystallisation the melt becomes undersaturated in Ca, Mg or Fe, and therefore high-temperature segregation of the leucocratic melt-rich zone at T > 900 °C occurs (Khodorevskaya, 2002). Finally, the zircons from the granulites and the orthogneisses of the Aydaly Complex display overgrowth rims that are variegated in CL (Figs. 10 and 11) and generally cover an age span of 444–466 Ma, corresponding to the Middle–Late Ordovician. The zircon rims are interpreted to have been formed during the overprinting processes. In the granulites, these overprinting processes are also reflected in the explicit chemical zoning of clinopyroxene, with a decrease of Mg from cores to rims, as well as the extensive development of epidote-clinozoisite associated with andradite-grossular (Fig. 4).

Thus, the Aydaly Complex rock types, represented by the predominant orthogneisses and granulites, demonstrate extensive evidence of a multi-stage tectono-thermal evolution, in which the Neoproterozoic (late Tonian) magmatism played a key role. The rocks were juxtaposed and synchronously deformed during their evolution, and also evidently experienced later metamorphic and/or metasomatic alterations in the Early Palaeozoic. It is worth noting that the granulites contain detrital zircon grains of mainly Palaeoproterozoic and, to a lesser extent, Neoarchean ages, indicating a sedimentary origin of the protolith, such as the mafic greywackes that were transformed to para-amphibolites prior to the main Neoproterozoic magmatic event, implying that the greywackes accumulated in the time range from the Palaeoproterozoic to the late Tonian.

In turn, the garnet-biotite schists of the Shukyr Complex were formed from the metamorphism of shales, according to their chemical compositions (Fig. S3a). In comparison to the Aydaly Complex rock types, the schists are characterised by a significantly lower grade of metamorphism at T ~600 °C, and are thought to represent moderate-temperature hornfels that formed at the contact between the protolith shales and the Ulken massif granitoids (Fig. 2B). The lower limit of accumulation for the shales is defined by the youngest age estimates from the detrital zircons of 548–560 Ma (Table S12), whereas the upper limit corresponds to the age of the cross-cutting granitoids of the Ulken massif of ~490 Ma. Hence, the accumulation of the protolith of the garnet-biotite schists occurred during the time range from the end of the Ediacaran to the Cambrian. The detrital zircon populations with preserved magmatic zoning cover the age intervals of ~2500 Ma, 1000 Ma and 780–860 Ma. The zircons with Neoproterozoic age estimates imply that the granitoids of the Aydaly Complex constitute one of the possible sources for the protolith of the garnet-biotite schists. Thus, based on the obtained detrital zircon ages, the formation of the protolith of the Shukyr Complex schists resulted from the erosion of Neo-, Meso- and Palaeoproterozoic, and to a lesser extent Neoarchean, felsic rocks. In addition, the geochemical signatures of these rock types indicate a notable contribution of mafic rocks in the source. The isotopic characteristics of these schists indicate a Palaeoproterozoic age of the source (2.3 Ga) and reflect an involvement of Palaeoproterozoic crust in the formation of all the younger complexes of the source area.

The Zhuantobe Complex represents an association of black shales, contrasting basaltic-rhyolitic volcanic rocks, jaspilites, sandstones and cherts, with middle- to upper-Cambrian conodonts. The basalts correspond to a tholeiitic series (Fig. S4) and display high TiO_2 contents, which is characteristic for an intraplate-derived formation. The rhyolites fall into the field of peraluminous series felsic rocks (Table S1). Based on the chemical compositions and structural positions, the Zhuantobe Complex sedimentary and volcanic rocks are interpreted to be of intraplate origin, formed in the Precambrian sialic basement. From these observations, we infer that the Zhuantobe Complex represents an analogue of the Cambrian black shale and terrigenous lithologies of the Kiintas and Ogiztau Formations, which are extensively developed in the southern part of the Chu Block (Abdulin, 1980). However, the presence of volcanic rocks in the sequence is unique to the Zhuantobe Complex, compared to the Kiintas and Ogiztau Formations. The observed low-grade metamorphic alterations of the Zhuantobe Complex volcanogenic rocks in the vicinity of the contact with the Aydaly Complex may be related to a thermal effect resulting from interaction with the exposed Aydaly Complex metamorphic formations in the Ordovician. To summarise, the Early Palaeozoic Shukyr and Zhuantobe Complexes may be inferred to represent a terrigenous shale cover overlying the Precambrian complexes of the Chu Block, formed during the time range from the end of the Ediacaran to the Cambrian, and that was subsequently metamorphosed to different extents.

The leucogabbros, plagiogranites and leucogranites of the Ulken massif have latest Cambrian ages (489 ± 5 Ma), cut all the studied older formations and are consistent with volcanic arc granitoids in terms of their compositions. The plagiogranite corresponds to a weakly ferroan series with low concentrations of Rb and Ba and high Sr contents, which is generally characteristic for I-type granites, derived from the melting of a metabasic source or the differentiation and/or crustal contamination of mafic melts. The leucogranite dykes of the Ulken massif display a higher ASI with a higher K_2O/Na_2O ratio compared to the plagiogranites, and correspond to a ferroan series. These features are common for rock types derived from the partial melting of metasedimentary sources, represented by metagreywackes or metapelites. The observed differences in the source compositions are supported by the distinctive $\varepsilon_{Nd(t)}$ values (-0.5 in the leucogabbro and −3.4 in the leucogranite, Table 6), which could indicate an isotopic heterogeneity of the sources due to variable proportions of juvenile and older crustal material. Moreover, the Ulken massif formations display similar Mesoproterozoic Nd model ages of 1.5 Ga. Thus, a mixed character of the source for the studied latest Cambrian granitoids may be related to the melting of Precambrian continental crust of the Chu-Kendyktas terrane, as a result of the intrusion of juvenile basic material of supra-subductional origin.

4.2. Regional correlations and Precambrian tectonic affinity of the Chu Block in the NW part of the Chu-Kendyktas terrane

The most widespread felsic formations of the Aydaly Complex in the Chu Block of the NW part of the Chu-Kendyktas terrane are Neoproterozoic orthogneisses and leucocratic granulites (tonalites) of 770–790 Ma. Similar age granitoids are known from the Aktyuz and Kemin Complexes in the Aktyuz Block of the SE part of the Chu-Kendyktas terrane (Kröner et al., 2007; Kröner et al., 2012) and from the Anrakhai Complex in the Zheltau terrane (Pilitsyna et al., 2019) (Fig. 1).

These granitoids show a predominance of K_2O over Na_2O, and mostly correspond to an alkalic–calcic and ferroan series with peraluminous or weakly metaluminous characteristics. These features allowed them to be classified as derived from the melting of the crustal tonalite-granodiorite material (Frost et al., 2011). The observed enrichment in REE and the absence of a depletion in HREE in the granitoids are common characteristics for A-type granites (Whalen et al., 1987), indicating a possible intraplate setting of the Neoproterozoic stage of magmatism. The observed granitoids display negative $\varepsilon_{Nd(t)}$ values and are thought to be derived from the Palaeoproterozoic continental crust complexes. Early Mesoproterozoic formations may have formed part of the structure of the Chu-Kendyktas terrane crust, which is supported by the presence of a Mesoproterozoic zircon core of 1450 Ma within the Neoproterozoic orthogneisses, as well as Nd model ages of ~1500 Ma for the Early Palaeozoic leucogabbro and leucogranite. Similarities in the tectono-magmatic evolution of the Chu-Kendyktas and Zheltau terranes are also indicated by the presence of Neoproterozoic felsic and basalt-rhyolite volcanogenic formations (the Yualy and Kopi Formations) with estimated ages of ~780 Ma (Kröner et al., 2007). An abundance of Late Neoproterozoic magmatic complexes of ~800 Ma within the different blocks of the Chu-Kendyktas and Zheltau terranes is also characteristic of the Ulutau-Moyunkum group of Precambrian terranes of the western CAOB (Degtyarev et al., 2017). The common features of this group also include the presence of Early Precambrian magmatic formations (Palaeoproterozoic orthogneisses of the Anrakhai Complex in the Zheltau terrane, Kröner et al., 2007; Pilitsyna et al, 2019), a wide distribution of Meso- and Early Neoproterozoic sedimentary lithologies (the Akbastau Formation of the Chu Block) and an absence of Late Mesoproterozoic magmatic formations of 1000–1100 Ma.

The studied Ediacaran–Cambrian sedimentary and volcanogenic rocks of the Shukyr and Zhuantobe Complexes have analogues in the south of the Chu Block (the Kiintas and Ogiztau Formations), within the Kendyktas Block (the Zhaisan Formation) and the Zheltau terrane (the Koyandy Complex). The Shukyr and Koyandy Complexes of the Chu-Kendyktas and Zheltau terranes contain detrital zircons with preserved magmatic zoning with predominant zircon populations covering the age span of 880–1360 Ma, with two prominent peaks at ~990 and 1080 Ma (Pilitsyna et al., 2019). Hence, the Grenville magmatic complexes, which are virtually lacking in the Ulutau-Moyunkum group of Precambrian terranes but are widespread in the Issedonian group of Precambrian terranes in the western CAOB (Degtyarev et al., 2017), are thought to represent the main sources for the observed Ediacaran–Cambrian formations. We note that the affinity of the Chu-Kendyktas and Zheltau terranes with the Ulutau-Moyunkum group, and the concurrent presence of the Issedonian group complexes as sources in the Ediacaran–Cambrian, are not in contradiction. The differences between the observed groups of Precambrian terranes are the most conspicuous in the Mesoproterozoic and the first half of the Neoproterozoic, when the terranes may have formed part of different continental blocks. However, at the end of the Neoproterozoic, the differences tend to become insignificant, whilst in the Ediacaran these differences disappear. Thus, the existence of a single continent, comprising all of the terranes of the western CAOB in the late Neoproterozoic–Ediacaran has been inferred (Degtyarev et al., 2017). Hence, for the Ediacaran–Cambrian period, both the Ulutau-Moyunkum and Issedonian groups of Precambrian terranes may represent possible sources of clastic material.

The late Precambrian tectono-magmatic evolution of the Ulutau-Moyunkum group of terranes is thought to be consistent with that of the north-east part of the Tarim craton (Kuruketage area) (Degtyarev et al., 2017). Within the Kuruketage area, Early Precambrian formations are similarly exposed and comprise Neoarchean TTG gneisses, calc-alkali and high Ba-Sr granites, as well as Palaeoproterozoic gneissic granites and high-potassium granites (Zhao and Cawood, 2012). Moreover, the Palaeoproterozoic complexes are unconformably overlain by weakly metamorphosed sedimentary Mesoproterozoic and possibly Early Neoproterozoic (Tonian) formations up to 3500 m thick (Zhao and Cawood, 2012; Zhang et al., 2013). Early Mesoproterozoic complexes have not been described in the north of the Tarim craton so far, however these are known from the south-western part of the craton and comprise A-type granites with an age of 1.4 Ga (Ye et al., 2016). Late Mesoproterozoic–Early Neoproterozoic magmatic and metamorphic formations are poorly developed in the northern part of the Tarim craton, where small granite bodies and Palaeoproterozoic gneisses metamorphosed at ~1.0 Ga occur (Shu et al., 2011; Zhang et al., 2012; He et al., 2013).

In turn, Late Neoproterozoic granitoids and other magmatic formations are the most widespread within the Kuruketage area, where the oldest magmatic complexes of this age comprise small bodies or dykes of ultramafic–mafic–carbonatite complexes, as well as granodiorites and granites with estimated ages of 800–820 Ma (Zhang et al., 2007). The larger massifs of the central part of the area are composed of younger quartz diorites, granodiorites and granites with ages ranging from 750 to 820 Ma (Long et al., 2011), and a similar age estimate of ~750 Ma was obtained for a contrasting volcanogenic succession of basalts, dacites, rhyolites and tuffs (Xu et al., 2009). The formation of the Neoproterozoic magmatic complexes from the north-east part of the Tarim craton is considered to be related to intraplate magmatism.

Importantly, Neoproterozoic high-temperature granulite metamorphism is another characteristic feature that unites the studied Chu-Kendyktas terrane and the Tarim craton. In the NE of the Kuruketage area, metasedimentary garnet-orthopyroxene granulites and overprinted amphibolites have been described (He et al., 2012), with an estimated age for the high-grade metamorphism of 790–820 Ma. Similarly, the metasedimentary formations of the Aydaly Complex in the Chu Block described in this study are thought to have undergone granulite facies re-equilibration at P-T conditions consistent with those obtained from the garnet-orthopyroxene granulites of the Tarim craton during the Neoproterozoic stage at 770–790 Ma. Furthermore, in the northern part of the Tarim craton, Early Neoproterozoic andesites (~900 Ma) (Aksu area) and blueschists with an estimated age for the metamorphism of not earlier than 760 Ma, are locally exposed (Zhang et al. 2013; He et al., 2019). The formation of the Neoproterozoic (900–760 Ma) granulites, andesites and blueschists in the Chu Block and the northern part of the Tarim craton may have occurred in suprasubductional settings.

To summarise, based on the ages, compositions and formation settings of the studied complexes, we suggest that the Chu Block, comprising the Chu-Kendyktas terrane, together with the other terranes of the Ulutau-Moyunkum group and the Tarim craton, belonged to a single large continental block in the Late Precambrian. At the end of the Neoproterozoic, the Issedonian group of Precambrian terranes apparently collided with that continental block, and the terranes were only separated again in the Early Palaeozoic as a result of the opening of the Palaeo-Asian and Turkestan Oceans.

4.3. Tectonic evolution of the Chu-Kendyktas terrane in the precambrian–early Palaeozoic

The Precambrian evolution of the Chu-Kendyktas terrane may be very roughly reconstructed based on the detrital zircon ages obtained

from the Aydaly Complex granulites and the Nd model ages of the studied Neoproterozoic granitoids. The Neoarchean-Palaeoproterozoic (~1.8–2.7 Ga) crustal complexes evidently formed part of the Chu-Kendyktas terrane, similarly to those described from the Zheltau and Naryn-Sarydzhaz terranes, and the Tarim craton (Kröner et al., 2007; Zhao and Cawood, 2012; Kröner et al., 2017; Pilitsyna et al, 2019). Hence, the observed Neoarchean-Palaeoproterozoic complexes of the Ulutau-Moyunkum group terranes and the Tarim craton are interpreted to have been formed within a single continental block, which may have been associated with the Columbia supercontinent (e.g. Shu et al., 2011). The existence of Early Mesoproterozoic complexes with ages of 1.4–1.5 Ga was ascertained from the inherited zircon core within the Neoproterozoic orthogneisses of the Aydaly Complex and the Nd model ages of the Early Palaeozoic granitoids of the Ulken massif, however the tectonic settings of the formation of the Early Mesoproterozoic complexes have been obscured. We have proposed that the Aydaly Complex para-amphibolites, which are thought to be the oldest formations and may be considered as precursors for the observed clinopyroxene-rich and melt-rich granulites, could be of Mesoproterozoic age. Several populations of detrital zircons indicate a sedimentary origin of the rocks' protolith and their chemical compositions are close to mafic greywackes, derived from the erosion of basic and intermediate magmatic complexes of supra-subductional origin. The available data are insufficient to determine the interval of time over which the accumulation of the sedimentary protolith of the para-amphibolites occurred. However, the presence of Palaeoproterozoic, and to a lesser extent Neoarchean, complexes in the source may be reasonably assumed. The accretion of the para-amphibolites' protolith to the Palaeoproterozoic continental block is therefore arbitrarily proposed to have occurred during the Mesoproterozoic. A thick sedimentary cover was accumulating within the Chu-Kendyktas Block and other terranes of the Ulutau-Moyunkum group, as well as the Tarim craton during the greater part of the Mesoproterozoic and Early Neoproterozoic.

In the Late Neoproterozoic, the Ulutau-Moyunkum group of terranes, together with the Tarim craton, formed part of the Rodinia supercontinent and were possibly located within its marginal parts. An inferred subduction zone existed in the vicinity of this margin, whereas the Rodinia supercontinent was mostly influenced by mantle-plume processes that initiated its subsequent breakup. The interaction of the Neoproterozoic Rodinian plume with the subduction zone led to voluminous and diverse magmatism, with both supra-subductional and intraplate geochemical signatures (Zhang et al., 2012). The formations related to this activity comprise the Neoproterozoic granitoids, which are extensively developed within the Chu-Kendyktas, Zheltau and other terranes of the Ulutau-Moyunkum group and the Tarim craton. Moreover, the observed granulite metamorphism of the para-amphibolites and the formation of the orthogneisses in the Aydaly Complex of the Chu Block, as well as analogous granulite metamorphism in the northern part of the Tarim craton (He et al., 2012), may have been related to interactions with the melts associated with the Late Neoproterozoic stage of magmatism. An alternative model for the occurrence of the Late Neoproterozoic granulite metamorphism within these regions proposes a collisional event in which the Ulutau-Moyunkum and Issedonian groups of Precambrian terranes were amalgamated (Degtyarev et al., 2017).

The Ediacaran–Cambrian complexes of the Chu-Kendyktas terrane (the Shukyr and Zhuantobe Complexes) along with the other terranes of the western CAOB were formed in intraplate settings and at the passive margins of the opened oceanic basins. It is worth nothing that both groups of Precambrian terranes are thought to represent sources of clastic material. The studied Ediacaran–Cambrian complexes are characterised by the presence of black shales, quartz-rich sandstones, and contrasting rhyolite-basalt volcanic rocks, which is indicative of the intraplate settings for the formation of these complexes. In the latest Cambrian, a closure of oceanic basins in the SW part of the CAOB was initiated (the Dzhalair-Naiman and Kyrgyz-Terskey oceans) and the marginal parts of the adjacent Precambrian terranes were transformed into active margins, where supra-subductional granitoid magmatism occurred. In the Chu Block, the formation of the Early Palaeozoic Ulken massif and the coeval granitoid massifs of the Kendyktas Block in the Chu-Kendyktas terrane (Kozakov, 1993) are thought to be associated with that stage. In the Middle Ordovician (460–445 Ma,) the oceanic basins were completely closed, which was followed by the subsequent collision of the framing Precambrian terranes. In the western part of the Palaeozoides of Kazakhstan and North Tien Shan, a supra-subductional volcano-plutonic continental arc was formed. In this process, the major part of the granite massifs was emplaced within the Precambrian terranes (e.g. Degtyarev, 2012; Kröner et al., 2012; Wang et al., 2012; Degtyarev et al., 2017; Kröner et al., 2013), and strong deformation of the Precambrian complexes is thought to have occurred at the same stage (Wang et al., 2011). Following this, the exhumation of the Aydaly Complex formations from deeper to shallower horizons was likely accompanied by the observed Middle Ordovician processes, which may also be related to the presence of the CL-dark zircon rims in the orthogneisses and granulites.

5. Conclusions

Based on our geological observations, along with whole-rock and mineral chemistry data and the results of zircon age determinations, as well as Nd isotopic investigations of the Chu Block rock types (the Chu-Kendyktas terrane), our main conclusions are as follows:

1. The Aydaly Complex formations include predominant orthogneisses with a Neoproterozoic protolith age of 790 Ma, as well as amphibolites–amphibole-rich granulites and their derivatives, comprising mesocratic, leucocratic and melanocratic granulites. The age estimates of the leucocratic melt-rich granulites, which form both veins or layers within the melanocratic clinopyroxene-rich host and more rarely separate bodies, correspond to the time range of 770–790 Ma and define the Neoproterozoic stage of magmatism and high-temperature metamorphism for this rock type. The spatial and structural proximity of the orthogneisses and granulites, together with the similar age estimations, could indicate a synchronous tectono-magmatic evolution, induced by the Neoproterozoic (late Tonian) magmatism;
2. The melanocratic clinopyroxene-rich granulites contain a number of detrital zircons with maximum concordant age estimates of 1794 and 1856 Ma, and to a lesser extent of 2290–2680 Ma, confirming a sedimentary origin of the protolith, which is thought to have been related to moderate-grade para-amphibolites (metagreywackes). Hence, the accumulation of the protolith for the Aydaly Complex granulites and its subsequent emplacement at mid-crustal levels are thought to have occurred in the time range from the middle Palaeoproterozoic (~1800 Ma) to the latter half of Tonian (~770–790 Ma). The subsequent interaction of the para-amphibolites with granitoid melts led to the formation of the granulite facies mineral assemblages of clinopyroxene and feldspar at T ~900 °C;
3. The Shukyr Complex is composed of metasedimentary garnet-biotite schists, the protolith of which corresponds to shales according to the chemical compositions. The protolith of these rocks was formed during the Ediacaran–Cambrian from the erosion of mainly Mesoproterozoic (1.0 Ga) and Palaeoproterozoic (2.46 Ga) complexes, which are lacking within the Chu-Kendyktas terrane. Detrital zircons with Neoproterozoic age estimates are also present in these garnet-biotite schists and are thought to have been at least partly sourced from the granitoids of the Aydaly Complex. The garnet-biotite schists are interpreted to represent moderate-temperature hornfels formed at the contact between the shales and the Early Palaeozoic granitoids of the Ulken massif at T ~600 °C, and subsequently became foliated in response to later episodes of deformation;

4. The formation of the protoliths of the rock types of the Aydaly and Shukyr Complexes is thought to have been related to the reworking of Palaeoproterozoic continental crust, according to the $\varepsilon_{Nd(t)}$ values and Nd model ages;
5. The ages and geochemical signatures of the Neoproterozoic formations of the Chu-Kendyktas terrane correspond to those of the Ulutau-Moyunkum group of Precambrian terranes in the western part of the CAOB. The late Precambrian tectono-magmatic evolution of the group is similar to that inferred for the northern part of the Tarim craton;
6. The observed Neoproterozoic granulite metamorphism in the Aydaly Complex is consistent with the formation of coeval garnet-orthopyroxene granulites in the NE part of the Tarim Craton, and may have resulted from either an interaction with the melts associated with the Late Neoproterozoic stage of magmatism or a collisional event that resulted in the amalgamation of the Ulutau-Moyunkum and Issedonian groups of Precambrian terranes in the Late Neoproterozoic.

Acknowledgements

The authors are thankful to T. Yu. Tolmacheva for conodont determinations and A.V. Ryazantsev for his help during the fieldwork. We are grateful to Professor Dmitry Gladkochub and an anonymous reviewer for their constructive and valuable comments and recommendations.

The expedition work and SHRIMP analyses were funded by research project № 14-27-00058 of the Russian Science Foundation. LA-ICP-MS studies were financed by a joint research project of the Russian Foundation for Basic Research (RFBR) and the Ministry of Science and Technology (MoST) of Taiwan № 19-55-52001. Other analytical procedures were funded by RFBR project № 17-05-00357.

Appendix A:. Analytical methods for the whole-rock and mineral chemistry studies

Major elements were determined by XRF using a Bruker AXS wavelength dispersive S4 PIONEER spectrometer with a 4 kW X-ray tube at Geological Institute of the Russian Academy of Sciences (RAS). Data processing was implemented using the «Spectra-Plus^{TM}» software package. The automatic registration of peak overlaps and correction for matrix effects were carried out during individual measurements of fundamental parameters for each sample. The intervals of analyzed concentrations obtained after recalculation to oxides (mass fraction %) were Si – 0.01–1.0, Ti – 0.01–5.0, Al – 1.0–60.0, Fe (total) – 1.0–40.0, Mn – 0.01–1.0, Ca – 1.0–50, Mg – 0.1–40, Na – 0.1–10.0, K – 0.1–10.0, and P – 0.01–5.0. Ferric and ferrous iron were calculated using the HCAM 50-X titrimetric bichromatic method (Kazakhstan Institute of Metrology; reg. number KZ.07.00.03141–2015 from 12.05.2015).

Trace elements were acquired by the Analytical Centre of the Institute of Microelectronics Technology and High-Purity Materials RAS using an ICP-MS on a Perkin Elmer ELAN 6100 DRC and by atomic emission spectrometry with ICP-MS (ICAP-61, Thermo Jarrell Ash; X-7, Thermo Elemental, USA). The relative standard deviation for all analyzed elements was not more than 0.2 for element contents below the five-fold detection limit and below 0.1 for contents above the fivefold detection limit. The major element concentrations are in wt.%, and the trace elements are in ppm.

Mineral compositions were determined using a JEOL-8200 electron probe microanalyzer (EPMA) in the Laboratory of Mineral Substances Analysis, Institute of Mineralogy, Geochemistry and Petrography of the RAS and a JEOL JXA-8230 EPMA at the Institut des Sciences de la Terre (ISTerre, University Grenoble Alpes, France). These were equipped with five wavelength dispersive spectrometers and an energy dispersive (EDX) spectrometer operating at an accelerating voltage of 20 kV, probe current of 20nA, and beam diameter of 1 μm. The standards were certified natural minerals and synthetic oxides: Wollastonite (Si, Ca), Corundum (Al), Orthoclase (K), Rhodonite (Mn), Albite (Na), Apatite (P), Rutile (Ti), Hematite (Fe), and Periclase (Mg). Ferric iron was recalculated for clinopyroxene, garnet, amphibole and chlorite on the basis of charge balance and stoichiometry (Droop, 1987). All iron in epidote-clinozoisite was taken as Fe^{3+} in accordance with the mineral formula. Mineral abbreviations are after Whitney and Evans (2010); a.p.f.u. is 'atom per formula unit'.

Appendix B:. Pseudosection modelling

Perple_X software (version 6.7.3; Connolly (1990), Connolly (2005)), in conjunction with the internally consistent thermodynamic database of Holland and Powell (1998) for the CaO-FeO-Fe_2O_3-MgO-Na_2O-K_2O-Al_2O_3-SiO_2-H_2O (amphibolite–amphibole-rich granulite of the Aydaly Complex), CaO-FeO-MgO-Na_2O-K_2O-Al_2O_3-SiO_2-H_2O (mesocratic and melanocratic clinopyroxene-rich granulites of the Aydaly Complex) and CaO-TiO_2-FeO-MgO-MnO-Na_2O-K_2O-Al_2O_3-SiO_2-H_2O (garnet-biotite schists of the Shukyr Complex) systems, was implemented to construct the pseudosections. Given that the Aydaly Complex rocks have been significantly changed by interactions with the haplogranitic melt and have experienced granulite facies re-equilibration, whole-rock compositions for each representative variety (reflecting the progressive alterations of the pre-existing para-amphibolite to amphibole-rich granulite, through to mesocratic and leucocratic with melanocratic (clinopyroxene-rich) granulites) were used to constrain the approximate P-T stability fields for the observed mineral assemblages and are considered to correspond to some extent to the reacting bulk compositions. Divided iron was taken for the least altered metamorphic variety of amphibolite–amphibole-rich granulite (X_{Fe3+} = 0.35), whereas for the mesocratic and melanocratic clinopyroxene-rich granulites of the Aydaly Complex the total iron was taken into recalculations due to the strong modifications resulting from interactions with the external melts, resulting in uncertainties related to the ferrous/ferric iron division. The total iron was also taken for the garnet-biotite schists of the Shukyr Complex, as the Fe^{3+} content in the main minerals of the schists is thought to be negligible. The introduced composition for the garnet-biotite schists represents an averaged bulk composition from all the analysed samples (Table 2), with corrected CaO contents by subtracting apatite.

The following solution models were applied for the granulites of the Aydaly Complex: Cpx(HP) for clinopyroxene (Holland and Powell, 1996), Amph(DHP) for amphibole (Dale et al., 2000), and feldspar (Fuhrman and Lindsley, 1988) for plagioclase with K-feldspar·H_2O was taken as a system component equal to the loss on ignition value, to model the melt proportions using a melt(HP) solution model for the haplogranitic melt (Holland and Powell, 2001; White et al., 2001). For the garnet-biotite schists, melting was not suggested therefore H_2O was taken as a saturated fluid phase and recalculated using the CORK equation of state (Holland and Powell, 1998). In addition, the solution models of Gt(HP) for garnet (Holland and Powell, 1998), Pl(I1, HP) for plagioclase (Holland and Powell, 2003), Bio(HP) for biotite (Powell and Holland, 1999), Mica(CHA) for white mica (Coggon and Holland, 2002; Auzanneau et al., 2010) and Chl(HP) for chlorite (Holland et al., 1998) were introduced.

The compositional isopleths and isomodes for all pseudosections were plotted using PyWerami software (Lexa, 2011).

Appendix C:. Analytical technique for zircon age determinations and Sm-Nd whole-rock isotopic studies.

The U-Pb ID-TIMS isotope investigations were carried out in the laboratory of Isotope Geology, Institute of Precambrian Geology and Geochronology RAS. Zircon morphology and internal structure were studied with an ABT 55 scanning electron microscopy with CL detector and LEICA DMLP microscope. The zircon grains selected for study were

washed in alcohol, acetone, and 1 M HNO3. Chemical abrasion was performed with a mixture of HF and HNO_3 (10:1) at 220 °C for 2 and 4 h, respectively (Mattinson, 1994). The dissolved parts of the zircons were decanted, and the residues were rinsed with concentrated HCl overnight and then several times on a hot plate with fresh portions of acid. The residues were then spiked, dissolved and analyzed following the method of Krogh (1973). Before decomposition, the zircons were spiked with a mixed ^{202}Pb – ^{235}U spike. Digestion of the zircons and U and Pb extractions were performed following a modified technique of Krogh (1973). The isotope analyses were performed using a TRITON TI multicollector mass-spectrometer in static and dynamic (with an electron multiplier) modes. The analytical uncertainties of the U and Pb concentrations were 0.5%, and the blanks were < 10 pg for Pb and 1 pg for U. The raw data were processed using PbDAT (Ludwig, 1989) and ISOPLOT (Ludwig, 2012). Common Pb correction was applied according to the model of Stacey and Kramers (1975). All errors are reported as 2σ means.

The SIMS U-Pb isotope analyses of zircon separates were carried out using a SHRIMP-II ion probe at the Center of Isotope Research of the Karpinsky Russian Geological Research Institute following conventional techniques (Williams, 1998; Larionov et al., 2004). The zircons were mounted in epoxy along with the zircon standards 91,500 (Wiedenbeck et al., 1995) and Temora (Black et al., 2003), polished to approximately half of the grain thicknesses and coated with 99.999% pure gold. The inner structure of the zircons was examined using optical microscopy and cathodoluminescence. Regions devoid of visible cracks and inclusions in euhedral crystals were chosen for analysis. The data were processed with the SQUID v1.12 and ISOPLOT/Ex 3.22 (Ludwig, 2005a; 2005b) programs using the decay constants of Steiger and Jager (1976). The correction for common Pb was applied according to the model of Stacey and Kramers (1975) using the measured $^{204}Pb/^{206}Pb$ ratio.

Zircon U-Th-Pb isotopic data were obtained using the LA-ICP-MS technique at the Department of Geosciences, National Taiwan University (NTU), Taipei, using an Agilent 7500 s quadrupole ICP-MS and a NewWave UP213 laser ablation system. The detailed analytical procedures can be found in Chiu et al. (2009). During the experiments, about 1 min was spent for measuring the gas blank, and the results indicate a sensitivity of less than 1000 counts per second for all measured isotopes. Spot analyses were done using a spot diameter of 30 μm. Calibration was performed using the GJ-1 zircon standard, with a well-established $^{207}Pb/^{206}Pb$ age and an intercept age, using isotope dilution thermal ionization mass spectrometry (ID-TIMS), of 608.5 ± 0.4 Ma (2σ) and 608.5 ± 1.5 Ma (2σ), respectively (Jackson et al., 2004). The Harvard 91,500 Wiedenbeck et al. (1995) and Plešovice (PLS) (Sláma et al., 2008) reference zircons were used as secondary standards for data quality control. All U-Th-Pb isotopic ratios were calculated using the GLITTER 4.0 (GEMOC) software (Van Achterbergh et al., 2001), and common lead was corrected using the common lead correction function proposed by Anderson (2002). Concordia ages were calculated using Isoplot v. 4.15 (Ludwig, 2008). Only Concordia ages with MSWD b 1 were used for construction of histograms, probability density plots and calculation of age peaks (Gehrels, 2012). Our $^{207}Pb/^{235}U$, $^{206}Pb/^{238}U$ and $^{207}Pb/^{206}Pb$ ages of zircon 91,500 obtained in the NTU are 1059 ± 8 Ma, 1055 ± 9 Ma and 1068 ± 10 Ma (2σ), respectively, which are in good agreement with the values reported by Wiedenbeck et al. (1995) using ID-TIMS methods. Our weighted average of $^{206}Pb/^{238}U$ ages for the PLS zircon is 336 ± 3 Ma (2σ, MSWD = 0.25, Probability = 1.00) and match the corresponding age of 337.13 ± 0.37 Ma recommended by (Sláma et al., 2008).

Whole-rock Sm-Nd isotopic analyses were performed at the Institute of Precambrian Geology and Geochronology, RAS, St. Petersburg. Approximately 100 mg of whole-rock powder were dissolved in a mixture of HF, HNO_3 and $HClO_4$. A ^{149}Sm–^{150}Nd spike solution was added to samples prior to dissolution. The REE were separated on BioRad AGW50-X8 200–400 mesh resin using conventional cation-exchange techniques. Sm and Nd were separated by extraction chromatography using a LN-Spec (100–150 mesh) resin. The total laboratory blanks were 0.1–0.2 ng for Sm and 0.1–0.5 ng for Nd. Isotopic compositions of Sm and Nd were measured on a TRITON TI multicollector mass-spectrometer in static mode. The precision (2σ) of Sm and Nd contents and $^{147}Sm/^{144}Nd$ ratios was ca. 0.5% and ca. 0.005% for the $^{143}Nd/^{144}Nd$ ratios. $^{143}Nd/^{144}Nd$ ratios were normalized against $^{146}Nd/^{144}Nd = 0.7219$ and adjusted relative to a value of 0.512115 for the JNdi-1 standard (Tanaka et al., 2000). During the period of analysis, the weighted average of 7 JNdi-1 Nd standard runs yielded 0.512101 ± 5 (2σ). The $\varepsilon_{Nd(t)}$ values were calculated using the present-day values for a chondritic uniform reservoir (CHUR) $^{143}Nd/^{144}Nd = 0.512638$ and $^{147}Sm/^{144}Nd = 0.1967$ (Jacobsen and Wasserburg, 1984). Whole-rock $Nd_{t(DM)}$ model ages were calculated using the model of Goldstein and Jacobsen (1988), according to which the Nd isotopic composition of the depleted mantle evolved linearly since 4.56 Ga ago and has a present-day value $\varepsilon_{Nd(0)}$ of + 10 ($^{143}Nd/^{144}Nd = 0.513151$ and $^{147}Sm/^{144}Nd = 0.21365$).

Appendix D. Supplementary data

Supplementary data to this article can be found online at https://doi.org/10.1016/j.precamres.2019.105397.

References

Abdulin, A.A., 1980. Chu-Yili Ore Belt: Geology of the Chu-Yili Region. Nauka, Alma Ata, p. 504 (in Russian).

Anderson, T., 2002. Correction of common lead in U-Pb analyses that do not report ^{204}Pb. Chem. Geol. 192, 59–79. https://doi.org/10.1016/S0009-2541(02)00195-X.

Auzanneau, E., Schmidt, M.W., Vielzeuf, D., Connolly, J.A.D., 2010. Titanium in phengite: a geobarometer for high temperature eclogites. Contrib. Mineral. Petrol. 159, 1–24. https://doi.org/10.1007/s00410-009-0412-7.

Bakirov, A.B., Tagiri, M., Sakiev, K.S., Ivleva, E.A., 2003. The Lower Precambrian rocks in the Tien Shan and their geodynamic setting. Geotectonics 37 (5), 368–380.

Barker, F., 1979. Trondhjemite: definition, environment and hypotheses of origin. In: Barker, F. (Ed.), Trondhjemites, Dacites, and Related Rocks. Elsevier, New York, pp. 1–12.

Black, L.P., Kamo, S.L., Allen, C.M., Aleinikoff, J.N., Davis, D.W., Korsch, R.J., Foudoulis, C., 2003. TEMORA 1: a new zircon standard for Phanerozoic U-Pb geochronology. Chem. Geol. 200, 155–170. https://doi.org/10.1016/S0009-2541(03)00165-7.

Chiu, H.-Y., Chung, S.-L., Wu, F.-Y., Liu, D., Liang, Y.-H., Lin, I.-J., Iizuka, Y., Xie, L.-W., Wang, Y., Mei-Fei Chu, M.-F., 2009. Zircon U-Pb and Hf isotopic constraints from eastern Transhimalayan batholiths on the precollisional magmatic and tectonic evolution in southern Tibet. Tectonophysics 477 (1–2), 3–19. https://doi.org/10.1016/j.tecto.2009.02.034.

Coggon, R., Holland, T.J.B., 2002. Mixing properties of phengitic micas and revised garnet phengite thermobarometers. J. Metamorph. Geol. 20, 683–696. https://doi.org/10.1046/j.1525-1314.2002.00395.x.

Condie, K.C., 1993. Chemical composition and evolution of the upper continental crust: contrasting results from surface samples and shales. Chem. Geol. 104, 1–37. https://doi.org/10.1016/0009-2541(93)90140-E.

Connolly, J.A.D., 1990. Multivariable phase-diagrams: an algorithm based on generalized thermodynamics. Am. J. Sci. 290, 666–718. https://doi.org/10.2475/ajs.290.6.666.

Connolly, J.A.D., 2005. Computation of phase equilibria by linear programming: a tool for geodynamic modeling and its application to subduction zone decarbonation. Earth Planet. Sci. Lett. 236 (1), 524–541. https://doi.org/10.1016/j.epsl.2005.04.033.

Cullers, R.L., 1994. The chemical signature of source rocks in size fractions of Holocene stream sediment derived from metamorphic rocks in the Wet Mountains region, Colorado, U.S.A. Chem. Geol. 113, 327–343. https://doi.org/10.1016/0009-2541(94)90074-4.

Cullers, R.L., 2000. The geochemistry of shales, siltstones and sandstones of Pennsylvanian-Permian age, Colorado, USA: implications for provenance and metamorphic studies. Lithos 51, 181–203. https://doi.org/10.1016/S0024-4937(99)00063-8.

Dale, J., Holland, T., Powell, R., 2000. Hornblende-garnet-plagioclase thermobarometry: a natural assemblage calibration of the thermodynamics of hornblende. Contrib. Mineral. Petrol. 140, 353–362. https://doi.org/10.1007/s004100000187.

Degtyarev, K.E., 2012. Tectonic Evolution of the Early Paleozoic Island Arcs and Continental Crust Formation in the Caledonides of Kazakhstan. GEOS, Moscow (in Russian).

Degtyarev, K., Yakubchuk, A., Tretyakov, A., Kotov, A., Kovach, V., 2017. Precambrian geology of the Kazakh Uplands and Tien Shan: an overview. Gondwana Res. 47, 44–75. https://doi.org/10.1016/j.gr.2016.12.014.

Depaolo, D.J., 1981. Neodymium isotopes in the Colorado Front Range and crust-mantle evolution in the Proterozoic. Nature 291, 193–196. https://doi.org/10.1038/291193a0.

Droop, T.R.G., 1987. A general equation for estimating Fe^{3+} concentrations in

ferromagnesian silicates and oxides from microprobe analyses, using stoichiometric criteria. Mineral. Mag. 51, 431–435. https://doi.org/10.1180/minmag.1987.051.361.10.
Frost, B.R., Barnes, C.G., Collins, W.J., Arculus, R.J., Ellis, D.J., Frost, C.D., 2001. A geochemical classification for granitic rocks. J. Petrol. 42, 2033–2048. https://doi.org/10.1093/petrology/42.11.2033.
Frost, C.D., Frost, B., 2011. On ferroan (A-type) granites: their compositional variability and modes of origin. J. Petrol. 52, 39–53. https://doi.org/10.1093/petrology/egq070.
Fuhrman, M.L., Lindsley, D.H., 1988. Ternary-feldspar modeling and thermometry. Am. Mineral. 73, 201–215.
Gao, J., Wang, X.-S., Klemd, R., Jiang, T., Qian, Q., Mu, L.-X., Ma, Y.-Z., 2015. Record of assembly and breakup of Rodinia in the southwestern Altaids: evidence from Neoproterozoic magmatism in the Chinese Western Tianshan Orogen. J. Asian Earth Sci. 113, 173–193. https://doi.org/10.1016/j.jseaes.2015.02.002.
G.E. Gehrels 2012. Detrital zircon U-Pb geochronology: current methods and new opportunities. C. Busby A. Azor Tectonics of Sedimentary Basins: Recent Advances. Wiley-Blackwell, Chichester, UK, 47–62. 10.1002/9781444347166.ch2.
Goldman, D.S., Albee, A.L., 1977. Correlation of Mg/Fe partitioning between garnet and biotite with $^{18}O/^{16}O$ partitioning between quartz and magnetite. Am. J. Sci. 277, 750–767. https://doi.org/10.2475/ajs.277.6.750.
Goldstein, S.J., Jacobsen, S.B., 1988. Nd and Sr isotopic systematics of rivers water suspended material: implications for crustal evolution. Earth Planet. Sci. Lett. 87, 249–265. https://doi.org/10.1016/0012-821X(88)90013-1.
Glorie, S., De Grave, J., Buslov, M.M., Zhimulev, F.I., Stockli, D.F., Batalev, V.Y., Izmer, A., Van den Haute, P., Vanhaecke, F., Elburg, M.A., 2011. Tectonic history of the Kyrgyz South Tianshan (Atbashi-Inylchek) suture zone: the role of inherited structures during deformation- propagation. Tectonics 30 (6), TC6016. https://doi.org/10.1029/2011TC002949.
Hammarstrom, J.M., Zen, E., 1986. Aluminum in hornblende: an empirical igneous geobarometer. Am. Mineral. 71, 1297–1313.
Henry, D.J., Novák, M., Hawthorne, F.C., Ertl, A., Dutrow, B.L., Uher, O., Pezzotta, F., 2011. Nomenclature of the tourmaline-supergroup minerals. Am. Mineral. 96, 895–913. https://doi.org/10.2138/am.2011.3636.
He, Z.-Y., Zhang, Z.-M., Zong, K.-Q., Wang, W., Santosh, M., 2012. Neoproterozoic granulites from the northeastern margin of the Tarim craton: petrology, zircon U-Pb ages and implications for the Rodinia assembly. Precambrian Res. 212–213, 21–33. https://doi.org/10.1016/j.precamres.2012.04.014.
He, Z.-Y., Zhang, Z.-M., Zong, K.-Q., Dong, X., 2013. Paleoproterozoic crustal evolution of the Tarim craton: constrained by zircon U-Pb and Hf isotopes of meta-igneous rocks from Korla and Dunhuang. J. Asian Earth Sci. 78, 54–70. https://doi.org/10.1016/j.jseaes.2013.07.022.
He, Z.Y., Klemd, R., Zhang, Z.-M., Zong, K.-Q., Sun, L.-X., Tian, Z.-L., Huang, B.-T., 2015. Mesoproterozoic continental arc magmatism and crustal growth in the eastern Central Tianshan Arc Terrane of the southern Central Asian Orogenic Belt: geochronological and geochemical evidence. Lithos 236–237, 74–89. https://doi.org/10.1016/j.lithos.2015.08.009.
He, Z., Wang, B., Zhong, L., Zhu, X., 2018. Crustal evolution of the Central Tianshan Block: Insights from zircon U-Pb isotopic and structural data from meta-sedimentary and meta-igneous rocks along the Wulasitai – Wulanmoren shear zone. Precambrian Res. 314, 111–128. https://doi.org/10.1016/j.precamres.2018.06.003.
He, J., Xu, B., Li, D., 2019. Newly discovered early Neoproterozoic (ca. 900 Ma) andesitic rocks in the northwestern Tarim Craton: implications for the reconstruction of the Rodinia supercontinent. Precambrian Res. 325, 55–68. https://doi.org/10.1016/j.precamres.2019.02.018.
Herron, M.M., 1988. Geochemical classification of terrigenous sands and shales from core or log data. J. Sediment. Res. 58 (5), 820–829. https://doi.org/10.1306/212F8E77-2B24-11D7-8648000102C1865D.
Holland, T., Powell, R., 1996. Thermodynamics of order-disorder in minerals: II. Symmetric formalism applied to solid solutions. Am. Miner. 81, 1425–1437. https://doi.org/10.2138/am-1996-11-1215.
Holland, T.J.B., Baker, J., Powell, R., 1998. Mixing properties and activity-composition relationships of chlorites in the system MgO-FeO-Al_2O_3-SiO_2-H_2O. Eur. J. Mineral. 10, 395–406. https://doi.org/10.1127/ejm/10/3/0395.
Holland, T.J.B., Powell, R., 1998. An internally consistent thermodynamic data set for phases of petrological interest. J. Metamorph. Geol. 16, 309–343. https://doi.org/10.1111/j.1525-1314.1998.00140.x.
Holland, T., Powell, R., 2001. Calculation of phase relations involving haplogranitic melts using an internally consistent thermodynamic dataset. J. Petrol. 42, 673–683. https://doi.org/10.1093/petrology/42.4.673.
Holland, T.J.B., Powell, R., 2003. Activity-composition relations for phases in petrological calculations: an asymmetric multicomponent formulation. Contrib. Mineral. Petrol. 145, 492–501. https://doi.org/10.1007/s00410-003-0464-z.
Hollister, L.S., Grissom, G.C., Peters, E.K., Stowell, H.H., Sisson, V.B., 1987. Confirmation of the empirical correlation of Al in hornblende with pressure of solidification of calcalkaline plutons. Am. Mineral. 72, 231–239.
Huang, Z., Long, X., Kröner, A., Yuan, C., Wang, Y., Chen, B., Zhang, Y., 2015. Neoproterozoic granitic gneisses in the Chinese Central Tianshan Block: implications for tectonic affinity and Precambrian crustal evolution. Precambrian Res. 269, 73–89. https://doi.org/10.1016/j.precamres.2015.08.005.
Huang, H., Cawood, P.A., Hou, M., Xiong, F., Ni, S., Gong, T., 2019. Provenance of latest Mesoproterozoic to early Neoproterozoic (meta)-sedimentary rocks and implications for paleographic reconstruction of the Yili Block. Gondwana Res. 72, 120–138. https://doi.org/10.1016/j.gr.2019.03.010.
Jacobsen, S.B., Wasserburg, G.J., 1984. Sm-Nd evolution of chondrites and achondrites. Earth Planet. Sci. Lett. 67, 137–150. https://doi.org/10.1016/0012-821X(84)90109-2.
Jackson, S.E., Pearson, N.J., Griffin, W.L., Belousova, E.A., 2004. The application of laser ablation-inductively coupled plasma-mass spectrometry to in situ U-Pb zircon geochronology. Chem. Geol. 211, 47–69. https://doi.org/10.1016/j.chemgeo.2004.06.017.
Johnson, M., Rutherford, M.J., 1989. Experimental calibration of the aluminium-in-hornblende geobarometer with application to Long Valley caldera. Geology 17, 837–841. https://doi.org/10.1130/0091-7613(1989) 017b0837:ecotaiN2.3.co;2.
Kanygina, N., Tretyakov, A., Kovach, V., Degtyarev, K., Wang, K.-L., Kotov, A., 2018. First results of study of detrital zircons from Late Precambrian quartzite–schist sequences of the Aktau-Mointy block. Central Kazakhstan. Dokl. Earth Sci. 479 (1), 320–323. https://doi.org/10.1134/S1028334X18030261.
Khodorevskaya, L.I., 2002. Diffusional interaction of haplogranite melt with amphibolite (experimental modeling). Exp. Geosci. 10 (1), 13–18.
Kovach, V., Degtyarev, K., Tretyakov, A., Kotov, A., Tolmacheva, E., Wang, K., Chung, S., Lee, H., Jahn, B., 2017. Sources and provenance of the Neoproterozoic placer deposits of the Northern Kazakhstan: implication for continental growth of the western Central Asian Orogenic Belt. Gondwana Res. 47, 28–43. https://doi.org/10.1016/j.gr.2016.09.012.
Kozakov, I.K., 1993. The Early Precambrian of the Central Asia Fold Belt. Nauka, St. Petersburg, p. 272 (in Russian).
Krogh, T.E., 1973. A low-contamination method for hydrothermal decomposition of zircon and extraction of U and Pb for isotopic age determination. Geochim. Cosmochim. Acta 37, 485–494. https://doi.org/10.1016/0016-7037(73), 90213-5.
Kröner, A.,Windley, B.F., Badarch, G., Tomurtogoo, O., Hegner, E., Jahn, B.M., Gruschka, S., Khain, E.V., Demoux, A., Wingate, M.T.D., 2007. Accretionary Growth and Crust Formation in the Central Asian Orogenic Belt and Comparison with the Arabian-Nubian Shield 181–209 (10.1130/2007.1200(11)).
Kröner, A., Alexeiev, D.V., Hegner, E., Rojas-Agramonte, Y., Corsini, M., Chao, Y., Wong, J., Windley, B.F., Liu, D., Tretyakov, A.A., 2012. Zircon and muscovite ages, geochemistry, and Nd-Hf isotopes for the Aktyuz metamorphic terrane: evidence for an early Ordovician collisional belt in the northern Tianshan of Kyrgyzstan. Gondwana Res. 21, 901–927. https://doi.org/10.1016/j.gr.2011.05.010.
Kröner, A., Alexeiev, D.V., Rojas-Agramonte, Y., Hegner, E., Wong, J., Xia, X., Belousova, E., Mikolaichuk, A.V., Seltmann, R., Liu, D., Kiselev, V.V., 2013. Mesoproterozoic (Grenville-age) terranes in the Kyrgyz North Tienshan: zircon ages and Nd-Hf isotopic constraints on the origin and evolution of basement blocks in the Southern Central Asian Orogen. Gondwana Res. 23, 272–295. https://doi.org/10.1016/j.gr.2012.05.004.
Kröner, A., Alexeiev, D.V., Kovach, V.P., Tretyakov, A.A., Mikolaichuk, A.V., Xie, H., Sobel, E.R., 2017. Zircon ages, geochemistry and Nd isotopic systematics for the Palaeoproterozoic 2.3–1.8 Ga Kuilyu Complex, East Kyrgyzstan – The oldest continental basement fragment in the Tianshan orogenic belt. J. Asian Earth Sci. 135, 122–135. https://doi.org/10.1016/j.jseaes.2016.12.022.
Lanari, P., Vho, A., Bovay, T., Airaghi, L., Centrella, S., 2018. Quantitative compositional mapping of mineral phases by electron probe microanalyser. Geol. Soc. London Special Publ. https://doi.org/10.1444/SP478.4.
Larionov, A.N., Andreichev, V.A., Gee, D.G., 2004. The Vendian alkaline igneous suite of northern Timan: ion microprobe U–Pb zircon ages of gabbros and syenite. In: Gee, D. G., Pease, V. (Eds.), The Neoproterozoic Timanide Orogen of Eastern Baltica. vol. 30. Geological Society, London, Memoirs, pp. 69–74.
Leake, B.E., Wooley, A.R., Arps, C.E., et al., 1997. Nomenclature of amphiboles: report of the subcommittee on amphiboles of the international mineralogical association, commission on new minerals and mineral names. Can. Mineral. 35, 219–246.
Lexa, O., 2011. PyWerami: Contour/3D Plotting Program for Perple_X WERAMI Data. (Version 2.0.1) [Software]. Available from. http://petrol.natur.cuni.cz/~ondro/pywerami:home.
Liu, H., Wang, B., Shu, L., Jahn, B.-M., Lizuka, Y., 2014. Detrital zircon ages of Proterozoic meta-sedimentary rocks and Paleozoic sedimentary cover of the northern Yili Block: Implications for the tectonics of microcontinents in the Central Asian Orogenic Belt. Precambrian Res. 252, 209–222. https://doi.org/10.1016/j.precamres.2014.07.018.
Long, X., Yuan, C., Sun, M., Kröner, A., Zhao, G., Wilde, S., Hu, A., 2011. Reworking of the Tarim craton by underplating of mantle plume-derived magmas: evidence from Neoproterozoic granitoids in the Kuluketage area, NW China. Precambrian Res. 187, 1–14. https://doi.org/10.1016/j.precamres.2011.02.001.
Ludwig, K.R., 1989. PBDAT for MS-DOS, a Computer Program for IBM-PC Compatibles for Processing Raw Pb- U- Th Isotopic Data: USGS Open-File Report 88–542.
Ludwig, K.R., 2005a. SQUID 1.12 a User's Manual. A Geochronological Toolkit for Microsoft Excel. Berkeley Geochronology Center Spec Pub, p. 22.
Ludwig, K.R., 2005b. User's Manual for ISOPLOT/Ex 3.22. A Geochronological Toolkit for Microsoft Excel. Berkeley Geochronology Center Spec Pub, p. 71.
Ludwig, K.R., 2008. Isoplot V. 4.15: a Geochronological Toolkit for Microsoft Excel. Special Publication, No. 4. 76. Berkeley Geochronology Center.
Ludwig, K.R, 2012. Isoplot/Ex, Rev. 3.75. A Geochronological Toolkit for Microsoft Excel. 5. Berkeley Geochronology Center Spec. Publ.
Mattinson, J.M., 1994. A study of complex discordance in zircons using step-wise dissolution techniques. Contrib. Mineral. Petrol. 116, 117–129.
McLennan, S.M., Hemming, D.K., Hanson, G.N., 1993. Geochemical approaches to sedimentation, provenance and tectonics. Geol. Soc. Am. Spec. Pap. 284, 21–40. https://doi.org/10.1130/SPE284-p21.
Morimoto, N., Fabries, J., Ferguson, A.K., et al., 1988. Nomenclature of pyroxenes. Am. Mineral. 73, 1123–1133.
Nesbitt, H.W.M., Young, G.M., 1982. Early Proterozoic climates and plate motions inferred from major element chemistry of lutites. Nature 299, 715–717. https://doi.org/10.1038/299715a0.

Pearce, J.A., Harris, N.B.W., Tindle, A.G., 1984. Trace element discrimination diagrams for the tectonic interpretation of granitic rocks. J. Petrol. 25, 956–983. https://doi.org/10.1093/petrology/25.4.956.

Perchuk, A.L., Lavrent'eva, I.V., 1983. Experimental investigation of exchange equilibria in the system cordierite-garnet-biotite. In: Saxena, S.K. (Ed.), Kinetics and Equilibrium in Mineral Reactions. Advances in Physical Geochemistry 1, 199–240.

Pilitsyna, A.V., Tretyakov, A.A., Degtyarev, K.E., Salnikova, E.B., Kotov, A.B., Kovach, V.P., Wang, K.-L., Batanova, V.G., et al., 2019. Early Palaeozoic metamorphism of Precambrian crust in the Zheltau terrane (Southern Kazakhstan; Central Asian Orogenic belt): P-T paths, protoliths, zircon dating and tectonic implications. Lithos 324–325, 115–1114. https://doi.org/10.1016/j.lithos.2018.10.033.

Powell, R., Holland, T., 1999. Relating formulations of the thermodynamics of mineral solid solutions: activity modeling of pyroxenes, amphiboles, and micas. Am. Mineral. 84, 1–14. https://doi.org/10.2138/am-1999-1-201.

Rozanov, S.B., Filatova, Kheraskova, L.I., 1974. Geology of Precambrian and Early Palaeozoic formations near the Zhuantobe Mount (East Betpak-dala). Izvestiya AS KazSSR. Geol. Ser. 6, 31–39 (in Russian).

Rozanov, S.B., 1976. Early Proterozoic spilite-jaspilite formation of Kazakhstan. In: Zaitsev, Yu.A. (Ed.), Precambrian Geology and Tectonics of. Central Kazakhstan. Moscow State University Publishing, pp. 11–178 (in Russian).

Sawyer, E.W., 2008. Atlas of migmatites. The Canadian Mineralogist, Special Publication 9. NRC Research Press, Ottawa, Ontario, Canada. 371 p.

Schmidt, M.W., 1992. Amphibole composition in tonalite as a function of pressure: an experimental calibration of the Al-in-hornblende barometer. Contrib. Mineral. Petrol. 110, 304–310. https://doi.org/10.1007/BF00310745.

Shi, W.X., Liao, Q.A., Hu, Y.Q., Yang, Z.F., 2010. Characteristics of Mesoproterozoic granites and their geological significance from Middle Tianshan Block, East Tianshan district, NW China. Geological Science and Technology Information 29, 29–37 (in Chinese with English abstract). https://doi.org/10.3109/10731190903495751.

Shu, L.S., Deng, X.L., Zhu, W.B., Ma, D.S., Xiao, W.J., 2011. Precambrian tectonic evolution of the Tarim Block, NW China: new geochronological insights from the Quruqtagh domain. J. Asian Earth Sci. 42, 774–790. https://doi.org/10.1016/j.jseaes.2010.08.018.

Skjerlie, K.P., Patino Douce, A.E., 1995. Anatexis of interlayered amphibolite and pelite at 10 kbar: effect of diffusion of major components on phase relations and melt fraction. Con-trib. Miner. Petrol. 122, 62–78.

Sláma, J., Košler, J., Condon, D.J., Crowley, J.L., Gerdes, A., Hanchar, J.M., Horstwood, M.S.A., Morris, G.A., Nasdala, L., Norberg, N., Schaltegger, U., Schoene, B., Tubrett, M.N., Whitehouse, M.J., 2008. Plešovice zircon—a new natural reference material for U-Pb and Hf isotopic microanalysis. Chem. Geol. 249, 1–35. https://doi.org/10.1016/j.chemgeo.2007.11.005.

Sun, S.-S., McDonough, W.F., 1989. Chemical and isotopic systematics of oceanic basalts: implications for mantle composition and processes. Geol. Soc. Lond. Spec. Publ. 42, 313–345. https://doi.org/10.1144/GSL.SP.1989.042.01.19.

Stacey, J.S., Kramers, I.D., 1975. Approximation of terrestrial lead isotope evolution by a two-stage model. Earth Planet. Sci. Lett. 26 (2), 207–221. https://doi.org/10.1016/0012-821X(75)90088-6.

Steiger, R.H., Jager, E., 1976. Subcomission of Geochronology: convension of the use of decay constants in geo- and cosmochronology. Earth Planet. Sci. Lett. 36 (2), 359–362. https://doi.org/10.1016/0012-821X(77)90060-7.

Tanaka, T., Togashi, S., Kamioka, H., Amakawa, H., Kagami, H., Hamamoto, T., Yuhara, M., Orihashi, Y., Yoneda, S., Shimizu, H., Kunimaru, T., Takahashi, K., Yanagi, T., Nakano, T., Fujimaki, H., Shinjo, R., Asahara, Y., Tanimizu, M., Dragusanu, C., 2000. JNdi-1: a neodymium isotopic reference in consistency with La Jolla neodymium. Chem. Geol. 168, 279–281. https://doi.org/10.1016/S0009-2541(00)00198-4.

Taylor, S.R., McLennan, S.M., 1985. The Continental Crust: Its Composition and Evolution. Blackwell, Oxford, pp. 312.

Tretyakov, A.A., Degtyarev, K.E., Kotov, A.B., Salnikova, E.B., Shatagin, K.N., Yakovleva, S.Z., Anisimova, I.V., Plotkina, Yu.V., 2011. Middle Riphean gneiss granites of the Kokchetav massif (northern Kazakhstan): structural position and age substantiation. Dokl. Earth Sci. 440 (4), 511–515.

Tretyakov, A.A., Degtyarev, K.E., Kotov, A.B., Salnikova, E.B., Yakovleva, S.Z., Anisimova, I.V., Shatagin, K.N., Letnikova, E.F., 2012. Age of the last episode of Precambrian regional metamorphic event in South Ulutau (central Kazakhstan): results of U-Pb geochronological studies of granites from the Aktas complex. Dokl. Earth Sci. 446 (1), 1037–1041.

Tretyakov, A., Degtyarev, K., Shatagin, K., Kotov, A., Salnikova, E., Anisimova, I., 2015. Neoproterozoic anorogenic rhyolite – granite volcano-plutonic association of the Aktau-Mointy sialic massif (Central Kazakhstan): age, source, and paleotectonic position. Petrology 23 (1), 22–44. https://doi.org/10.1134/S0869591115010063.

Tretyakov, A.A., Degtyarev, K.E., Sal'nikova, E.B., Shatagin, K.N., Kotov, A.B., Ryazantsev, A.V., Pilitsyna, A.V., Yakovleva, S.Z., Tolmacheva, E.V., Plotkina, Y.V., 2016. Paleoproterozoic anorogenic granitoids of the Zheltav sialic massif (Southern Kazakhstan): Structural position and geochronology. Dokl. Earth Sci. 466 (2), 1–6. https://doi.org/10.1134/S1028334X16010165.

Turkina, O.M., Letnikov, F.A., Levin, A.V., 2011. Mesoproterozoic granitoids of the basement of the Kokchetav microcontinent. Dokl. Earth Sci. 436 (4), 499–503.

Van Achterbergh, E., Ryan, C.G., Jackson, S.E., Griffin, W.L., 2001. In: Sylvester, P.J. (Ed.), LA ICP-MS in the Earth Sciences – Appendix 3, Data Reduction Software for LA-ICP-MS. Vol. 29. Mineralogical Association of Canada, St. John's, pp. 239–243 Short Course Volume.

Wang, B., Jahn, B.-M., Lo, C.-H., Shu, L.-S., Wu, C.-Y., Li, K.-Sen, Wang, F., 2011. Structural analysis and 40Ar/39Ar thermochronology of Proterozoic rocks in Sailimu area (NW China): Implication to polyphase tectonics of the North Chinese Tianshan. J. Asian Earth Sci. 42, 839–853. https://doi.org/10.1016/j.jseaes.2011.07.022.

Wang, B., Jahn, B.-M., Shu, L., Li, K., Chung, S.-L., Liu, D., 2012. Middle-Late Ordovician arc-type plutonism in the NW Chinese Tianshan: implication for the accretion of the Kazakhstan continent in Central Asia. J. Asian Earth Sci. 49, 40–53. https://doi.org/10.1016/j.jseaes.2011.11.005.

Wang, B., Liu, H., Shu, L., Jahn, B.-M., Chung, S., Zha, Y., Liu, D., 2014a. Early Neoproterozoic crustal evolution in Northern Yili Block: insights from migmatite, orthogneiss and leucogranite of the Wenquan metamorphic complex in the NW Chinese Tianshan. Precambrian Res. 242, 58–81. https://doi.org/10.1016/j.precamres.2013.12.006.

Wang, B., Shu, L., Liu, H., Gong, H., Ma, Y., 2014b. First evidence for ca. 780 Ma intraplate magmatism and its implication for Neoproterozoic rifting of the North Yili Block and tectonic origin of the continental block in the southwest of Central Asia. Precambrian Res. 254, 258–272. https://doi.org/10.1016/j.precamres.2014.09.005.

Whalen, J.B., Currie, K.L., Chappell, B.W., 1987. A-type granites: geochemical characteristics, discrimination and petrogenesis. Contrib. Mineral. Petrol. 95, 407–419. https://doi.org/10.1007/BF00402202.

White, R.W., Powell, R., Holland, T.J.B., 2001. Calculation of partial melting equilibria in the system Na_2O-CaO-K_2O-FeO-MgO-Al_2O_3-SiO_2-H_2O (NCKFMASH). J. Metamorph. Geol. 19, 139–153. https://doi.org/10.1046/j.0263-4929.2000.00303.x.

Whitney, D.L., Evans, B.W., 2010. Abbreviations for names of rock-forming minerals. Am. Mineral. 95, 185–187. https://doi.org/10.2138/am.2010.3371.

Wiedenbeck, M., Alle, P., Corfu, F., Griffin, W.L., Meier, M., Oberli, F., von Quadt, A., Roddick, J.C., Spiegel, W., 1995. Three natural zircon standards for U-Th-Pb, Lu-Hf, trace-element and REE analyses. Geostand. Newslett. 19, 1–23. https://doi.org/10.1111/j.1751-908X.1995.tb00147.x.

Williams, I.S., 1998. U-Th-Pb geochronology by ion microprobe. In: McKibben, M.A., Shanks III, W.C., Ridley, W.I. (Eds.), Applications of Microanalytical Techniques to Understanding Mineralizing Processes. Reviews in Economic Geology, pp. 1–35. https://doi.org/10.5382/Rev.07.

Wyllie, P.G., Wolf, M.B., 1993. Amphibolite dehydration-melting: sorting out the solidus. Geol. Soci., London, Spec. Publ. 76 (1), 405–416. https://doi.org/10.1144/gsl.sp.1993.076.01.20.

Xiong, F., Hou, M., Cawood, P.A., Huang, H., Ducea, M.N., Ni, S., 2019. Neoproterozoic I-type and highly fractionated A-type granites in the Yili Block, Central Asian Orogenic Belt: petrogenesis and tectonic implications. Precambrian Res. 328, 235–249. https://doi.org/10.1016/j.precamres.2019.04.017.

Xu, B., Xiao, S., Zou, H., Chen, Y., Li, Z.-X., Song, B., Liu, D., Zhou, C., Yuan, X., 2009. SHRIMP zircon U-Pb age constraints on Neoproterozoic Quruqtagh diamictites in NW China. Precambrian Res. 168, 247–258. https://doi.org/10.1016/j.precamres.2008.10.008.

Ye, X.-T., Zhang, C.-L., Santosh, M., Zhang, J., Fan, X.-K., Zhang, J.-J., 2016. Growth and evolution of Precambrian continental crust in the southwestern Tarim terrane: New evidence from the ca. 1.4 Ga A-type granites and Paleoproterozoic intrusive complex. Precambr. Res. 275, 18–34. https://doi.org/10.1016/j.precamres.2015.12.017.

Zhang, C.-L., Li, X.-H., Li, Z.-X., Lu, S.-N., Ye, H.-M., Li, H.-M., 2007. Neoproterozoic ultramafic–mafic-carbonatite complex and granitoids in Quruqtagh of northeastern Tarim Block, western China: geochronology, geochemistry and tectonic implications. Precambrian Res. 152, 149–169. https://doi.org/10.1016/j.precamres.2006.11.003.

Zhang, C.-L., Li, H.-K., Santosh, M., Li, Z.-X., Zou, H.-B., Wang, H., Ye, H., 2012. Precambrian evolution and cratonization of the Tarim Block, NW China: petrology, geochemistry, Nd-isotopes and U-Pb zircon geochronology from Archaean gabbro-TTG–potassic granite suite and Paleoproterozoic metamorphic belt. J. Asian Earth Sci. 47, 5–20. https://doi.org/10.1016/j.jseaes.2011.05.018.

Zhang, C.-L., Zou, H.-B., Li, H.-K., Wang, H.-Y., 2013. Tectonic framework and evolution of the Tarim Block in NW China. Gondwana Res. 23, 1306–1315. https://doi.org/10.1016/j.gr.2012.05.009.

Zhao, G., Cawood, P., 2012. Precambrian geology of China. Precambrian Res. 222–223, 13–54. https://doi.org/10.1016/j.precamres.2012.09.017.

Zhu, X., Wang, B., Cluzel, D., He, Z., Zhou, Y., Zhong, L., 2019. Early Neoproterozoic gneissic granitoids in the southern Yili Block (NW China): Constraints on microcontinent provenance and assembly in the SW Central Asian Orogenic Belt. Precambrian Res. 325, 111–131. https://doi.org/10.1016/j.precamres.2019.02.019.